Vol. 69 • No. 2

February 2026

Microwave Journal

horizon house®

Founded in 1958

mwjournal.com

MILLER MMIC

Advancing RFIC Design Through Human-AI collaboration and competition

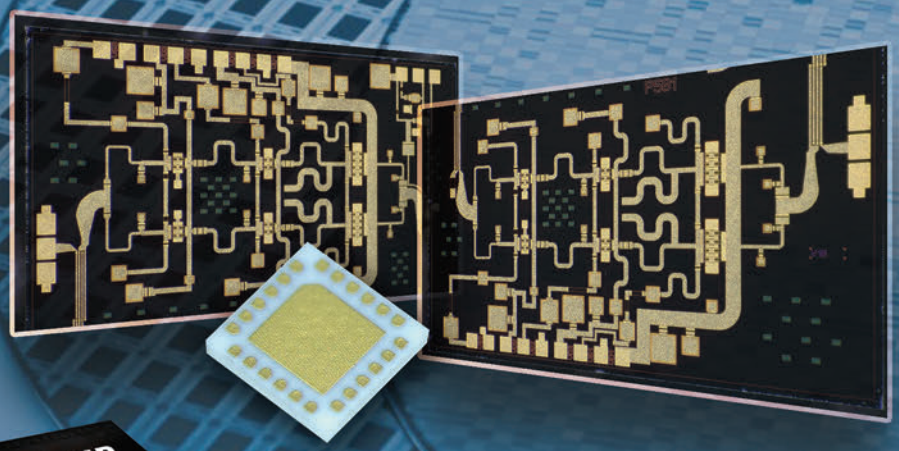

Miller MMIC is a global provider of RF semiconductor solutions with expertise in GaAs and GaN processes. We offer a diverse range of products tailored to various wireless applications. Our product lineup encompasses a wide array of offerings, including Low Noise Amplifiers, Distributed Amplifiers, Power Amplifiers, Driver Amplifiers, RF Switches, RF PIN Diode Switches, and numerous other voltage- and digitally-controllable RF components.

QFN and SiP (System-In-Package) available

RF Distributed Low Noise Amplifiers

PN	Freq Low (GHz)	Freq High (GHz)	Gain (dB)	NF(dB)	P1dB (dBm)	Voltage (VDC)	Current (mA)	Package
MMW001T	DC	20.0	17~19	1~3.5	23 @ 10GHz	8.0	145	die
MMW4FP	DC	50.00	16.00	4.00	24.00	10	200	die
MMW507	0.20	22.0	14.0	4 - 6	28.0	10.0	350	die
MMW508	DC	30.0	14.0	2.5dB @ 15GHz	24.5	10.0	200	die
MMW509	30KHz	45.0	15.0		20.0	6.0	190	die
MMW510	DC	45.0	11.0	4.5	15.5	6.0	100	die
MMW510F	DC	30.00	20.00	2.50	22.00			die
MMW511	0.04	65.0	10.0	9.0	18.0	8.0	250	die
MMW512	DC	65.0	10.0	5.0	14.5	4.5	85	die
MMW5FN	DC	67.00	14.00	2.00	19.00	4.5	81	die
MMW5FP	DC	67.00	14.00	4.00	21.00	8	140	die
MMW011	DC	12.0	14.0		30.5	12.0	350	die

Low Noise Amplifiers

PN	Freq Low (GHz)	Freq High (GHz)	Gain (dB)	NF(dB)	P1dB (dBm)	Voltage (VDC)	Current (mA)	Package
MML040	6.0	18.0	24.0	1.5	14.0	5.0	35	die
MML058	1.0	18.0	15.0	1.7	17.0	5.0	35	die
MML063	18.0	40.0	11.0	2.9	15.0	5.0	52	die
MML080	0.8	18.0	16.5/15.5	1.9/1.7	18/17.5	5.0	65/40	die
MML081	2.0	18.0	25/23	1.0/1.0	16/9.5	5.0	37/24	die
MML083	0.1	20.0	23.0	1.6	11.0	5.0	58	die

RF Driver Amplifier

PN	Freq Low (GHz)	Freq High (GHz)	Gain (dB)	NF(dB)	P1dB (dBm)	Voltage (VDC)	Current (mA)	Package
MM3006	2.0	20.0	19.5	2.5	22.0	7.0	130	die
MM3014	6.0	20.0	15.0	-	19.5	5.0	107	die
MM3017T	17.0	43.0	25.0		22.0	5.0	140	die
MM3031T	20.0	43.0	20.0		24.0	5.0	480	die
MM3051	17.0	24.0	25.0	-	25.0	5.0	220	die
MM3058	18.0	40.0	20/19.5	2.5/2.3	16/14	5/4	69/52	die
MM3059	18.0	40.0	16/16	2.5/2.3	16/15	5/4	67/50	die

GaAs Medium Power Amplifier

PN	Freq Low (GHz)	Freq High (GHz)	Gain (dB)	P1dB (dBm)	Psat (dBm)	Voltage (VDC)	Current (mA)	Package
MMP107	17.0	21.0	19.0	30.0	30.0	6.0	400	die
MMP108	18.0	28.0	14.0	31.5	31.0	6.0	650	die
MMP111	26.0	34.0	25.5	33.5	33.5	6.0	1300	die
MMP112	2.0	6.0	20.0	31.5	32.0	8.0	365	die
MMP501	20.0	44.0	15.0	27 -- 32	29 - 34	5.0	1200	die
MMP502	18.0	47.0	14.0	28.0	30.0	5.0	1500	die

PN : MMW5FP

RF GaAs MMIC DC-67GHz

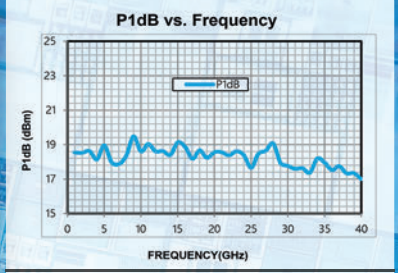

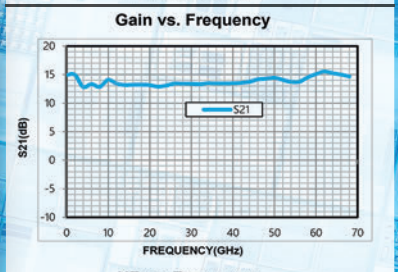

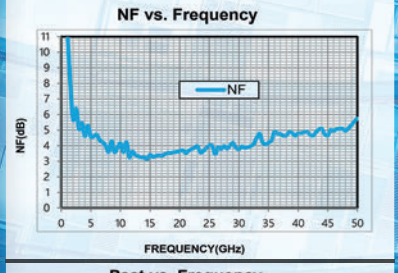

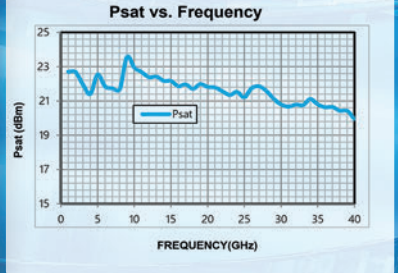

CALL US 1-833-2MILLER(264-5537)
WWW.MILLERMMIC.COM

MILLER MMIC

sales@millermmic.com
support@millermmic.com

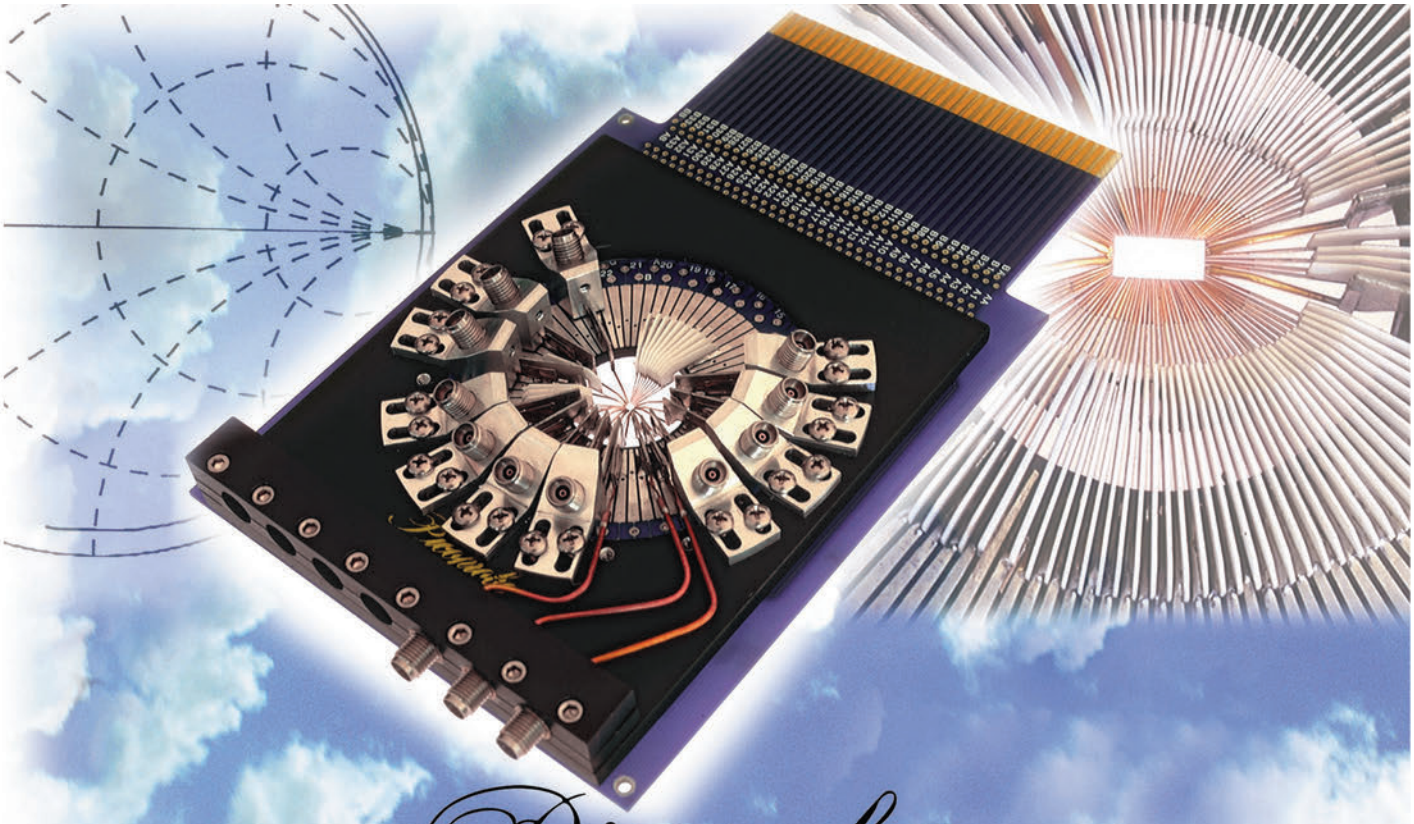

Picoprobe®

Picoprobe elevates probe cards to a higher level…

(…110 GHz to be exact.)

Since 1981, GGB Industries, Inc., has blazed the on-chip measurement trail with innovative designs, quality craftsmanship, and highly reliable products. Our line of custom microwave probe cards continues our tradition of manufacturing exceptional testing instruments.

Through unique modular design techniques, hundreds of low frequency probe needles and a variety of microwave probes with operating frequencies from DC to 40, 67, or even 110 GHz can be custom configured to your layout.

Our patented probe structures provide the precision and ruggedness you require for both production and characterization testing. And only Picoprobe® offers the lowest loss, best match, low inductance power supplies, and current sources on a single probe card.

Our proven probe card design technology allows full visibility with inking capability and ensures reliable contacts, even when probing non-planar structures.

Not only do you get all the attractive features mentioned, but you get personal, professional service, rapid response, and continuous product support--all at an affordable price so your project can be completed on time and within budget.

Typical Specs	10GHz	20GHz	40GHz
Insertion Loss	0.6 dB	0.8 dB	1.3 dB
Return Loss	22 dB	18 dB	15 dB

For technical assistance, custom product designs, or off-the-shelf delivery,call GGB Industries, Inc., at (239) 643-4400.

GGB INDUSTRIES, INC. • 4196 CORPORATE SQUARE • NAPLES, FL 34104

Telephone (239) 643-4400 • E-mail email@ggb.com • www.picoprobe.com

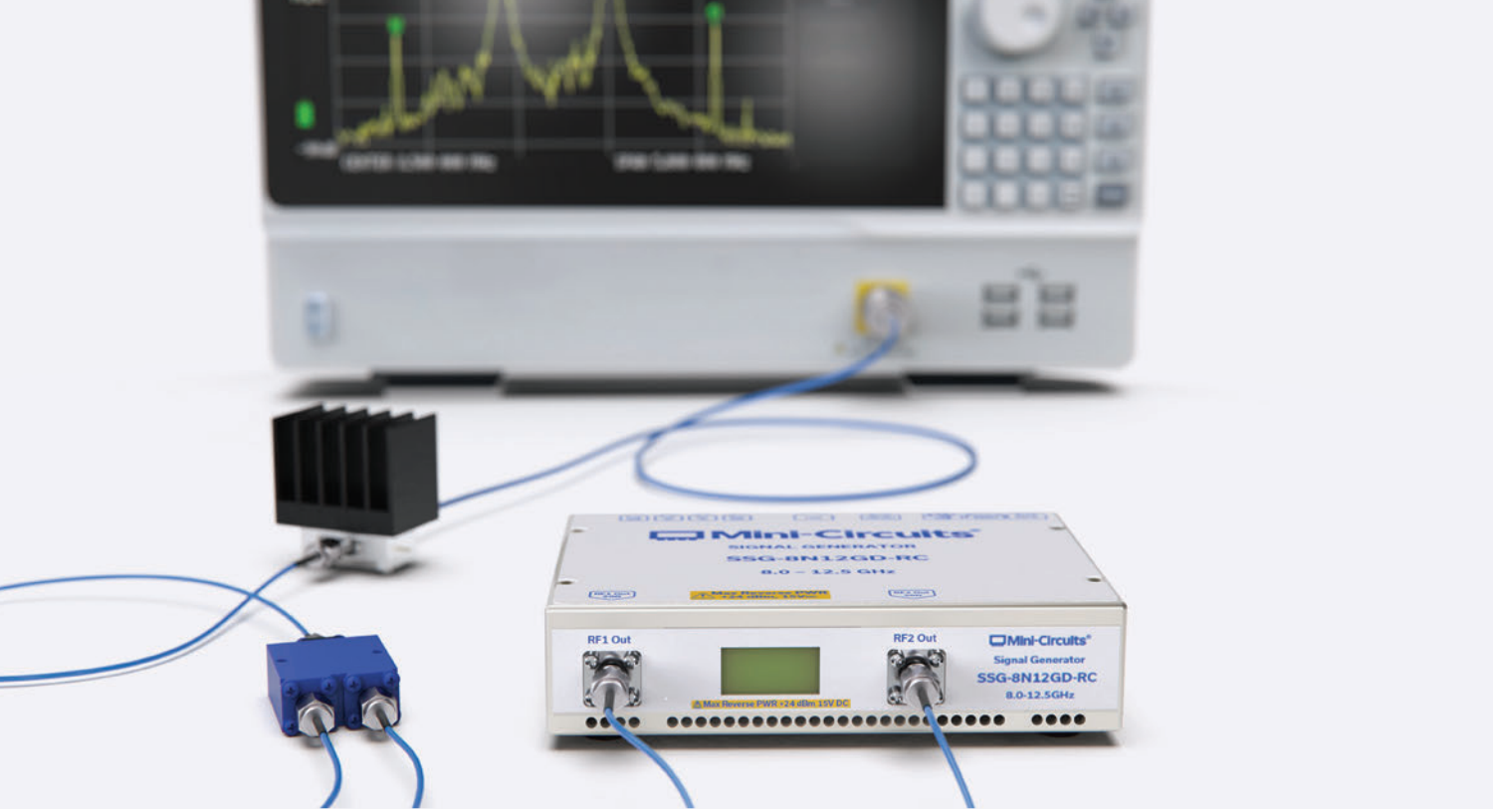

SSG SERIES

Signal Generators

Single-Channel & Dual Channel

LEARN MORE

Highlights

- Wide output power range
- Dual outputs with 360° independent phase control
- Pulsed, CW, AM, FM, and chirp modulations
- USB, Ethernet & PoE control interfaces
- Daisy chain port for multi-module control
- Compact housing, 3.6 x 5.1 x 1.2″

Model Number	Frequency	Output Power	# Channels	Release Status
SSG-8N12G-RC	8 to 12.5 GHz	-55 to 23 dBm	1	Production
SSG-8N12GD-RC	8 to 12.5 GHz	-55 to 23 dBm	2	Production
SSG-5N9G-RC	5 to 9 GHz	-55 to 23 dBm	1	Production
SSG-5N9GD-RC	5 to 9 GHz	-55 to 23 dBm	2	Production
SSG-9G-RC	0.01 to 9 GHz	-50 to 15 dBm	1	Q2, 2025
SSG-9GD-RC	0.01 to 9 GHz	-50 to 15 dBm	2	Q2, 2025
SSG-R7N6G-RC	0.7 to 6 GHz	-55 to 23 dBm	1	Q2, 2025
SSG-R7N6GD-RC	0.7 to 6 GHz	-55 to 23 dBm	2	Q3, 2025
SSG-1R5G-RC	0.02 to 1.5 GHz	-55 to 23 dBm	1	Q3, 2025
SSG-1R5GD-RC	0.02 to 1.5 GHz	-55 to 23 dBm	2	Q3, 2025

PWR SERIES

Power Sensors

Turn Your PC into a High-Performance Power Meter

LEARN MORE

- Dynamic range options spanning -60 to +20 dBm
- CW, true RMS, peak and average measurement capability
- Sample rates up to 80 million samples per second
- 50 and 75Ω models
- Software package supports automated measurement with statistical analysis and time domain plots
- No external calibration required

Model #	Control Interface	Measurement Type	Freq. Range (MHz)	Input Power Range (dBm)	Measurement Speed (ms)
PWR-40PW-RC	USB & Ethernet	Peak & Avg.	500-40000	-20 to 20	5.00E-05
PWR-18PWHS-RC	USB & Ethernet	Peak & Avg.	50-18000	-60 to 20	1.30E-05
PWR-18RMS-RC	USB & Ethernet	RMS	50-18000	-60 to 20	0.5
PWR-9PWHS-RC	USB & Ethernet	Peak & Avg.	50-9000	-60 to 20	0.000013
PWR-9RMS-RC	USB & Ethernet	RMS	50-9000	-60 to 20	0.5
PWR-8P-RC	USB & Ethernet	Peak & Avg.	10-8000	-60 to 20	0.002
PWR-8FS	USB	CW	1-8000	-30 to 20	10
PWR-8GHS	USB	CW	1-8000	-30 to 20	30
PWR-8GHS-RC	USB & Ethernet	CW	1-8000	-30 to 20	30
PWR-8PW-RC	USB & Ethernet	Peak & Avg.	10-8000	-60 to 20	0.00005

NIC

ASCENDING
TO NEW HEIGHTS

PROGRAMS:

- GPS III
- GOES
- Oceansat-2
- Iridium NEXT
- Chandrayaan 1
- Mangalyaan

MILITARY & COMMERCIAL SPACE SOLUTIONS

HIGH RELIABILITY

EEE-INST-002 & TOR Compliant Workflows

25+ YEARS **SPACE** HERITAGE

LC Filters | Crystal Filters | Ceramic Filters | Printed Filters | Switched Filter Banks | Integrated Assemblies

ISO 9001:2015
AS9100
CERTIFIED

NIC NETWORKS INTERNATIONAL CORPORATION
www.nickc.com

913.685.3400
15237 Broadmoor
Overland Park, KS
e-mail: sales@nickc.com

WE STAND AMONG GIANTS

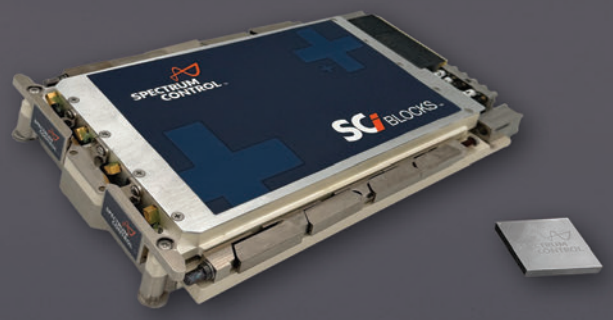

Innovation that cuts giants down to size.

Miniature. Modular. Intelligent.

SPECTRUM CONTROL™

spectrumcontrol.com/sci-blocks

ACCESS

ERAVANT
MAKING MILLIMETERWAVE ACCESSIBLE

CAPABLE.
COMPACT.
ACCESSIBLE.

VNA Frequency Extenders

- **Extended** Frequency Bands
- Excellent Dynamic Range
- Pricing built for scalability

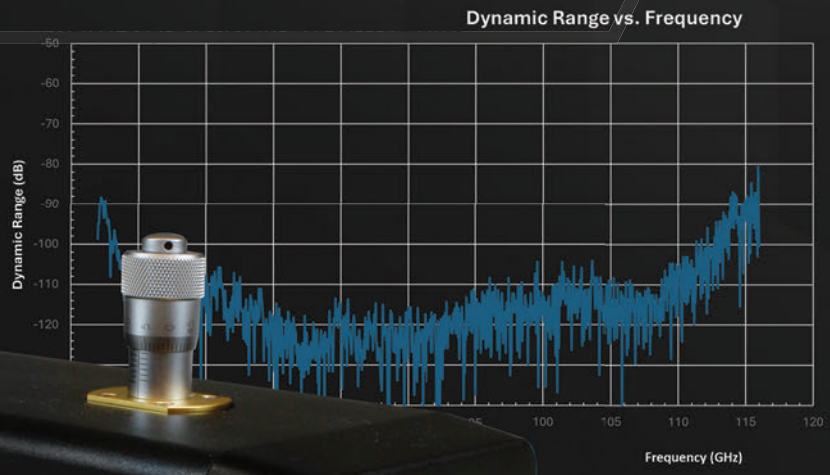

WG Port	Frequency Range	Dynamic Range (Typical @ 10Hz BW)	Test Port Output Power (Typical)	Phase Stability (@300 Hz BW)	Magnitude Stability (@300 Hz BW)	Directivity (Typical)
V-Band	45 to 80 GHz	120 dB	+13 dBm	±2 °	±0.3 dB	30 dB
E-Band	55 to 95 GHz	120 dB	+13 dBm	±2 °	±0.3 dB	30 dB
W-Band	67 to 116 GHz	120 dB	+7 dBm	±2 °	±0.3 dB	30 dB

**** Additional frequency bands & configurations are available online—scan the QR code to explore the full ACCESS lineup.**

WWW.ERAVANT.COM

www.eravant.com 501 Amapola Avenue Torrance, CA 90501
T: 424-757-0168 F: 424-757-0188 support@eravant.com

Adapters • Amplifiers • Antenna Feeds • Antennas • Attenuators • Bias Tees • Cable Assemblies • Corner Reflectors • Couplers • DC Blocks • Detectors • Ferrite Devices • Filters • Frequency Converters • Frequency Multipliers • Limiters • Magic Tees • Mixers • Noise Sources • Oscillators • Phase Shifters • Power Dividers • Radar Sensors • Subassemblies • Switches • Termination Loads • Test Equipment • Test Hardware & Accessories • TX/RX Modules • Uni-Guide™ • Waveguide Sections

RF-LAMBDA

THE LEADER OF RF BROADBAND SOLUTIONS

BROADBAND SSPA / EMC BENCHTOP

SOLID STATE POWER AMPLIFIER

0.1-22GHZ ULTRA BROADBAND SSPA

RFLUPA01M22GA
4W 0.1-22GHZ

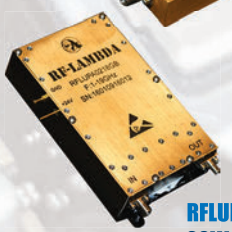

RFLUPA0218GB
20W 1-19GHZ

6-18GHZ 800W
CW REMC06G18GG

18-40GHZ 200W
CW REMC18G40GQ

MADE IN USA

0.1-6GHZ VHZ, UHF, L, S, C BAND

RFLUPA02G06GC
100W 2-6GHZ

RFLUPA0706GD
30W 0.7-6GHZ

6-18GHZ C, X, KU BAND

RFLUPA0618GD
60W 6-18GHZ

RFLUPA08G11GA
50W 8-11GHZ

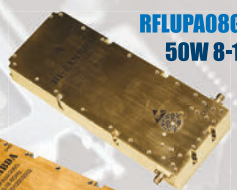

RFLUPA06G12GB
25W 6-12GHZ

18-50GHZ K, KA, V BAND

RFLUPA18G47GC
2W 18-47GHZ

RFLUPA27G34GB
15W 27-34GHZ

RFLUPA47G53GA2
10W 47-53GHZ

RFLUPA27G34GB
30W 18-40GHZ

BENCHTOP RF MICROWAVE SYSTEM POWER AMPLIFIER

REMC02G06GE
600W 2-6GHZ

REMC18G40GC2
40W 18-40GHZ

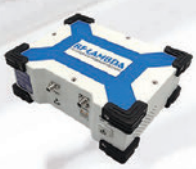

RAMP30G65GG
8W 30-65GHZ

RAMP06G18GA
10W 6-18GHZ

RAMP00M65GA
DC-65GHZ

www.rflambda.com
sales@rflambda.com

1-888-976-8880
1-972-767-5998

San Diego, CA, US
Carrollton, TX, US

Ottawa, ONT, Canada
Frankfurt, Germany

Microwave Journal
CONTENTS

February 2026
Vol. 69 • No. 2
Satellite & Radio Communications
mwjournal.com

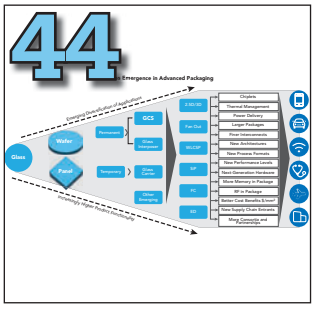

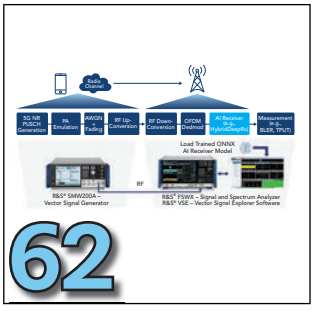

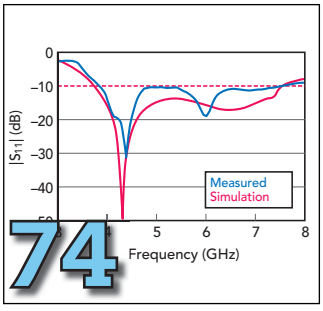

Cover Feature

Special Report

Technical Features

Has Amplifier Performance or Delivery Stalled Your Program?

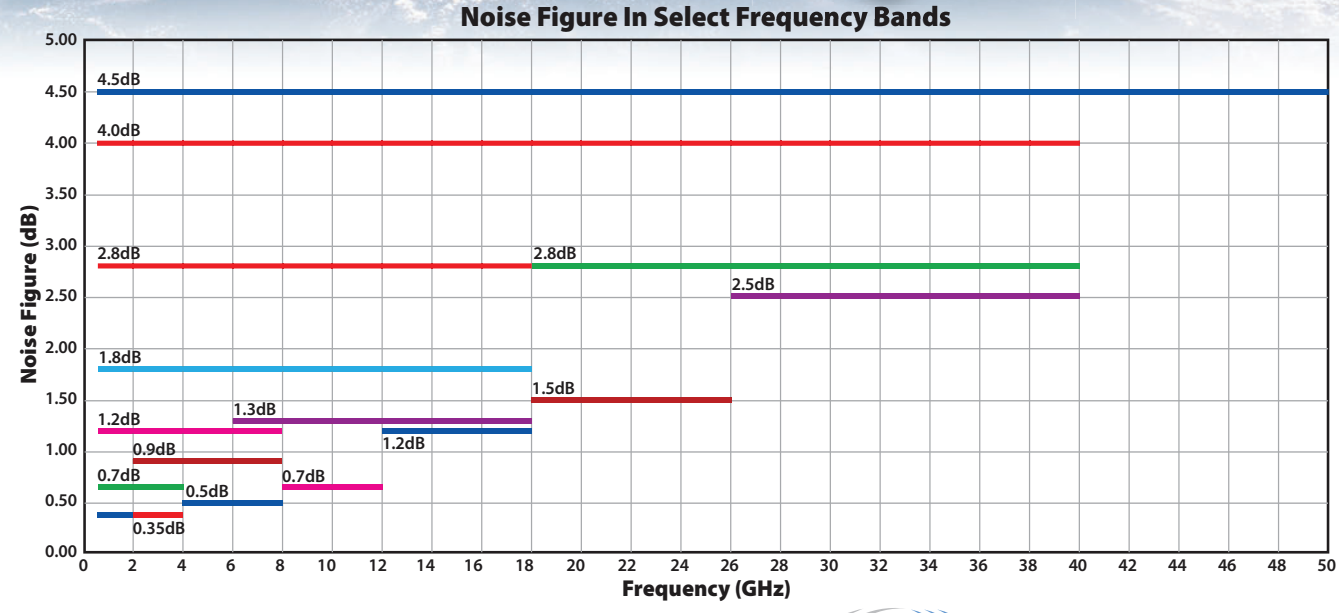

B&Z TECHNOLOGIES
Innovating to Excel

www.bnztech.com

Microwave Journal

CONTENTS

mwjournal.com

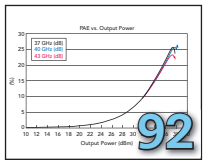

Product Features

Tech Briefs

Departments

Microwave Journal (USPS 396-250) (ISSN 0192-6225) is published monthly by Horizon House Publications Inc., 685 Canton St., Norwood, MA 02062. Periodicals postage paid at Norwood, MA 02062 and additional mailing offices.

POSTMASTER: Email address corrections to mwj@e-circ.net.com. Subscription information: (978) 671-0446. This journal is issued without charge upon written request to qualified persons working in the RF & microwave industry. Other subscriptions are: domestic, $130.00 per year, two-year subscriptions, $200.00; foreign, $225.00 per year, two-year subscriptions, $400.00; back issues (if available) and single copies, $20.00 domestic and $30.00 foreign. Claims for missing issues must be filed within 90 days of date of issue for complimentary replacement.

Posted under Canadian international publications mail agreement #PM40612608

STAFF

EXECUTIVE EDITORIAL OFFICE
685 Canton Street, Norwood, MA 02062
Tel: (781) 769-9750
FAX: (781) 769-5037
e-mail: mwj@mwjournal.com

EUROPEAN EDITORIAL OFFICE
16 Sussex Street, London SW1V 4RW, England
Tel: Editorial: +44 207 596 8730 Sales: +44 207 596 8740
FAX: +44 207 596 8749

SUBSCRIPTION SERVICES
Send subscription inquiries and address changes to:
Tel: (978) 671-0446
e-mail: mwj@e-circ.net

www.mwjournal.com

Printed in the USA

Design with Confidence. Source with Speed.

Fixed attenuators from the Spectrum Control brands you trust. Available at RFMW.

Powerfilm™

Chip Attenuators

Attenuation: up to 30 dB
Frequency: up to 40 GHz
Power: up to 250W
Cryo models also available

Inmet & Weinschel™

Coaxial Attenuators

Attenuation: up to 60 dB
Frequency: up to 50 GHz
Power: up to 500W
Cryo models also available

Model	Frequency	Power	DB Values in Stock
PCAAF Wrap around terminal & ground	DC-8 GHz	0.75 - 5W	1 - 12
PCAAW Wrap around ground	DC-18 GHz	0.75 - 4W	0 - 20
PCAA No wrap	DC-18 GHz	0.75 - 5W	1 - 8
PCAL Tabbed	DC-12.4 GHz	1.5W	1, 3, 12
PCAF Wrap around terminal & ground	DC-4 GHz	1.5W	0 - 5

Model	Frequency	Power	DB Values in Stock
18A - SMA *Hex connector available	DC-18 GHz	2W	0 - 40
40A – 2.9mm *Hex connector available	DC-40 GHz	0.5W	2, 11, 30
53 – Type N Conduction/ Convection Cooled	DC-2.5Gz	500W	3, 20, 30
50EH – 2.4mm (Hex)	DC-50 GHz	0.5W	3, 10, 30
86 – 3.5mm Conduction Cooled/ Bi-directional	DC-22 GHz	50W	3, 6, 10

Quick Links To In-Stock Attenuators

spectrumcontrol.com/rfmw-att

SPECTRUM CONTROL™

RFMW®

Online Panel

March 4

Chiplets and 3D Heterogenous Integration

This panel of experts will discuss the challenges of advanced packaging technologies such as Chiplets and 3D Heterogenous Integration including integration, stacking, signal integrity and thermal concerns. The group will discuss simulation, testing and performance advantages of these approaches.

WHITE PAPERS

Coilcraft **The Fundamentals of RF Inductors**

Pat Hindle talks with Andrea Goldsmith, President of Stony Brook University and 2025 IEEE Mildred Dresselhaus Medal Winner, about how her wireless communications insights have affected wireless technology, the future of communications and her vision/strategy leading Stony Brook University into a new era.

https://podcasts.microwavejournal.com/category/industry-icons

Jason Cohenour, retired former CEO of Sierra Wireless, shares his story of transforming Sierra Wireless from a data card designer and supplier to the leading IoT and device-to-cloud solutions provider.

Executive Interview

Join Us Online

Follow us @Pathindle @MWJEditor

Join us at the RF and Microwave Community

Become a fan at facebook.com/microwavejournal

Catch *Frequency Matters*, the industry update from *Microwave Journal*, microwavejournal.com/FrequencyMatters

Visit us @ mwjournal.com

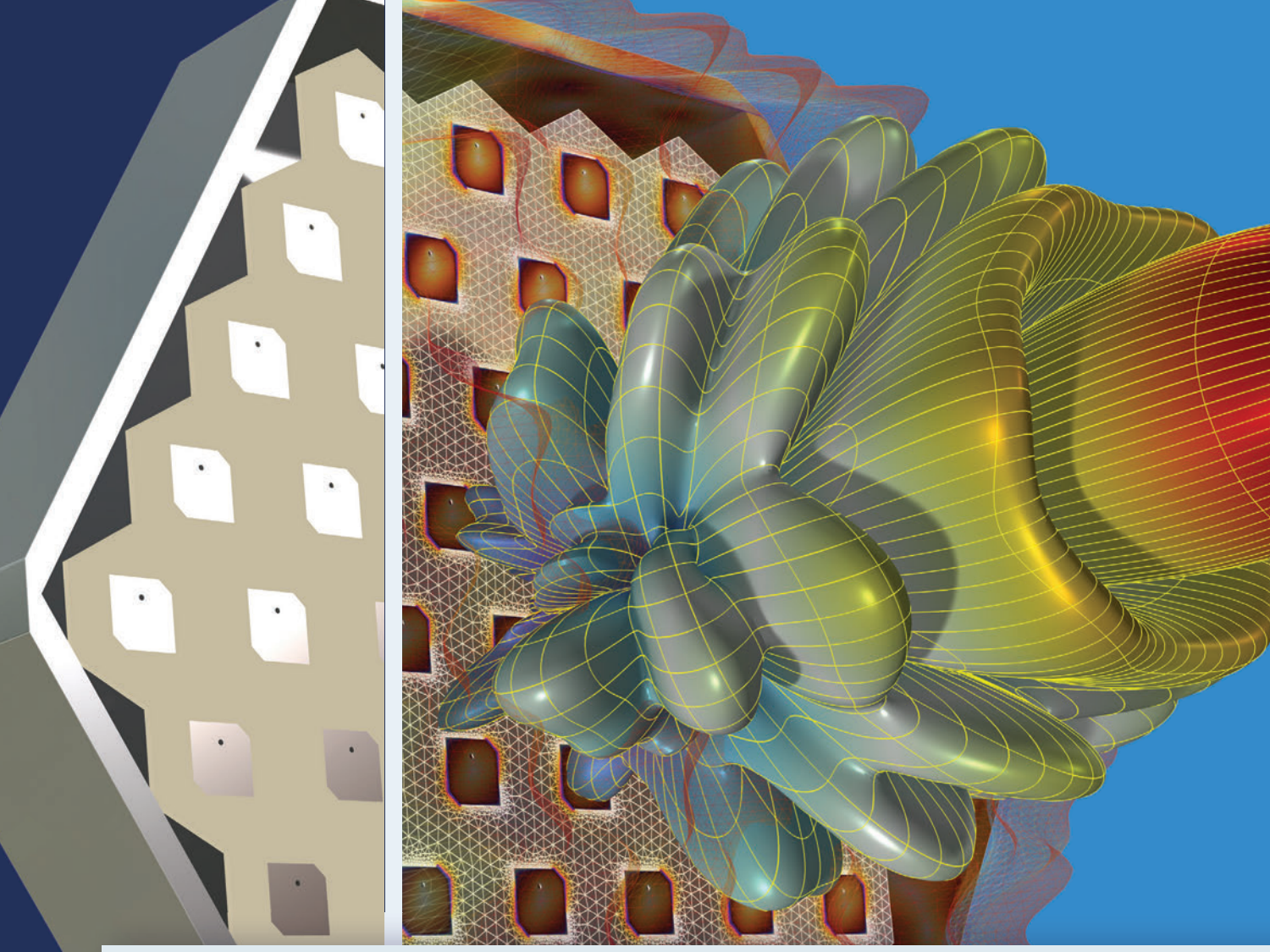

Take the Lead in RF Design

with COMSOL Multiphysics®

Multiphysics simulation is expanding the scope of RF analysis to higher frequencies and data rates. Accurate models of microwave, mmWave, and photonic designs are obtained by accounting for coupled physics effects, material property variation, and geometry deformation. Ultimately, this helps you more quickly see how a design will perform in the real world.

» *comsol.com/feature/rf-innovation*

COMSOL

LOVE AT FIRST SPEC

Not Flowers

When Compatibility Really Matters, Choose the Perfect Cable

LEARN MORE

Key Features

- 400+ models in stock (custom lengths & configurations available)
- Cable construction options from jumpers to VNA cables & more
- Wide range of connector types, genders, orientations and mounts
- Rugged construction for high reliability & long life

Mini-Circuits

MARK YOUR CALENDAR

STAY CONNECTED TO COMING EVENTS

FEBRUARY

24-26
DesignCon
Santa Clara, Calif.
www.designcon.com

MARCH

2-5
MWC Barcelona
Fira Gran Via, Barcelona
www.mwcbarcelona.com

9-11
German Microwave Conference
Karlsruhe, Germany
www.gemic2026.kit.edu

23-26
Satellite x GovMilSpace
Washington DC
www.SATShow.com

24-26
EMV
Cologne, Germany
https://emv.mesago.com

APRIL

13-16
IEEE WCNC
Kuala Lumpur, Malaysia
https://wcnc2026.ieee-wcnc.org

19-24
EuCAP
Dublin, Ireland
www.eucap2026.org

20-21
IEEE WAMICON
Clearwater, Fla.
www.ieeewamicon.org

20-22
IC-MAM
Barcelona, Spain
https://icmam-ieee.org

20-22
CS International
Brussels, Belgium
https://csinternational.net

20-22
PIC International
Brussels, Belgium
https://picinternational.net

MAY

18-21
CS Mantech
Portland, Ore.
https://csmantech.org

JUNE

16-18
Annual Microwave Power Symposium (IMPI)
New Orleans, La.
https://impi.org/events/symposium/

Call for Papers Deadlines

3/27
EuMW

5/1
IEEE RFID-TA 2026

FOR DETAILS VISIT MWJOURNAL.COM/EVENTS

Q/V-Band Frequency Converters for Next-Generation Satcom Systems

Korkut Yegin and Paul Gouws
ETL Systems, Rickmansworth, U.K.

INTRODUCTION

Next-generation satellite communication (satcom) systems targeting data rates in excess of Tb/s, such as ViaSat 3, are expected to replace traditional, aging broadband systems. High-throughput satellite (HTS) and very high-throughput satellite (VHTS) systems operating at multiple Ka-, Q- and V-Bands are gaining popularity in practical realisation of such data rates, which were perceived as almost impossible to achieve in commercial applications not long ago.[1-3] These new generation satellite systems are deemed vital to a diverse range of applications from mega-constellation LEOs, future MEOs and high-altitude platforms to unmanned aerial vehicles, drones and cellular backhaul.

The effective use of the Q- and V-Bands has the potential to double the total satellite bandwidth available. The Q/V spectrum is currently sparsely populated, and physically smaller antenna sizes offer many advantages, including reduced mass in satellite hardware. Narrower beam widths allow reduced satellite spacing and a denser constellation. Q/V-Band feeder links reduce the number of gateways required to support system capacity and free up spectrum allocated to Ka-Band gateways, which can be used for user links, as illustrated in ***Figure 1***.

The main drawbacks of the Q/V satellite system are the increased propagation and atmospheric losses compared to Ka-Band counterparts and less mature technology in the choice of high frequency components such as amplifiers, mixers, filters and passive components, which inevitably increase the cost of these converters. These are the main reasons that Q/V-Band implementation of satcom is currently limited to gateways and satellites rather than to direct users.

In a typical uplink to satellite scenario, the V-Band frequency converter is utilized after the modem and before the high power amplifier (HPA), as illustrated in ***Figure 2***. The output power of the V-Band frequency converter itself would be too low to overcome the signal path loss, which is mostly composed of propagation loss, atmospheric loss, depolarization due to Faraday rotation and ionospheric scintillation. Although pencil-beam high gain antennas are employed at the ground station terminals, there is still a need for an HPA to establish seamless communication between the ground station and the satellite. Furthermore, most modems have data ports through fibre or Ethernet, which makes them more suited for indoor units where they can be managed effectively. HPAs, on the other hand, need to be close to the antenna or to the antenna control room to minimize losses and electromagnetic shielding. As signal loss increases with frequency, it becomes necessary to co-locate the frequency converter and HPA as close to one another as practical, and likewise HPA to the antenna feed as possible.

The RF characteristics of HPAs

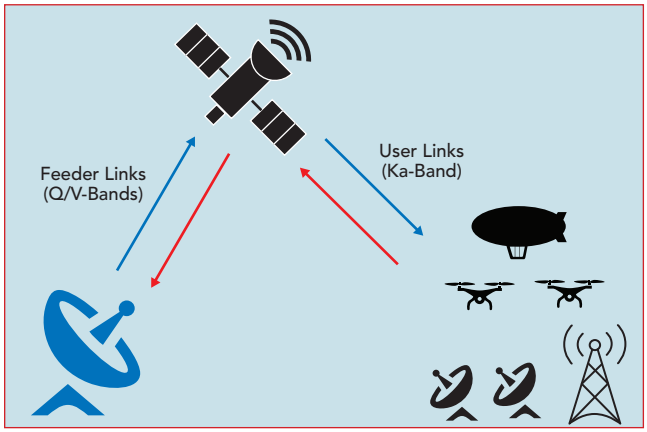

Fig. 1 **Typical application scenario.**

The only QPL Certified **MECHANICAL SWITCH** House!

Quick Turn **RF FILTER** Prototypes are in our DNA!

Huge Library of **PASSIVES** with Best in Show **HIGH POWER COUPLER** offering!

RUGGED & RELIABLE

AGILE & ADAPTIVE

HIGH POWER & VARIETY

RF MECHANICAL SWITCHES, RF FILTERS & RF PASSIVES

AS9100 CERTIFIED, MADE IN USA

High Performance Precision Microwave Components
Serving the world-wide aerospace & defense community since 1959

Robust Catalog Portfolio - no hassle, quick turn, custom solutions our specialty

RLC Electronics | 83 Radio Circle, Mt. Kisco, NY 10549 | 914-241-1334 | sales@rlcelectronics.com | www.rlcelectronics.com

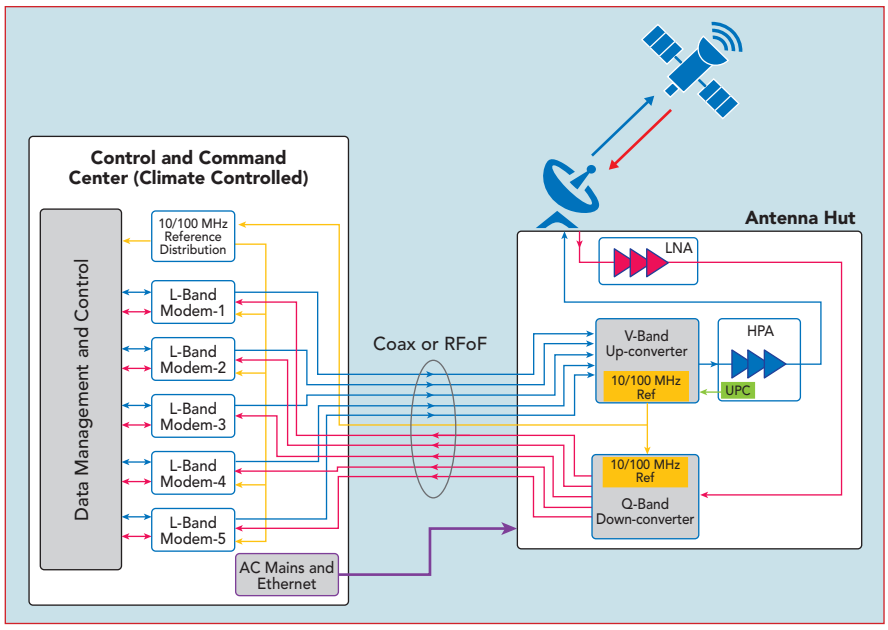

Fig. 2 **Satellite link configuration for Q/V-Band satcom.**

are also different than modems as their linearity, group delay and efficiency depend on the levels of input and output signal and their physical operational environment. Thus, an up-converter not only translates the L-Band modem frequency to V-Band but also serves as an intermediary to maintain the linearity requirements of both modem and HPA while providing adequate gain to overcome the loss between the two ends of the communication link.

The downlink scenario of the communication link resembles that of the up-converter for most traditional and legacy satcom systems. However, with the usage of spot-beams, satellite frequency reuse and polarization diversity of traditional bent-pipe architectures have been replaced with more complicated systems, where software-defined radio architectures gained increased popularity with adaptive and reconfigurable frequency translation and signal routing. Thus, the downlink signal bandwidth, data rate and signal modulation can dynamically change, which must be accounted for at the down-converter. Unlike HPAs, the low noise amplifiers (LNAs) are more standard, and the noise figure, linearity and signal distortion requirements are well known to affect the system performance within a predefined signal bandwidth. However, traditional LNAs aim to minimize noise figure and maximize gain over a narrow bandwidth, tuned to be reconsidered for wideband systems, where gain variation should be corrected before the HPA. The distortion added to the received satellite signal should be minimal at the frequency conversion stage, namely at the down-converter. Thus, the linearity requirement of the Q-Band down-converter is expected to be considerably better than that of a typical Ku-Band down-converter.

To describe multiple modems connected to a V-Band up-converter, the term multi-channel is often used in product specifications. In strict terms, a communication channel refers to a physical transmission medium such as wire, fibre or radio in the context of telecommunications. However, in broadcasting terminology, a channel is usually referred to as a data stream within the transmission or reception bandwidth. Thus, a bandwidth can be divided into sub-bands, where each sub-band is called a channel. This can be regarded as the classical definition of channel, which is somewhat different than its modern usage, where multiple access sys-

4,500+ COTS

High-Reliability Components & IMAs for Mission-Critical Applications

PMI
PLANAR MONOLITHICS

- Select from over 4,500+ available RF, Microwave, mmWave products online
- Eliminate Non-Recurring Engineering Fees (NRE), long lead times, and reduce your inventory burden
- Orders shipped same day
- Check stock easily using the "Buy Now" Button on the PMI website product specification sheets or select from the available "Stock Items"
- Industry-leading customer & applications support


Solid State Amplifiers


Attenuators


Detector Logarithmic Video Amplifiers


Filters


Frequency Converters


Frequency Discriminators & IFM


Frequency Sources


IQ Vector Modulators


Limiters


Phase Shifters & Bi-Phase Modulators


Solid State Switches


Detectors


Mixers & Active Mixers


Gain & Loss Equalizers


Integrated Microwave Assemblies (IMAs)


Isolators & Circulators


Monopulse Comparators


Power Dividers/ Combiners


Receiver Front Ends & Transceivers


Switch Filter Banks

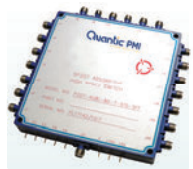
Switch Matrices


SMT & QFN Products


Couplers (90°, 180°, & Directional)


USB Products

Get a complete list of our components, integrated module portfolio, and available options, download product features and other technical data at **pmi-rf.com**

Or contact us at **1-877-752-6271** or **sales@pmi-rf.com**

SATELLITE x GovMilSpace

Visit us March 23 - 26, Booth #1726
satshow.com

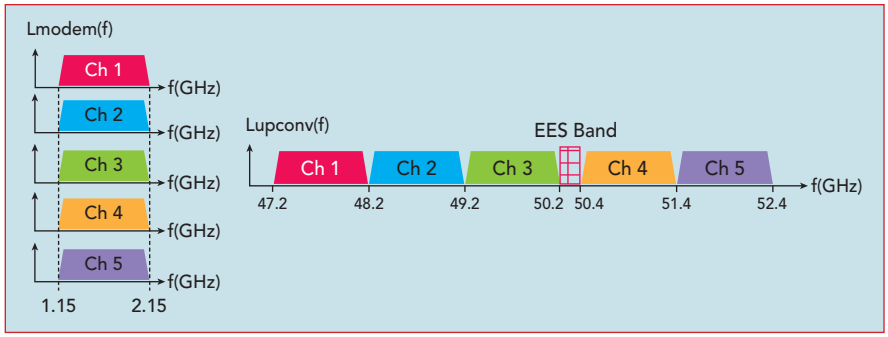

Fig. 3 L-Band translation of input bands to V-Band.

tems, such as code-division or time-division, utilize the entire bandwidth for all user channels to increase the capacity and data rate. L-Band modems shown in Figure 2 are combined to form a wideband signal that has been translated to V-Band and transmitted to the satellite (see ***Figure 3***). In classical frequency division systems, the channels are separated by guard bands to minimize inter-channel interference and leakage. Adjacent channel power ratio (ACPR) is usually a very strict parameter that directly impacts the system performance. In the satellite broadcasting industry, the distribution of channels within a given satellite bandwidth is usually controlled by the satellite operators and system engineers. Unlike a typical wireless link, where there is no or minimal control over the source frequency and information, satellite operators can define modem output frequencies for minimal interference. Satellite system operators are usually experts in link configuration and would rather control the frequency distribution of combined signals than reduce the expensive bandwidth for fixed channel separation. In a typical wireless system, usually 10 percent of the bandwidth from each end, which amounts to 20 percent of the allocated bandwidth, would be reserved for guard bandwidth, which translates to almost 200 MHz of unused bandwidth in satcom. With high peak-to-average ratio modulated signals, this guard band would be widened even further to maintain the same ACPR value. This allocation of bandwidth is deemed to be an underutilized resource in satellite broadcasting and communication. Therefore, edge-to-edge stacking up of L-Bands without leaving any guard band is possible with appropriate reservations in communication planning.

General specifications for frequency converters are outlined next. Critical converter features that impact Q/V-Band frequency converters, such as isolation, phase noise and group delay, are also detailed in subsequent sections.

GENERAL SYSTEM SPECIFICATIONS

Single or multi-channel L-Band signals can be translated to V-Band

RapidRF

World's 1st AI Driven RFIC DESIGN PLATFORM

A PUSH-BUTTON GDS TAPE-OUT READY SOLUTION

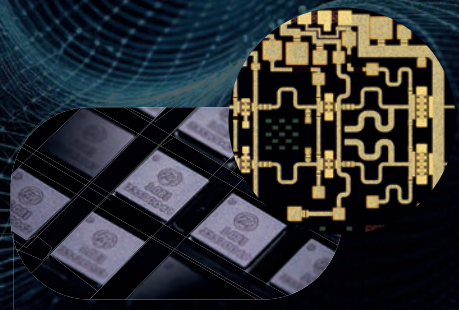

END APPLICATIONS CUSTOMERS

PERFORMANCE-DRIVEN FOCUS
EXPANDED DESIGN CHOICES
ENHANCED SECURITY AND CONFIDENTIALITY
REDUCED DEPENDENCE ON IC VENDORS
SIGNIFICANT COST SAVINGS

SEMICONDUCTOR COMPANIES

HUGE DESIGN COST REDUCTION
TAILORED TO CUSTOMER NEEDS
100X, 1000X FASTER
SUCCESSFUL RATE INCREASE

RapidRF

TRULY ENABLES A "DIRECT INTERACTION" MODEL FOR THE RFIC INDUSTRY ACROSS EVERY SECTOR.

FOUNDRIES

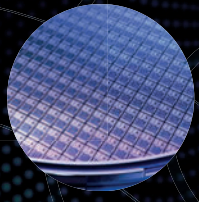

HIGHER REVENUE GREATER DESIGN VOLUME
EXPANDED CUSTOMER BASE LOWERING DESIGN ENTRY BARRIERS
ACCELERATED PRODUCT ITERATION

SIMPLE 3 STEPS

- LOGIN WWW.RAPIDRF.AI
- ENTER DESIGN TARGET
- PRESS "GENERATE"

A TAPE-OUT-READY GDS FILE WILL BE GENERATED AND **AVAILABLE FOR DOWNLOAD.**

TABLE 1
SYSTEM SPECIFICATIONS OF Q/V-BAND FREQUENCY CONVERTERS

	V-Band Up-converter	*Q-Band Down-converter*
Input Frequency (GHz)	1.15 - 2.15	37.5 - 42.5
Output Frequency (GHz)	47.2 - 52.4	1.15 - 2.15
Number of Channels	5	5
Gain Flatness (dB) over 5 GHz over 1 GHz Channel any 40 MHz (in Channel)	 +/- 1.5 +/- 1.0 +/- 0.3	 +/- 1.5 +/- 1.0 +/- 0.3
Mean Conversion Gain (dB)	30	30
Gain Control Range (dB)	0-30	0-30
Uplink Power Control (UPC) Programmable	Yes	N/A
Electronic Slope Equalizer (dB)	0-6	0-6
Noise Figure (dB)	16	14
OP1dB (dBm)	+5	+10
OIP3 (dB)	+15	+25
Input Return Loss	18	14
Output Return Loss	14	18
Spectral Inversion	Non-inverting	Non-inverting
In-band/Out-of-band Spur (dBc)	-60	-60
Phase Noise (dBc/Hz)	10 Hz Offset: -47 100 Hz Offset: -67 1 kHz Offset: -85 10 kHz Offset: -85 100 kHz Offset: -92 1 MHz Offset: -102	10 Hz Offset: -47 100 Hz Offset: -67 1 kHz Offset: -85 10 kHz Offset: -85 100 kHz Offset: -92 1 MHz Offset: -102
Group Delay Variation	3 ns (p-p)	3 ns (p-p)
External Reference (MHz)	10/100	10/100
Input/Output Connector	N / WR19	WR22 / N
Indoor/Outdoor	Outdoor	Outdoor

using either a single or dual conversion. Using legacy L-Band modems, a general dual-stage architecture can provide enough flexibility in system design and component selection. With the emergence of C-Band modems, a single channel with an excess of 2 GHz instantaneous bandwidth can also be considered. However, the limited availability of such modems precludes their widespread use in commercial markets at present.

The down-converter architecture is similar to that of the up-converter, but the RF specifications can be different. In the up-converter, the linearity of the wideband signal that is formed from L-Band signals is mostly dictated by the last stage V-Band section, whereas in the down-converter, this requirement is mostly transferred to the final L-Band output stage. The presence of an LNA at the front-end eases noise figure requirements of the down-converter and places greater emphasis on the linearity of subsequent sections.

General system specifications for up- and down-converters are summarized in ***Table 1***.

CHANNEL-TO-CHANNEL ISOLATION

Apart from in-band and out-of-band spurs, adjacent channel leakage at the input or output is also undesirable and must be kept as low as possible. A possible leakage scenario is illustrated in ***Figures 4*** and

Nxbeam

Ku/ Ka/ V/ E-Band Power Amplifier MMICs

Maximized performance for linear power applications

Ku/Ka-Band MMIC Die and Packaged MMICs

MMIC Die:

NPA1020-DE	12.5 - 14.5 GHz	15 W
NPA2020-DE	23.0 - 25.0 GHz	10 W
NPA2001-DE	26.5 - 29.5 GHz	35 W
NPA2002-DE	27.0 - 30.0 GHz	35 W
NPA2003-DE	27.5 - 31.0 GHz	35 W
NPA2004-DE	25.0 - 27.5 GHz	40 W
NPA2030-DE	27.5 - 31.0 GHz	20 W
NPA2040-DE	27.5 - 31.0 GHz	10 W

QFN Packaged MMICs:

NPQ2101-SM	27.5 - 31.0 GHz	5 W
NPQ2103-SM	27.5 - 31.0 GHz	8 W
NPQ2105-SM	27.5 - 31.0 GHz	12 W
NPQ2107-SM	27.5 - 31.0 GHz	17 W

Contact Nxbeam for Flange Packaged Options

V-Band MMICs

MMIC Die:

NPA4000-DE	47.0 - 52.0 GHz	1.5 W
NPA4010-DE	47.0 - 52.0 GHz	3.0 W

E-Band MMICs

MMIC Die:

NPA7000-DE	65.0 - 76.0 GHz	1.0 W

5, where Channel 2 is coupling to other channels. The coupled signal would appear at the input modem band of other channels for input-to-input coupling in Figure 4, where the conducted coupling must go through the combiner and reverse direction of the victim converter channel, which is usually much better than its forward gain. Thus, input-to-input coupling can be as low as -60 dBc. The out-to-out coupling is solely determined by the converter selectivity and combiner/splitter isolation between the channels. Since L-Band channels are stacked back-to-back, band edges shared by adjacent channels can only be isolated by the combiner isolation theoretically.

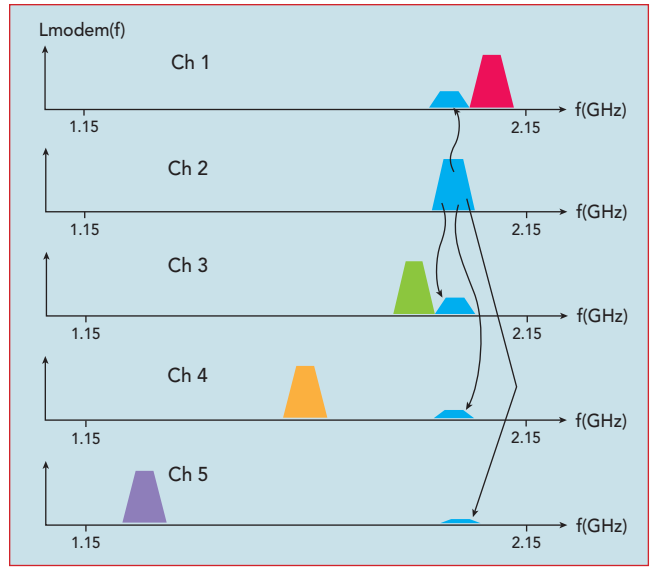

Fig. 4 **Channel 2 leakage to other channels (input-input coupling).**

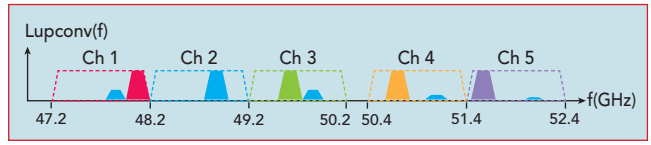

Fig. 5 **Channel 2 leakage in output spectrum.**

PHASE NOISE

Phase noise is one of the most critical metrics that impacts system performance. In a typical digital constellation, the relation between PN and error vector magnitude (EVM), as seen in ***Figure 6***, can be established. EVM can be expressed by ***Equation 1***:

$$EVM = \sqrt{\frac{\int [v_{ref}(t) - v_{meas}(t)]^2 dt}{\int [v_{ref}(t)]^2 dt}} \quad (1)$$

where v_{ref} (t) and v_{meas} (t) are expected and measured signals, respectively. For $|\varphi(t)|<<1$, the expression can be approximated by ***Equation 2***:

$$[E]^2 = 2R^2 - 2R^2\cos(\phi) \approx R^2\phi^2 \quad (2)$$

and EVM can be readily stated as seen in ***Equation 3***:

$$EVM \approx \phi_{rms} = 100\% \times \sqrt{2 \times \int L(f)\,df} \quad (3)$$

Therefore, the maximum EVM for a chosen digital modulation also sets the upper bound for maximum phase noise. Although this integrated phase noise is a critical factor, spurs in the phase noise spectrum can also lead to increased EVM and translation of unwanted signals into the band.

The IESS-308 Standard is often an adequate performance metric for Ku-Band systems.[4] The U.S. military, however, has been using slightly tighter phase noise specifications as outlined in MIL-STD-188-164C.[5-6] Both specifications are summarized in ***Table 2***.

In the up-converter module, a 36 GHz signal source is used to translate the intermediate band (IF) to V-Band. The phase noise of this signal would be the dominant contributor

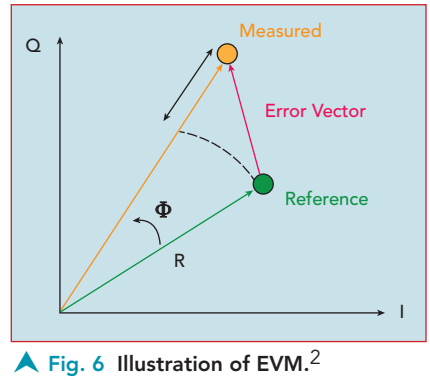

Fig. 6 **Illustration of EVM.**[2]

Proven Solutions
From Ground to Deep Space

- Commercial off-the-shelf rad tolerant parts
- Complex, large format RF/MW PCBs
- High power microwave solutions from L to Q-band
- RF/MW components, modules and integrated assemblies
- High speed IP modems with TRANSEC capability
- Ultra reliable switching solutions
- Microwave & high voltage ruggedized interconnects

Aerospace & Defense Electronics
TeledyneADE.com

TELEDYNE

to the up-converter phase noise. The signal is first generated using a synthesized source of 18 GHz, and with the help of a doubler, 36 GHz is obtained. The phase noise at 18 GHz is shown in ***Figure 7***.

The phase noise for the entire five-channel V-Band block up-converter is also measured, and its performance at the upper band edge, namely 52.4 GHz, is displayed in ***Figure 8***. Even at this extreme band edge, the unit easily satisfies IESS standards and performs very close to MIL standards.

GROUP DELAY

Group delay variation is also a critical metric in system design and link calibration. A waveguide filter at the final output of the V-Band up-converter and input of the Q-Band down-converter is needed to provide good rejection for out-of-band signals and spurs. This filter is built and measured, and its measured group delay response is shown in ***Figure 9***. Measured data are processed in AWR Microwave Office with other building blocks.

TABLE 2
COMMON PHASE NOISE STANDARDS

Offset Freq.	IESS-308 (dBc/Hz)	MIL-STD-188-164C (dBc/Hz)
10 Hz	-30	-32
100 Hz	-60	-62
1 kHz	-70	-72
10 kHz	-80	-82
100 kHz	-90	-92
1 MHz	-90	-102
10 MHz	-90	-102

CONCLUSION

Critical design aspects of wideband Q/V-Band frequency converters are discussed. Apart from legacy converter designs, the target 5 GHz conversion bandwidth has key design challenges in terms of in-band (channel-to-channel) leakage and spurs, low phase noise to accommodate higher modulation and coding and low group delay variation. To overcome these critical issues, the design is made flexible and scalable in terms of submodules that separate the final translation band from the L-Band and intermediate bands. That way, wider single-channel modems such as 2 GHz C-Band modems can also be utilized with the modification of submodules. The use of IF combiners/splitters permits such scalability.

Uplink power control (UPC) settable up-converters would be an essential part of these systems, as fade margins would be higher compared to Ka-Band counterparts. UPC based solely on beacon feedback in an open loop system is usually inferior to systems that employ an additional closed loop system based on a test-loop-translator of the pilot channel. In traditional systems, UPC is used to adjust HPA with a limited linearity range. When UPC is simultaneously utilized in the up-converter and HPA, the dynamic range or the linearity range of the satellite link can be enhanced.

RF-LAMBDA

MADE IN USA

THE LEADER OF RF BROADBAND SOLUTIONS

EMC Broadband RF Power Amplifier

High Power Solid State

HUNDREDS IN STOCK

FAST SHIPPING

FREQUENCY UP TO 90GHZ

POWER UP TO 2KW CW

BENCHTOP AND RACKMOUNT

REMC06G18GG 6-18GHZ 400W

- AUTOMATIC BUILT IN SELF CALIBRATION AND BIAS ADJUSTMENT.
- OVER TEMPERATURE, CURRENT, INPUT POWER PROTECTION.
- VSWR MEASUREMENT AND OPEN CIRCUIT PROTECTION.
- USER FRIENDLY CONTROL INTERFACE.
- REMOTE ETHERNET CONTROL AND FIRMWARE UPDATE.
- HIGH POWER EFFICIENCY AND LIGHTWEIGHT.

RAMP42G47GA 42-47GHZ 8W

RAMP18G40GB-U 18-40G 20W

RAMP05M80GC 0.5-80GHZ

REMC02G06GE 2-6GHZ 500W

REMC18G40GQ 18-40GHZ 200W CW

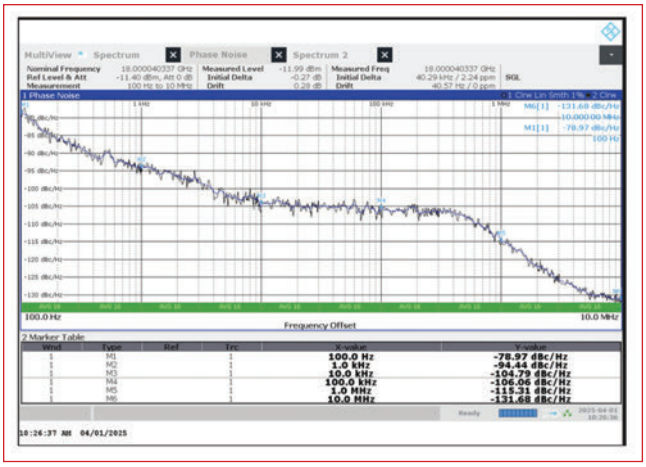

Fig. 7 **Measured phase noise at 18 GHz.**

Another important feature of these new generation converters is their ability to synchronize all other subcomponents in the satellite link to a common reference for minimum frequency translation error. With the emergence of software modems and digital IF products, not only frequency reference but also time reference through 1 pps GPS would become essential. Hence, these converters are expected to lock or derive their internal reference from GPS disciplined references and synchronize all internal sources to this common time reference to maintain commercial-grade target Tb/s high throughput rates. ■

ACKNOWLEDGEMENT

This work is partly funded by the European Space Agency under Contract No. 4000128210/19/NL/MM/ra.

References

1. H. Fenech, S. Amos, A. Tomatis and V. Soumpholphakdy, "High Throughput Satellite Systems: An Analytical Approach," *IEEE Transactions on Aerospace and Electronic Systems*, Vol. 51, No. 1, January 2015, pp. 192–202, doi: 10.1109/TAES.2014.130450.
2. K. Yegin, B.L. Brown and P.G. Gouws, "Phase Noise Modelling for Ka-Band VHTS Systems," *ARMMS Conference*, September 2023, pp. 1–6.
3. M. M. Bilgic and K. Yegin, "Low Profile Wideband Antenna Array With Hybrid Microstrip and Waveguide Feed Network for Ku Band Satellite Reception Systems," *IEEE Transactions on Antennas and Propagation*, Vol. 62, No. 4, April 2014, pp. 2258-2263, doi: 10.1109/TAP.2013.2297696.
4. "Digital Video Broadcasting (DVB); Second Generation Framing Structure, Channel Coding and Modulation Systems for Broadcasting, Interactive Services, News Gathering and other Broadband Satellite Applications; Part 1: DVB-S2, DVB-S2," ETSI EN 302 307-1 V1.4.1 (2014-11).
5. "Interoperability of Superhigh Frequency (SHF) Satellite Communications Phase-Shift Keying (PSK) Modems," *MIL-STD-188-165B*, March 26, 2018.
6. L. Gonzalez, J. Rippon and J. Besse, "Phase Noise, SATCOM and MIL-STD-188-165B," *IEEE Military Communications Conference (MILCOM)*, 2019, pp.13–16.

Fig. 8 **Measured phase noise at 52.4 GHz.**

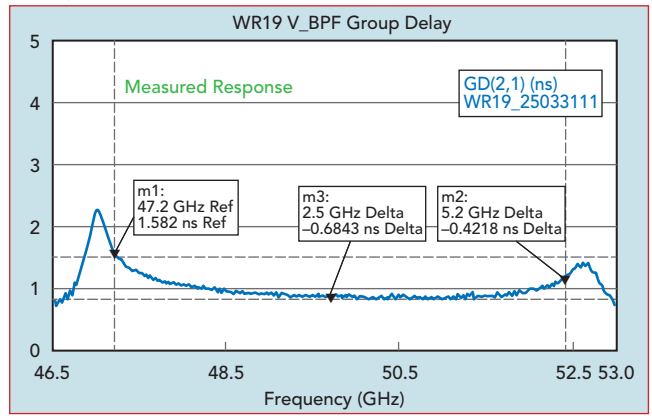

Fig. 9 **Measured group delay of waveguide filter at V-Band.**

ROHDE&SCHWARZ

Mastering the Orbit: Comprehensive NTN Testing with the CMX500

The CMX500 is the versatile solution designed for testing various NTN technologies.

The rise of non-terrestrial networks (NTN) leveraging satellites and high-altitude platforms promises ubiquitous connectivity, particularly for underserved areas, global IoT applications and emergency communications. As NTN matures alongside 5G and looks towards 6G, overcoming significant technical hurdles is key to realizing its potential. To address these hurdles, Rohde & Schwarz has upgraded its tried-and-tested CMX500 5G one-box signaling tester, supporting NR-NTN, NB-NTN and Direct-to-Cell (D2C/DTC) technologies in a single platform.

UNIQUE CHALLENGES OF NON-TERRESTRIAL NETWORKS

Unlike terrestrial networks, NTN introduces unique challenges due to the dynamic nature of satellite communication: LEO satellites move rapidly relative to ground-based UEs, creating constantly shifting radio environments characterized by Doppler frequency shifts, variable propagation delays and substantial path loss. This demands sophisticated channel emulation capable of accurately replicating real-world satellite conditions. Further complicating matter is the multi-orbit and multi-band nature of NTN. Services operate across LEO, MEO and GEO, each presenting unique handover, latency, and coverage considerations. NTNs also utilize diverse frequency bands, including sub-6 GHz and higher FR2, requiring Frequency Division Duplex (FDD) instead of the more common Time Division Duplex (TDD) used in terrestrial FR2 transmissions.

CRITICAL REQUIREMENTS FOR SEAMLESS NTN CONNECTIVITY

Seamless connectivity in NTNs relies on frequent and reliable handovers between satellite beams and between satellites themselves, a critical aspect for fast-moving LEO constellations with limited coverage areas. Effective handovers necessitate precise real-time ephemeris data, tracking satellite and UE positions, alongside interoperability with terrestrial network segments. Finally, testing requires simulating extended operational periods to account for complex handover scenarios triggered by factors like signal strength or distance.

A VERSATILE PLATFORM FOR NTN TESTING

The CMX500 supports two primary testing configurations: Full Satellite Access Network (SAN) emulation for device manufacturers, simulating the complete NTN architecture for comprehensive device testing, and gNB and 5G core network emulation for satellite network operators, validating satellite components against standards-compliant cellular technologies. The CMX500 platform creates a high-fidelity digital twin of the sky, simulating orbits, bands and impairments like Doppler shifts and fading. Key features include dedicated internal FPGAs for channel emulation and signaling, over-the-air testing capabilities using anechoic chambers and robotic arms for higher frequencies, and comprehensive RF and QoS testing via external IP networks.

Rohde & Schwarz also offers an **XLAPI Python Test Case package**, which includes a range of **Starlink LTE-DTC** test scenarios. These scenarios cover critical aspects such as LTE attach time and success rates in DTC mode, Event A3 handover, cell reselection between intra-frequency LTE DTC cells, and recovery after Radio Link Failure (RLF) on LTE DTC cells, among others. An AI-powered script generation tool (ScriptAssist) further supports users.

Enhancing the CMX500 is the **Constellation Insights Tool**, a software solution offering powerful management features for NTN testing. By allowing engineers to visualize satellite constellations, analyze coverage gaps and observe trajectories, it tackles complex aspects like mobility management, constellation behavior and long-duration simulations. It displays crucial fading parameters like path loss and Doppler shifts, providing a comprehensive view of link conditions.

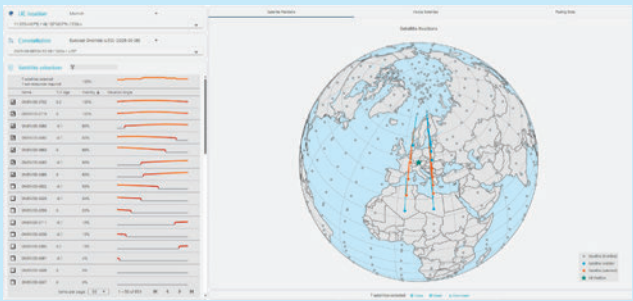

Configure and visualize a simulation period with the Constellation Insights Tool.

ENABLING THE FUTURE OF CONNECTIVITY

As 5G NTN evolves, advanced testing solutions like the CMX500 and the Constellation Insights Tool are vital for accelerating development, ensuring quality and guaranteeing the reliability of these transformative networks. The future of NTN connectivity is rapidly becoming a reality, driven by advancements in testing and simulation.

MWC GSMA BARCELONA 2 – 5 MARCH 2026

Visit Rohde & Schwarz at MWC Barcelona at booth 5A80 for a live demo of the CMX500: www.rohde-schwarz.com/mwc

Find out how the CMX500 can enable you to shape the future of NTN connectivity: www.rohde-schwarz.com/cmx-ntn

RF Amplifiers and Sub-Assemblies for Every Application

Delivery from Stock to 2 Weeks ARO from the catalog or built to your specifications!

- Competitive Pricing & Fast Delivery
- Military Reliability & Qualification
- Various Options: Temperature Compensation, Input Limiter Protection, Detectors/TTL & More
- Unconditionally Stable (100% tested)

ISO 9001:2000 and AS9100B CERTIFIED

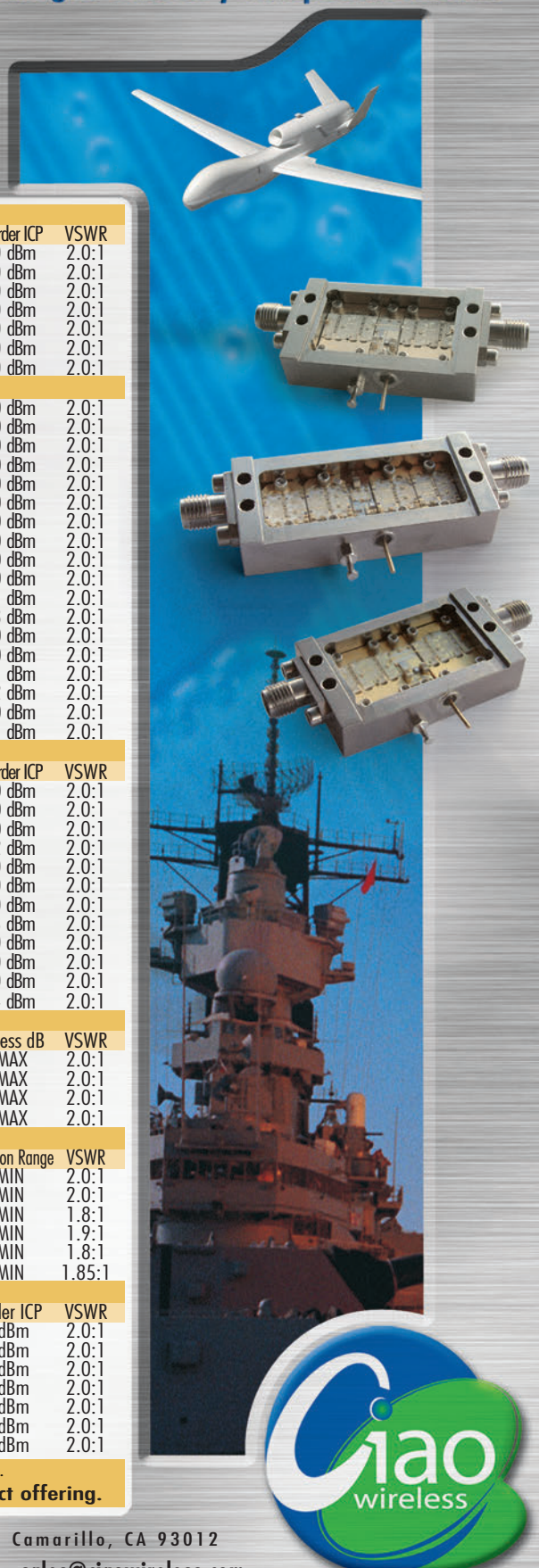

OCTAVE BAND LOW NOISE AMPLIFIERS

Model No.	Freq (GHz)	Gain (dB) MIN	Noise Figure (dB)	Power-out @ P1-dB	3rd Order ICP	VSWR
CA01-2110	0.5-1.0	28	1.0 MAX, 0.7 TYP	+10 MIN	+20 dBm	2.0:1
CA12-2110	1.0-2.0	30	1.0 MAX, 0.7 TYP	+10 MIN	+20 dBm	2.0:1
CA24-2111	2.0-4.0	29	1.1 MAX, 0.95 TYP	+10 MIN	+20 dBm	2.0:1
CA48-2111	4.0-8.0	29	1.3 MAX, 1.0 TYP	+10 MIN	+20 dBm	2.0:1
CA812-3111	8.0-12.0	27	1.6 MAX, 1.4 TYP	+10 MIN	+20 dBm	2.0:1
CA1218-4111	12.0-18.0	25	1.9 MAX, 1.7 TYP	+10 MIN	+20 dBm	2.0:1
CA1826-2110	18.0-26.5	32	3.0 MAX, 2.5 TYP	+10 MIN	+20 dBm	2.0:1

NARROW BAND LOW NOISE AND MEDIUM POWER AMPLIFIERS

Model No.	Freq (GHz)	Gain (dB) MIN	Noise Figure (dB)	Power-out @ P1-dB	3rd Order ICP	VSWR
CA01-2111	0.4 - 0.5	28	0.6 MAX, 0.4 TYP	+10 MIN	+20 dBm	2.0:1
CA01-2113	0.8 - 1.0	28	0.6 MAX, 0.4 TYP	+10 MIN	+20 dBm	2.0:1
CA12-3117	1.2 - 1.6	25	0.6 MAX, 0.4 TYP	+10 MIN	+20 dBm	2.0:1
CA23-3111	2.2 - 2.4	30	0.6 MAX, 0.45 TYP	+10 MIN	+20 dBm	2.0:1
CA23-3116	2.7 - 2.9	29	0.7 MAX, 0.5 TYP	+10 MIN	+20 dBm	2.0:1
CA34-2110	3.7 - 4.2	28	1.0 MAX, 0.5 TYP	+10 MIN	+20 dBm	2.0:1
CA56-3110	5.4 - 5.9	40	1.0 MAX, 0.5 TYP	+10 MIN	+20 dBm	2.0:1
CA78-4110	7.25 - 7.75	32	1.2 MAX, 1.0 TYP	+10 MIN	+20 dBm	2.0:1
CA910-3110	9.0 - 10.6	25	1.4 MAX, 1.2 TYP	+10 MIN	+20 dBm	2.0:1
CA1315-3110	13.75 - 15.4	25	1.6 MAX, 1.4 TYP	+10 MIN	+20 dBm	2.0:1
CA12-3114	1.35 - 1.85	30	4.0 MAX, 3.0 TYP	+33 MIN	+41 dBm	2.0:1
CA34-6116	3.1 - 3.5	40	4.5 MAX, 3.5 TYP	+35 MIN	+43 dBm	2.0:1
CA56-5114	5.9 - 6.4	30	5.0 MAX, 4.0 TYP	+30 MIN	+40 dBm	2.0:1
CA812-6115	8.0 - 12.0	30	4.5 MAX, 3.5 TYP	+30 MIN	+40 dBm	2.0:1
CA812-6116	8.0 - 12.0	30	5.0 MAX, 4.0 TYP	+33 MIN	+41 dBm	2.0:1
CA1213-7110	12.2 - 13.25	28	6.0 MAX, 5.5 TYP	+33 MIN	+42 dBm	2.0:1
CA1415-7110	14.0 - 15.0	30	5.0 MAX, 4.0 TYP	+30 MIN	+40 dBm	2.0:1
CA1722-4110	17.0 - 22.0	25	3.5 MAX, 2.8 TYP	+21 MIN	+31 dBm	2.0:1

ULTRA-BROADBAND & MULTI-OCTAVE BAND AMPLIFIERS

Model No.	Freq (GHz)	Gain (dB) MIN	Noise Figure (dB)	Power-out @ P1-dB	3rd Order ICP	VSWR
CA0102-3111	0.1-2.0	28	1.6 Max, 1.2 TYP	+10 MIN	+20 dBm	2.0:1
CA0106-3111	0.1-6.0	28	1.9 Max, 1.5 TYP	+10 MIN	+20 dBm	2.0:1
CA0108-3110	0.1-8.0	26	2.2 Max, 1.8 TYP	+10 MIN	+20 dBm	2.0:1
CA0108-4112	0.1-8.0	32	3.0 MAX, 1.8 TYP	+22 MIN	+32 dBm	2.0:1
CA02-3112	0.5-2.0	36	4.5 MAX, 2.5 TYP	+30 MIN	+40 dBm	2.0:1
CA26-3110	2.0-6.0	26	2.0 MAX, 1.5 TYP	+10 MIN	+20 dBm	2.0:1
CA26-4114	2.0-6.0	22	5.0 MAX, 3.5 TYP	+30 MIN	+40 dBm	2.0:1
CA618-4112	6.0-18.0	25	5.0 MAX, 3.5 TYP	+23 MIN	+33 dBm	2.0:1
CA618-6114	6.0-18.0	35	5.0 MAX, 3.5 TYP	+30 MIN	+40 dBm	2.0:1
CA218-4116	2.0-18.0	30	3.5 MAX, 2.8 TYP	+10 MIN	+20 dBm	2.0:1
CA218-4110	2.0-18.0	30	5.0 MAX, 3.5 TYP	+20 MIN	+30 dBm	2.0:1
CA218-4112	2.0-18.0	29	5.0 MAX, 3.5 TYP	+24 MIN	+34 dBm	2.0:1

LIMITING AMPLIFIERS

Model No.	Freq (GHz)	Input Dynamic Range	Output Power Range Psat	Power Flatness dB	VSWR
CLA24-4001	2.0 - 4.0	-28 to +10 dBm	+7 to +11 dBm	+/- 1.5 MAX	2.0:1
CLA26-8001	2.0 - 6.0	-50 to +20 dBm	+14 to +18 dBm	+/- 1.5 MAX	2.0:1
CLA712-5001	7.0 - 12.4	-21 to +10 dBm	+14 to +19 dBm	+/- 1.5 MAX	2.0:1
CLA618-1201	6.0 - 18.0	-50 to +20 dBm	+14 to +19 dBm	+/- 1.5 MAX	2.0:1

AMPLIFIERS WITH INTEGRATED GAIN ATTENUATION

Model No.	Freq (GHz)	Gain (dB) MIN	Noise Figure (dB)	Power-out @ P1-dB	Gain Attenuation Range	VSWR
CA001-2511A	0.025-0.150	21	5.0 MAX, 3.5 TYP	+12 MIN	30 dB MIN	2.0:1
CA05-3110A	0.5-5.5	23	2.5 MAX, 1.5 TYP	+18 MIN	20 dB MIN	2.0:1
CA56-3110A	5.85-6.425	28	2.5 MAX, 1.5 TYP	+16 MIN	22 dB MIN	1.8:1
CA612-4110A	6.0-12.0	24	2.5 MAX, 1.5 TYP	+12 MIN	15 dB MIN	1.9:1
CA1315-4110A	13.75-15.4	25	2.2 MAX, 1.6 TYP	+16 MIN	20 dB MIN	1.8:1
CA1518-4110A	15.0-18.0	30	3.0 MAX, 2.0 TYP	+18 MIN	20 dB MIN	1.85:1

LOW FREQUENCY AMPLIFIERS

Model No.	Freq (GHz)	Gain (dB) MIN	Noise Figure dB	Power-out @ P1-dB	3rd Order ICP	VSWR
CA001-2110	0.01-0.10	18	4.0 MAX, 2.2 TYP	+10 MIN	+20 dBm	2.0:1
CA001-2211	0.04-0.15	24	3.5 MAX, 2.2 TYP	+13 MIN	+23 dBm	2.0:1
CA001-2215	0.04-0.15	23	4.0 MAX, 2.2 TYP	+23 MIN	+33 dBm	2.0:1
CA001-3113	0.01-1.0	28	4.0 MAX, 2.8 TYP	+17 MIN	+27 dBm	2.0:1
CA002-3114	0.01-2.0	27	4.0 MAX, 2.8 TYP	+20 MIN	+30 dBm	2.0:1
CA003-3116	0.01-3.0	18	4.0 MAX, 2.8 TYP	+25 MIN	+35 dBm	2.0:1
CA004-3112	0.01-4.0	32	4.0 MAX, 2.8 TYP	+15 MIN	+25 dBm	2.0:1

CIAO Wireless can easily modify any of its standard models to meet your "exact" requirements at the Catalog Pricing.

Visit our web site at **www.ciaowireless.com** for our complete product offering.

Ciao Wireless, Inc. 4000 Via Pescador, Camarillo, CA 93012

Tel (805) 389-3224 Fax (805) 389-3629 sales@ciaowireless.com

Boeing Delivers B-52 with New Radar to USAF for Testing

Boeing has delivered the first B-52 Radar Modernization Program (RMP) flight test aircraft to the U.S. Air Force for testing with the 412th Test Wing at Edwards Air Force Base in California. The test aircraft was fitted with an APQ-188 active electronically scanned array radar system that is akin to those on fighter aircraft.

The RMP upgrades are a critical part of the B-52's broader modernization efforts that will keep U.S. global strike capability ahead of threats through the 2050 and beyond. The testing at Edwards AFB follows ground integration and initial system functional checks completed at Boeing's San Antonio facility.

"The new radar will significantly increase B-52 mission effectiveness by improving situational awareness, speeding target prosecution and enhancing aircrew survivability in contested environments," said Troy Dawson, vice president of Boeing Bombers. "This phase of the program is dedicated to getting it right at the start so that we can execute the full radar modernization program."

B-52 (Source: Boeing)

Data gathered during testing will inform subsequent developmental test phases and the planned retrofit of the 76 operational B-52 aircraft.

RMP also includes two Display and System Sensor Processors as its mission computers to integrate the radar with B-52 systems, along with two large 8×20 in. high-definition touchscreens at the Nav and Radar Nav stations for radar imagery, control and legacy displays and two fighter-like hand controllers for radar operation. The system features upgraded cooling, providing liquid cooling for the radar and engine bleed-air heating for very cold conditions.

Viasat Introduces Next-Gen Global Ka-Band Network to Support Resilient Government Satcom

Viasat Inc. announced a significant evolution of its network for government customers by unifying Viasat Ka-Band satellites, the Global Xpress satellite fleet and select partner satellites into a fully integrated global Ka-Band satcom network. Fully interoperable with MILSATCOM Ka-Band networks, this evolved Ka-Band network capability will provide seamless global, multi-orbit Ka-Band connectivity for government and military users, offering increased performance, expanded coverage and greater resiliency for missions across air, land and sea.

Leveraging an integrated waveform, upgraded gateways and common ground architecture, Viasat's expanded global Ka-Band connectivity for government will enable customers to seamlessly roam between Ka-Band satellite networks, including Viasat satellites, Global Xpress Ka-Band satellites (part of Viasat's global fleet following the acquisition of Inmarsat in 2023) and other commercial and government Ka-Band satellites. Moving forward, government users operating across domains will be able to access this evolved Ka-Band network through upgraded, single terminal solutions rather than needing multiple hardware solutions.

Supports High Speed, Resilient Multi-Network Connectivity for Multi-Domain Mission Operations

Viasat's integrated Ka-Band network will offer government users ubiquitous roaming and faster connectivity, with data rates up to 200 Mbps with a 45 cm or equivalent antenna, and it features electronically and mechanically steered beams that offer the flexibility to dynamically allocate bandwidth and deliver dedicated secure connectivity for mobile government platforms. The unified Ka-Band network will incorporate the ultra-high-capacity ViaSat-3 satellites, each designed to move significant bandwidth to meet real-time demand in high-concentration areas. The recently launched ViaSat-3 F2 satellite will provide additional resilience for the Americas and the ViaSat-3 F3 satellite is planned to deliver coverage over the Asia-Pacific region.

Viasat's global network is designed to support national security and mission operations in contested environments, including dedicated Mil-Ka access and specific features built-in for increased resilience against threats attempting jamming, interference and denial attacks to disrupt communications. Viasat's integrated Ka-Band network is part of Viasat's global, multi-orbit network roadmap, helping Viasat further deliver resilient and secure connectivity with the flexibility to meet different customer and mission needs.

With abundant bandwidth capacity and redundant layers across the unified network, Viasat government satcom, part of communication services, offers customers scalable service models that enable multi-mission flexibility for entire military fleets, including dedicated beams that provide sovereign control and predictable performance.

For More Information

Visit mwjournal.com for more defense news.

SAMP/T NG: Thales Contributes to the Success of the European Air Defense System's Firing Campaign

On Monday, December 15, 2025, the first test firing of the French version of the SAMP/T NG system was successfully performed from the DGA Essais de Missiles test range in Biscarosse (Nouvelle-Aquitaine region). Each system features a Thales Ground Fire radar with a performance range of up to 400 km and panoramic coverage at 360 degrees and 90 degrees elevation. The Ground Fire radar, which has been in series production since the beginning of 2025, was demonstrated during this firing of the French version of the SAMP/T NG system.

This firing campaign has once again demonstrated the high level of performance of this long-range air defense system developed by Eurosam, a joint venture between Thales and MBDA. After a successful first firing in Italy on December 3, 2025, this new firing in France demonstrated the innovations and performance of the SAMP/T NG fire control system with its new modernized Engagement Module when coupled with the Thales Ground Fire radar.

Based on fully digital active electronically scanned antennas technology, the Ground Fire radar provides a very high level of performance for the detection, tracking and classification of all types of targets in the most difficult environments (sea, mountains, intense traffic density, jamming, etc.). This multifunction radar features a refresh rate of only 1 second and a surveillance capacity of up to 400 km, with panoramic coverage at 360- and 90-degree elevations. It is capable of simultaneously detecting drones, fighter jets and ballistic missiles while benefiting from the mobility of a tactical radar.

SAMP/T NG (Source: DGA Essais de Missiles)

This success is a further step toward the operational deployment of the SAMP/T NG system in France and Italy, with the first deliveries scheduled for 2026.

The SAMP/T NG system has thus established itself as the only European alternative for medium- and long-range protection against all types of threats, including ballistic, maneuvering and saturating threats.

The SAMP/T NG program is supervised by the Organisation Conjoint de Coopération en matière d'Armement (OCCAR). Eurosam, a joint venture between Thales and MBDA, is the prime contractor for the entire system.

Reactel, Inc.

Reacting First to All Your Filter Needs.

Filter Solutions For Mission Critical Applications

High Performance, Rugged Packaging, Small Size and Weight

Great things *can* come in small packages. Reactel filters are ideally suited for the demanding environments that unmanned vehicles encounter.

Many manufacturers rely on Reactel to provide units which are:
High performance - Lightweight - Low profile

Contact a Reactel engineer with your filter or multiplexer requirements. We can create a unit which will be the perfect fit for your applications.

RF & Microwave Filters - Multiplexers - Multifunction Assemblies

8031 Cessna Avenue • Gaithersburg, Maryland 20879 • (301) 519-3660 • reactel@reactel.com • reactel.com

Intertek

RoHS Compliant 2002/95/EC

MADE IN MD
Since 1979

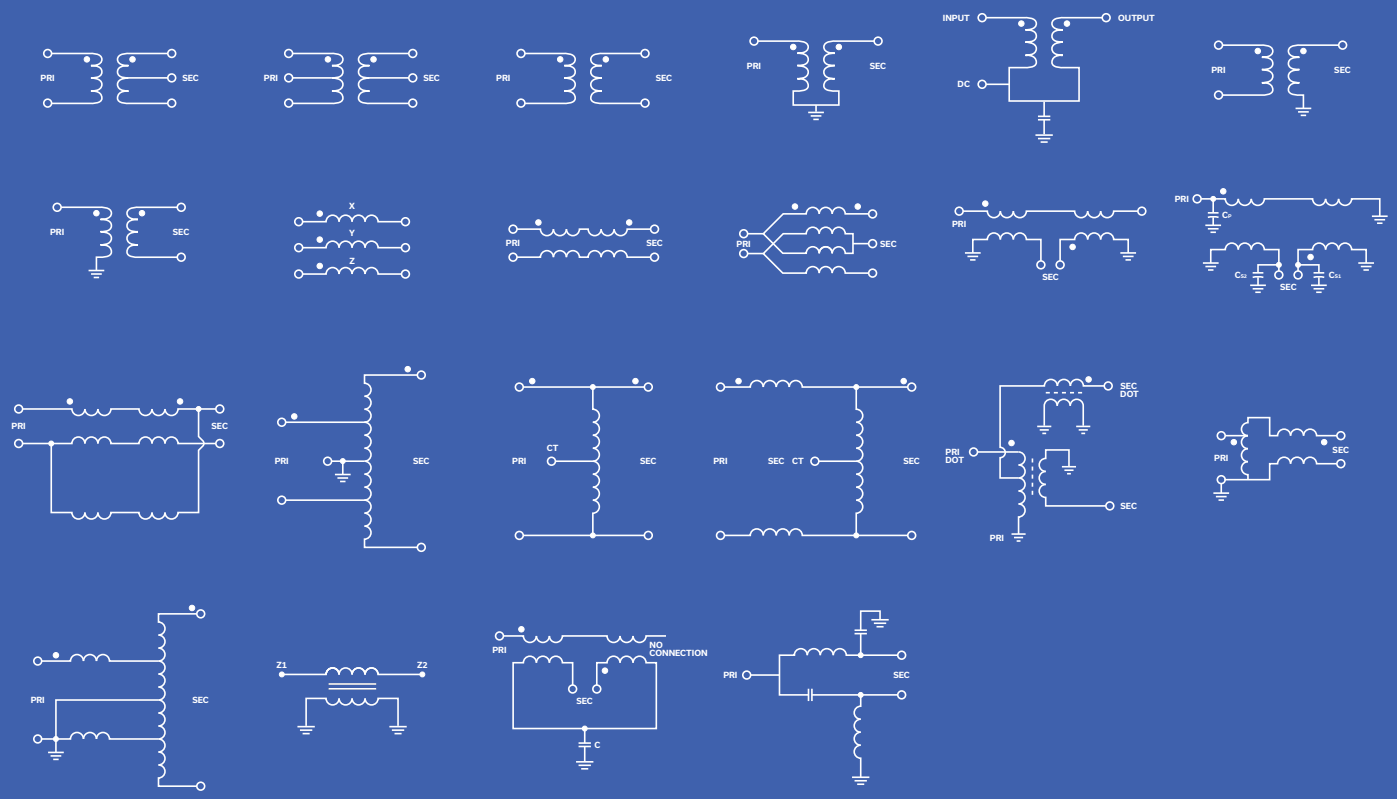

DC TO 24 GHz

Transformers from A to Z...

Configurations for Every Requirement

- 350+ models in stock plus custom designs
- 22 configurations
- MMIC, µCeramIQ™ and core & wire construction
- Impedance ratios from 0.11 to 36
- SMT, connector, plug-in & die form factors

LEARN MORE

Mini-Circuits®

U.S. Nears Universal 5G Adoption as North America Leads the World

The global wireless industry continued its rapid expansion in the third quarter of 2025, with global 5G connections reaching 2.8 billion worldwide, according to data from Omdia and 5G Americas. North America remains one of the world's most technologically advanced 5G markets, achieving exceptionally high adoption levels driven by strong consumer uptake and strong technological leadership, including enhanced 5G features that improve performance, efficiency and real-world network intelligence for consumers and enterprises alike.

In terms of 5G penetration, the U.S. accounts for 341 million 5G connections against a population of 344 million, one of the highest 5G penetration rates globally. As a region, North America leads the world in 5G penetration, reaching 363 million 5G connections in Q3 2025, representing nearly 95 percent of the region's population. While Asia leads in absolute 5G volume with 2 billion 5G connections today, North America leads in per capita 5G adoption, significantly outperforming the global average of 36 percent.

North America's 5G connections are forecast to grow to 867 million by 2030, more than doubling from current levels. This growth reflects a shift toward multi-device 5G environments, supporting advanced mobility, fixed wireless access and a broad array of connected platforms.

Additionally, fixed wireless access (FWA) continues to be a growing driver of multi-device adoption, expanding high speed broadband choice for households and small businesses, particularly in markets where fiber deployment is limited or still underway. Globally, 4G LTE and 5G FWA accounted for 78.14 million connections at the end of Q3 2025, with a year-over-year (YoY) growth rate of 27 percent.

As of November 2025, there were 379 commercial 5G networks deployed worldwide, including 17 in North America, alongside 707 LTE networks globally. This infrastructure expansion is key to supporting skyrocketing demand for ultra-reliable, low latency connectivity. Looking ahead, NTNs like satellite connectivity are emerging as a complementary layer to terrestrial 5G, extending coverage to remote areas, supporting resiliency during emergencies and enabling seamless service continuity across land, sea and air.

Industry Report Finds 62% of Survey Respondents More Confident to Invest in Wi-Fi Than 12 Months Ago

The Wireless Broadband Alliance (WBA) published the "WBA Industry Report 2026," which contains the results of its annual industry survey across the Wi-Fi, cellular and enterprise ecosystem. Among its chief findings is that 62 percent of respondents have grown more confident to invest in Wi-Fi over the last 12 months (18 percent are as confident). Wi-Fi 7 is the technology most likely to be deployed in 2026, with 38 percent of respondents planning deployments. Closely behind that is the impact of AI, with 32 percent planning to deploy AI/cognitive networks, which can transform Wi-Fi networking with an ability to improve the performance and reliability of networks.

The survey details where respondents expect to see overall network and traffic growth. Smart Home IoT led the top three with 36 percent, followed by AI (33 percent) and industrial/manufacturing applications & IoT (24 percent).

The 2026 survey highlights a positive outlook for Wi-Fi, strong momentum behind Wi-Fi 7 and 6 GHz and growing confidence in OpenRoaming as a foundation for seamless, secure connectivity across public, private and carrier networks. Together, the findings underline the importance of WBA's core focus areas, including OpenRoaming, Wi-Fi 7, AI-enabled Wi-Fi, QoS/QoE, security and Wi-Fi/5G convergence.

When asked about the role of Wi-Fi in converged networks with both 5G and private enterprise implementations, responses reinforced the view that the technologies are complementary and together benefit organizations. 60 percent said combining them would give their organization greater enterprise flexibility. The same proportion expect Wi-Fi and 5G to co-exist rather than be a binary choice for enterprise networks.

The industry survey shows OpenRoaming transitioning into a period of mainstream planning, with the need for seamless onboarding and roaming between Wi-Fi and cellular networks now seen as central business drivers. 38 percent of respondents say they had already deployed an OpenRoaming and/or Passpoint-compliant network with a further 32 percent wishing to deploy in 2026 and 18 percent in 2027.

When asked what is driving investment in OpenRoaming/Passpoint, the top three reasons given were enablement of frictionless Wi-Fi (63 percent), seamless access between Wi-Fi and 5G/LTE (60 percent) and seamless access across different networks (40 percent). Each of these responses relates to network access, highlighting that this element is the most important factor for the industry.

The WBA Industry Survey 2026 collected input from 185 participants worldwide, with diverse job roles ranging from the C-suite and business strategy to those in research and development and product management in a wide range of sectors.

LiDAR for Automotive 2025: The Intensifying Global Battle for IP Leadership

KnowMade released its latest patent landscape report, "LiDAR for Automotive – Patent Landscape Analysis 2025," a compre-

For More Information Visit mwjournal.com for more commercial market news.

hensive study capturing how global innovation and IP strategies are shaping the future of LiDAR technologies for ADAS and autonomous vehicles. As LiDAR transitions from an advanced sensor option to a core enabler of vehicle perception, patenting activity has accelerated at unprecedented speed. As of October 2025, the global patent landscape for automotive LiDAR includes more than 36,200 patent families and over 62,900 individual patents. LiDAR patent filings have tripled since 2021, underscoring the sector's rapid move from initial research to full-scale industrial deployment. Between 2020 and 2025, patent activity shows an estimated CAGR of 27 percent.

Innovation now spans all layers of the LiDAR technology stack: ranging principles, beam steering architectures, photonic integration, advanced detectors, packaging, calibration and increasingly AI-driven perception and fusion. This broadening of technical domains demonstrates a transition from early research toward large-scale IP consolidation, with companies striving to secure strategic positions in high-growth segments such as FMCW, integrated photonics and solid-state architectures.

The expansion also reflects a rapidly diversifying ecosystem comprising LiDAR pure players, Tier-1 suppliers, automotive OEMs, autonomous-driving developers, semiconductor companies and research institutes. Their collective activity highlights the growing maturity of LiDAR technologies and a stronger alignment between IP strategies and long-term technological roadmaps.

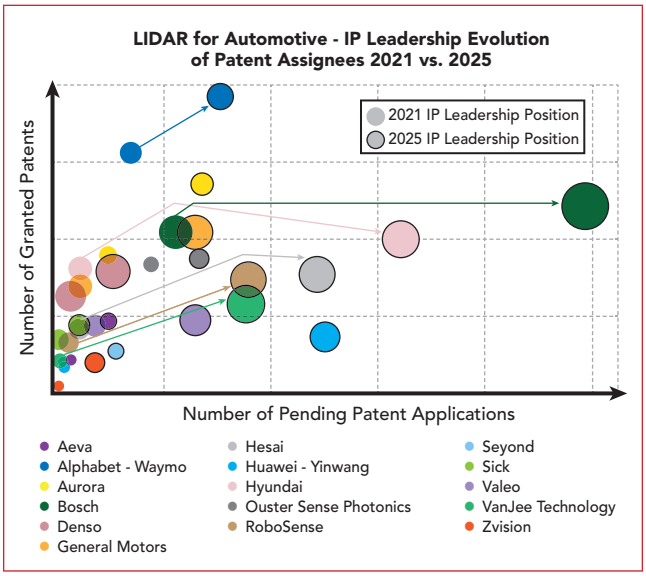

The more a company combines a high number of granted patents with a high number of pending patent applications, the greater its IP leadership in a field. The bubble size represents the number of patent families selected for the study. *Source:* LIDAR for Automotive - Patent Landscape, KnowMade December 2025.

ENGINEERED FOR EXCELLENCE, PROVEN BY PERFORMANCE

LC • CERAMIC • CAVITY • PRINTED • MULTIPLEXERS • SWITCHED FILTER BANKS • MULTI-FUNCTION ASSEMBLIES

3H Comunication Systems offers high quality, cost-effective solutions for RF and microwave filter products and other front-end solutions for multiple markets including military defense, commercial, public safety, aerospace and medical industries - all with a 5-year warranty.

3H Communication Systems

AS9100 & ISO9001:2015 CERTIFIED

949.529.1583 | sales@3hcomm.com

3HCommunicationSystems.com

Around the **Circuit**

Barbara Walsh, Multimedia Staff Editor

COLLABORATIONS

Anritsu announced the launch of an advanced acoustic evaluation solution for next-generation automotive emergency call systems (NG eCall), developed in collaboration with **HEAD acoustics**, an acoustic measurement and analysis company. The new solution, which is compliant with ITU-T Recommendation P.1140, enables precise assessment of voice communication quality between vehicle occupants and public safety answering points, supporting faster and more effective emergency response. With NG eCall over 4G (LTE) and 5G (NR) now mandatory in Europe as of January 1, 2026, ensuring high-quality, low-latency voice communication during vehicle emergencies has become essential. After a collision, calls are conducted hands-free inside the vehicle cabin, where high noise levels, echoes and other acoustic challenges can significantly degrade speech clarity.

Keysight Technologies, Inc. announced the signing of a five-year Master Research Collaboration Agreement (MRCA) with Singapore's leading quantum research institutions: the **Agency for Science, Technology and Research (A*STAR)**, the **National University of Singapore (NUS)** through the **Centre for Quantum Technologies (CQT)** and **Nanyang Technological University, Singapore (NTU Singapore)**, to advance capabilities in quantum computing. This collaboration covers the design, measurement and control of qubits. Quantum computing holds immense promise for transformative applications. However, realizing this potential requires overcoming significant challenges in scalability, connectivity and architectural flexibility. This new partnership addresses hurdles in the design and control of quantum processor chips through targeted collaborative initiatives.

ST Engineering iDirect, a satellite communications company, announced that it is collaborating with **Capgemini**, an AI-powered global business and technology transformation company, to develop a 5G non-terrestrial network (NTN) satellite base station. Based on cloud-native fundamentals, the solution will enable seamless integration between satellite and terrestrial networks, accelerating the adoption of standards-based, software-defined 5G NTN technology. The core of this collaboration is the development of a satellite-optimized radio access technology within ST Engineering iDirect's cloud-native Intuition ground system. Built using Capgemini's gNodeB software stack, the NTN satellite base station has been uniquely optimized to address the nuances of satellite connectivity.

HENSOLDT is equipping air defence systems from Rheinmetall subsidiary **Rheinmetall Air Defence AG** with radars from its SPEXER 2000 product family. The companies have now signed a long-term framework agreement that will remain valid until the 2030s. The agreement covers the flexible provision and delivery of large quantities of radars for ground-based air defence applications, in particular for drone defence solutions, and the Skyranger 30 air defence system from Rheinmetall Air Defence. The contract thus has a potential volume in the high three-digit range. With the framework agreement now in place, both companies have laid the foundation for predictable, efficient and reliable cooperation.

ACHIEVEMENTS

Leonardo DRS Inc. announced the successful first on-orbit test of its revolutionary multi-channel software-defined radio (SDR) with integrated advanced cryptography. This milestone marks a significant advance in validating a technology poised to establish a new standard for secure U.S. military satellite data transport at the tactical edge. The eXtended Crypto Module3-Space (XCM3-Space) adapts the company's next-generation crypto and multi-channel SDR capabilities to the space domain, addressing emerging cyber and electronic warfare threats to military satellite data transport. Leonardo DRS developed this capability to enable high performance secure satcom across multiple frequencies and networks simultaneously.

Eviden, the Atos Group product brand of advanced computing, cybersecurity products, mission-critical systems and Vision AI, announced that it has been selected by the **NATO Support and Procurement Agency (NSPA)** to modernize the ground-to-air-to-ground communication systems of the Spanish Air and Space Force. The €12 million contract includes the supply, installation and maintenance of next-generation communication systems that will enhance operations at air traffic control towers across various air bases, Air Force airfields and Air Surveillance Squadron bases of the Spanish Air and Space Force.

MatrixSpace is the winner in the **U.S. Army**'s xTech-Counter Strike competition, part of Operation Flytrap 4.5. MatrixSpace was the only active sensing provider selected among 15 finalists, highlighting the company's capabilities in rapidly deployable airspace awareness. Operation Flytrap is the U.S. Army's key initiative to accelerate innovative, scalable C-UAS technologies through live soldier experimentation, rapid acquisition pathways and transition to operational units. MatrixSpace showcased its Expeditionary AI Radar and 360 AI Radar, powered by AiEdge software, demonstrating fast setup, seamless integration into the Army's FAAD-C2 via the NATO-standard SAPIENT protocol and real-time situational awareness at the tactical edge.

NTT DOCOMO INC. announced that they have successfully conducted the world's first outdoor demonstration using real-time transceiver systems with AI-powered wireless technology for 6G mobile communications. The demonstration was carried out in collaboration with NTT, Inc., Nokia Bell Labs and SK Telecom Co., Ltd.

For More Information **For up-to-date news briefs, visit mwjournal.com**

GOLD STANDARD

GSDRO series

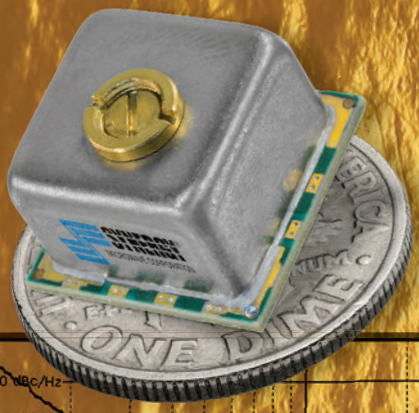

0.75" x 0.75" x 0.53"

* Typical For 10 GHz RF Output

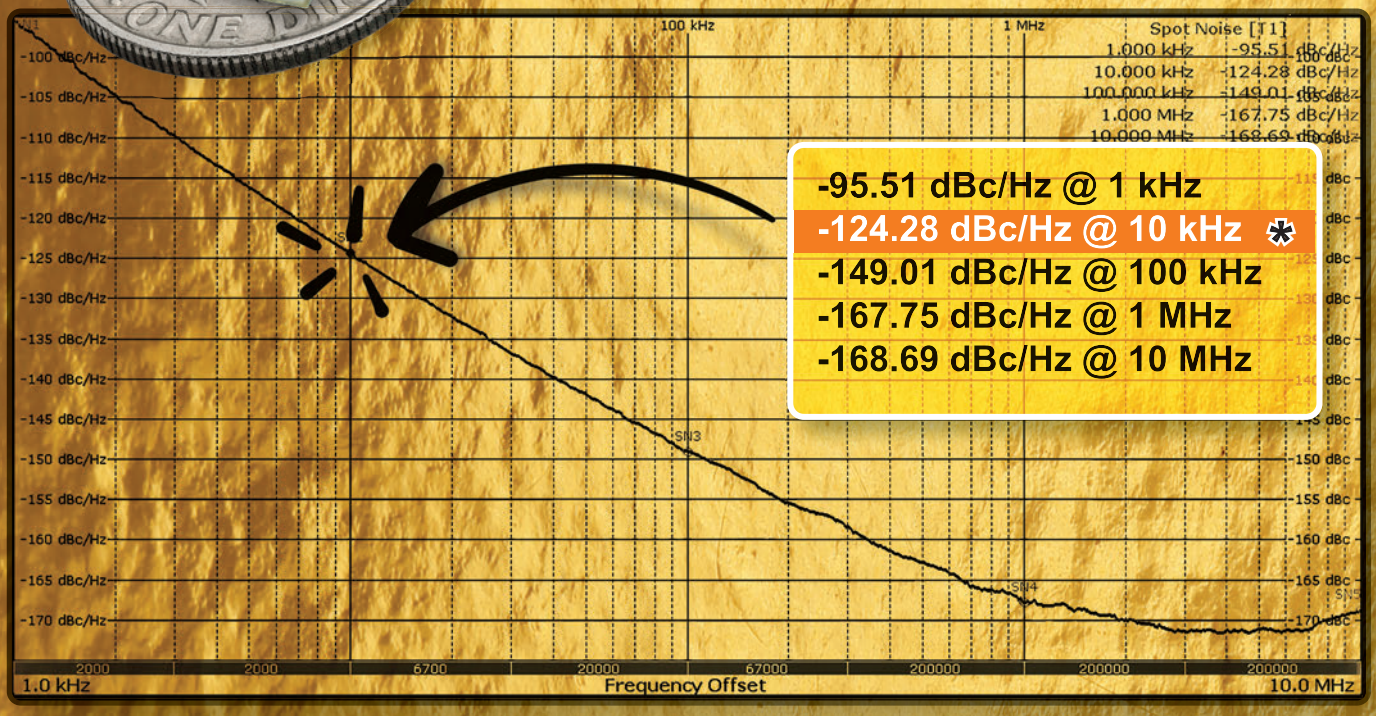

-95.51 dBc/Hz @ 1 kHz
-124.28 dBc/Hz @ 10 kHz *
-149.01 dBc/Hz @ 100 kHz
-167.75 dBc/Hz @ 1 MHz
-168.69 dBc/Hz @ 10 MHz

FEATURES:

- *Exceptional Phase Noise*
- *Lead Free RoHS Compliant*
- *Patented Technology*

Applications:
Radar, Test Equipment,
5G, Frequency Synthesizer

Now Up To 22 GHz!

Check out our website for available frequencies.

Talk To Us About Your Custom Requirements.

SYNERGY® MICROWAVE CORPORATION

Phone: (973) 881-8800 | Fax: (973) 881-8361
E-mail: sales@synergymwave.com | Web: www.synergymwave.com
Mail: 201 McLean Boulevard, Paterson, NJ 07504

Around the **Circuit**

CONTRACTS

Verus® Research has been awarded a four-year, $6 million effort to support the **Naval Surface Warfare Center Dahlgren Division (NSWCDD)** via the **Naval Surface Technology & Innovation Consortium (NSTIC)**. Under this award, Verus Research will implement its concept referred to as Adaptive Radio Frequency Chamber and Hardware in the loop for Integrated Missile Subsystem Evaluation and Assessments (ARCHIMES).

Applied Physical Electronics, L.C. (APEL) has been awarded a $1.73 million Small Business Innovation Research (SBIR) Phase II contract by the **U.S. Air Force** to develop a transportable array structure to support high-power RF and high-altitude electromagnetic pulse (HEMP) sources. This two-year project focuses on solving a key structural challenge within EMP array development. As multiple organizations race to advance EMP technologies, APELC's award aims to fill a significant interest — designing a reconfigurable, transportable array frame capable of supporting large, heavy pulsed power systems in a variety of field environments.

PEOPLE

▲ *Tim Filteau*

Naprotek announced the appointment of **Tim Filteau** as its new CEO. This strategic leadership transition underscores the company's commitment to blending proven expertise with bold innovation to shape the future of technology. Filteau brings a distinguished track record of executive leadership, guiding organizations through periods of growth, transformation and market expansion. His career spans decades of experience in technology, operations and strategic development, making him uniquely positioned to lead Naprotek into its next chapter. As CEO, Filteau will focus on expanding Naprotek's innovation pipeline, strengthening customer partnerships and driving sustainable growth across global markets.

Delft Circuits, a company focused on high-density I/O solutions for quantum computers, announced the appointment of **Martin Danoesastro** as CEO and an €8 million extension of the company's previous financing round, bringing the total capital raised to €15 million. The appointment comes during a period of strong momentum for Delft Circuits, marked by new partnerships, expanded production capacity and advancements in product research and development. Recent milestones include the publication of a next-generation product roadmap and a partnership with Bluefors to offer cutting-edge quantum I/O solutions integrating Delft Circuits' Cri/oFlex® technology into Bluefors' dilution refrigerators.

▲ *Martin Danoesastro*

EXODUS

Best in Class
RF Amplifier SSPA's

POWER REVEALED

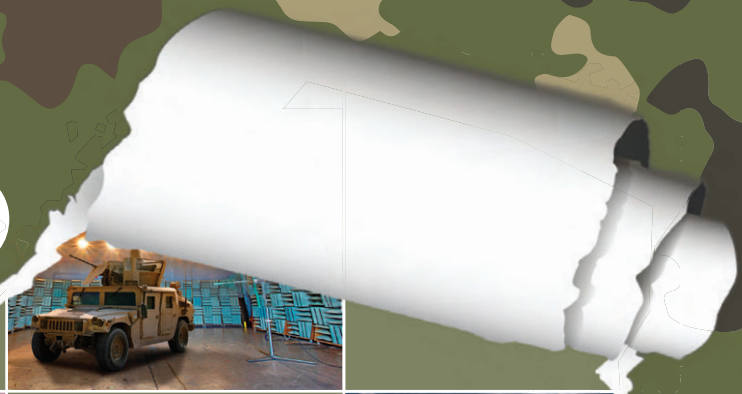

AMP20184
0.8-2.5 GHz, 500W

AMP20130
80-1000 MHz, 1300W

RF & Microwave Amplifiers
10KHz-75GHz

AMP20192
1.0-2.0 GHz, 10KW

AMP20191
2.0-4.0 GHz, 10KW

AMP20182
4.0-8.0 GHz, 10KW

AMP20178
6.0-18.0 GHz, 400W

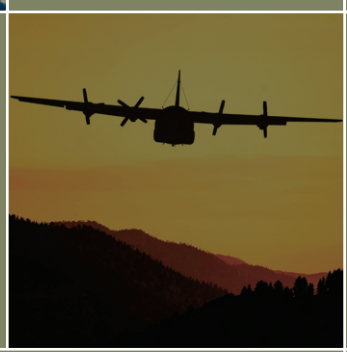

AMP20160
1.0-6.0 GHz, 750W

EXODUS ADVANCED COMMUNICATIONS

3674 E. Sunset Road, # 100
Las Vegas, Nevada 89120
Tel: 1-702-534-6564 ***www.exoduscomm.com***

AMP20141
400-1000 MHz, 4 KW Pulse

INVITED PAPER

Glass as a Versatile Platform for Advanced Packaging and RF Systems

Bilal Hachemi
Yole Group, Villeurbanne, France

Advanced packaging has become the scaling vector for computing power, and it is increasingly the scaling vector for RF systems, too. The same forces that reshaped compute, such as chiplets, 2.5D/3D stacking, denser redistribution layers and new production formats, are now reshaping RF front ends as they expand in band count, antenna count and integration level. Packaging is no longer just an enclosure: at mmWave and sub-THz bands, it becomes part of the electromagnetic design, the thermal architecture and the cost structure.

That shift is widening the materials palette. One of the most consequential additions is glass, as shown in ***Figure 1***. Historically linked to displays and optics, glass is now emerging in advanced packaging through multiple entry points, and that multi-entry nature is precisely what makes it strategically interesting. Glass is arriving at different "levels" of packaging: carrier, interposer, substrate and even board-level, each solving different bottlenecks and each reinforcing the others through shared equipment, process know-how and supply chain investments.

In parallel, RF system requirements are converging with the compute packaging roadmap. RF wants low losses, stable geometry, dense vertical interconnects for shielding and waveguide structures and compact antenna-feeding networks. Compute wants dimensional stability for ultra-fine routing and large body sizes, as well as scalable manufacturing formats. Glass sits at that intersection.

Glass fits both "compute scaling" and "frequency scaling." At the material level, glass offers a mix that is unusual in one substrate family: a wide dielectric constant range (3.7 to 21), CTE tunability (3 to 12 ppm/K) and very smooth surfaces (<10 nm roughness), with zero moisture absorption listed in comparative packaging tables. These features become increasingly valuable as frequencies rise and line widths shrink. Glass also aligns with the manufacturing direction of travel: it can be produced and processed in large-panel formats, positioning it between expensive silicon interposers and cost-sensitive organic laminates for mmWave applications.

For RF specifically, the physics drivers get harsher above ~100 GHz, where the conductor roughness penalties grow, discontinuities matter more and parasitics that were tolerable at 6 to 28 GHz become dominant error terms. Glass-based approaches

The Future of Filters Is Clear

Our next-generation, high-performance filters reset the bar in RF design, powered by Marki Microwave's proprietary OmniFlow design engine. Built on a new high-Q glass substrate, they deliver MMIC-level repeatability and push our filter portfolio into the MHz range. Verified models enable true first-pass success, with measurements that tightly match simulation data. Offered in compact footprints (LP/HP: 4.25 × 4 mm; BP: 7.5 × 4.2 mm), these filters drive the next wave of RF from 100 MHz to 6 GHz.

- **Replaces lumped-element and ceramic filters from VHF through C-Band**
- **Optimized for IF signal conditioning and anti-aliasing filter applications**
- **Handles up to 15 W CW with robust, reliable performance**

Contact: sales@markimicrowave.com
www.markimicrowave.com

The Trusted Leader When Performance Matters

Marki® microwave

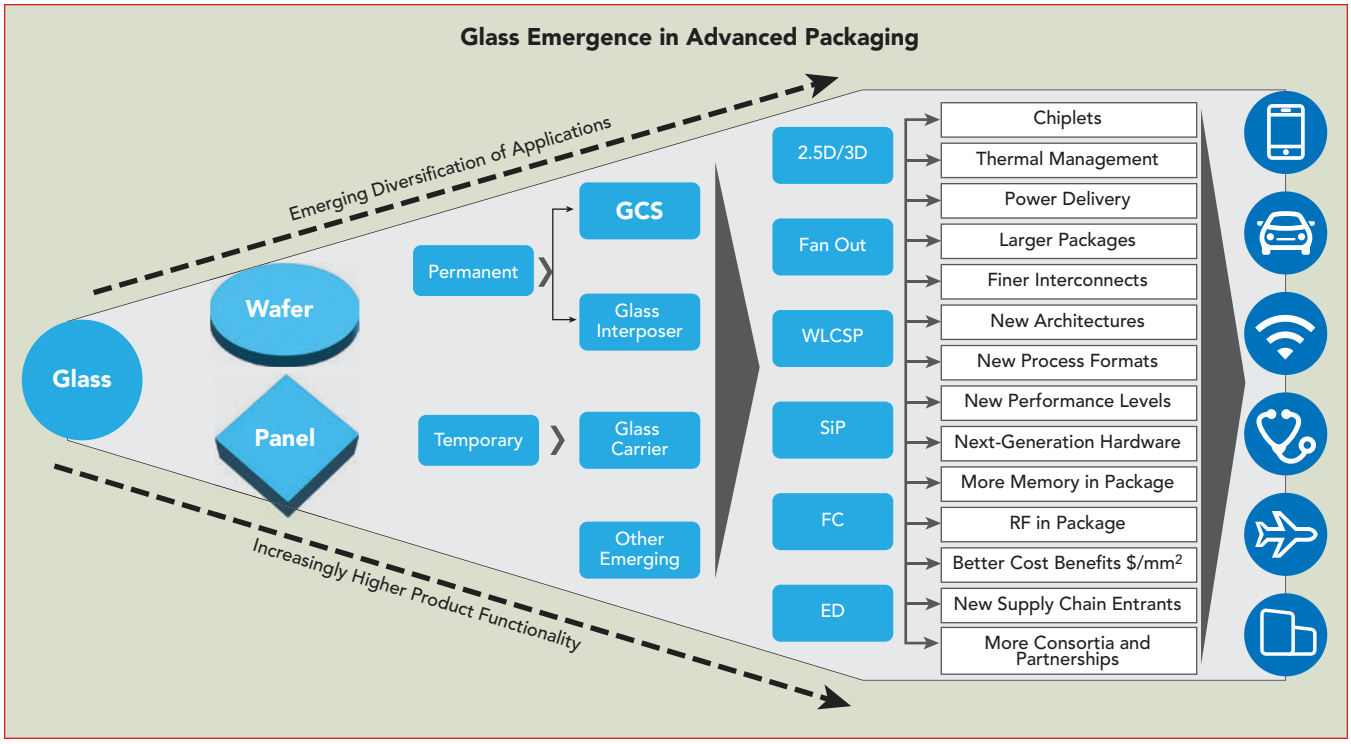

Fig. 1 **Glass emergence in advanced packaging.** ***Source:*** **Glass Materials for Packaging 2025 report, Yole Group.**

are being actively discussed for W-Band, D-Band and even G-Band packaging. This is why packaging choices increasingly translate into system cost and performance, not just manufacturability.

For the system architecture, the direction is clear: tighter co-location of antennas, RFICs/MMICs, mixed-signal and compute. The "antenna-to-AI" concept popularized for 6G is essentially a packaging roadmap that compactly integrates MMICs, passives and compute to collapse latency, loss and form factor across the RF-to-data path. Glass becomes relevant because it can serve as both an RF-friendly substrate and a scalable integration medium.

MULTI-ENTRY ADOPTION OF GLASS IN PACKAGING

The multiple entry points allow glass to be treated not as a single product, but as a platform with four entry points and practical roles, including glass carriers, glass interposers, glass-core substrates and glass at the board level, as shown in ***Figure 2***. Each role has its own adoption curve, RF relevance and bottlenecks.

Glass is already widely used, often "quietly," as a carrier in advanced packaging flows, particularly when thin wafers or fragile stacks require stiffness and planarity. This includes fan-out processes, thin-die handling and some 3D stacking steps. The carrier role is one reason why glass's ecosystem is maturing faster than usual for a new material; CapEx investments can be justified even before glass becomes the permanent substrate.

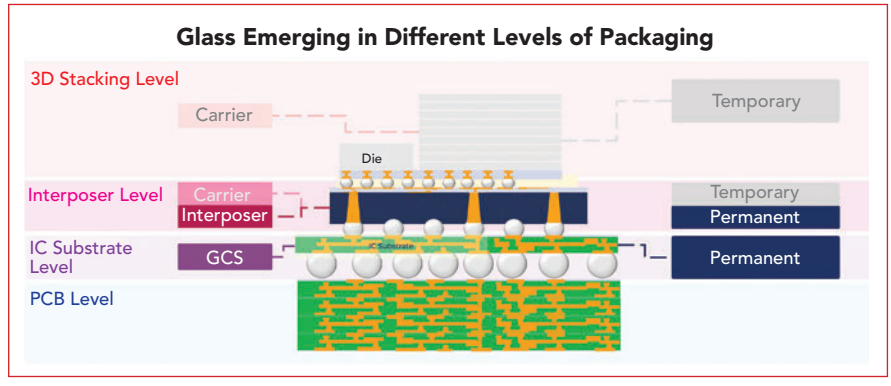

Fig. 2 **Glass emerging in different packaging levels.** ***Source:*** **Glass Materials in Semiconductor Manufacturing 2025 report, Yole Group.**

Glass Interposers

A glass interposer is the closest conceptual analog to a silicon interposer. A thin dielectric plate with dense through-glass vias (TGVs) and fine redistribution layers (RDL), used as an intermediate routing and interconnect layer between dies/chiplets and the package substrate.

Why does this matter in compute packaging? Computing is pushing 2.5D/3D into a regime where interposer size and routing density can dominate cost and yield. Silicon interposers deliver superb density and alignment, but cost and wafer-size constraints become painful as body sizes grow. Organic and molded interposers offer cost advantages, but face limitations in geometry control, moisture behavior and ultra-fine scaling. Glass interposers occupy the "middle ground." They aim for the precision of silicon-like routing without silicon RF's leakage behavior and with an eventual path to panel-

Dalicap
DALICAP TECH. CORPORATION

Microwave / RF Ceramic Capacitor

DLC70 Series High Q,NP0(C0G) RF/Microwave MLCC

Product Features

- High Q
- C0G:0±30PPM.TCC
- Low ESR/ESL
- Low Noise
- Ultra-Stable Performance
- Extended WVDC available

SIZE:0603,0505,0805, 1111,2225,3838 for RF/Microwave; 6040,7575,130130 for High RF Power

DLC70B Performance Curve

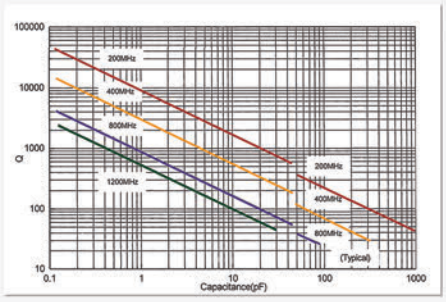

DLC:70B(1111) Q Value and Capacitance Curve

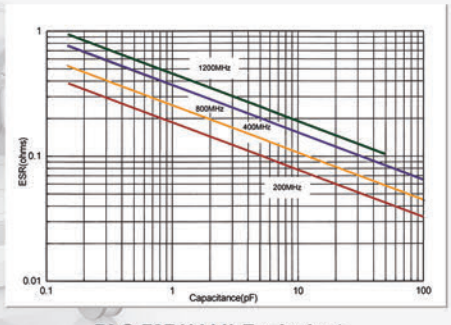

DLC:70B(1111) Equivalent Series Resistances（ESRs）

Single LayerChip Ceramic Capacitor (SLC)


General SLC


Margin SLC


Surface Mounting SLC


Array SLC

Product Features

- Broadband application for microwave and mmWave up to 100GHz
- Capacitance: 0.1pF to Max. 5000pF
- Voltage Rating: up to 100 WVDC
- Used for DC Blocking, Low Noise Amplifiers, Power Amplifiers, tuning and Filters.

SIZE: 0.25 X 0.25 to 1.25 X1.25
Custom size is available

Dalicap

Dalicap Tech. Corporation is a global leader in Precision RF/Microwave Solutions. As the No.1 leader in China’s RF capacitor niche market and ranked among the top globally, Dalicap is a trusted strategic partner for Tier-1 international market leaders in medical MRI and semiconductor RF power sectors.

We provide high-performance solutions through a fully self-controlled manufacturing process, offering a comprehensive portfolio including High Q MLCCs, SLCCs,Power Capacitor Assemblies (Modules),Bracket Capacitors,Thin Film circuits and DPC ceramic PCBs for high-power RF modules.

Our veteran R&D teams ensure rapid response to customized requests, leveraging a unique RF lab and specialized testing to guarantee superior product realization in the world’s most demanding RF environments.

www.dalicap.com
dalicap@dalicap.com
+86-411-87632359

scale throughput. Glass keeps resurfacing due to the equipment ecosystem and its adaptability to panel formats adapted from the flat panel display industry.

RF receives a second benefit. Glass interposers are not just dense routing planes, they can be engineered as electromagnetic structures, including as via fences and ground cages for isolation between RF channels and between RF/digital regions, substrate integrated waveguides (SIW) and waveguide-like cavities (especially attractive at D-Band+), antenna feed networks with tighter phase and amplitude control and embedded passive integration (filters, couplers, transitions) that reduces board-level loss and assembly complexity.

The telecommunications industry can commercialize it faster "in RF" because the value proposition (loss, integration and size) is so immediate for mmWave front ends and backhaul modules. In practice, RF modules increasingly need low loss routing to arrays, tight tolerances to maintain beam patterns and compact transitions that do not destroy match and efficiency. Glass interposers directly target these requirements, as demonstrated in ***Figure 3***.

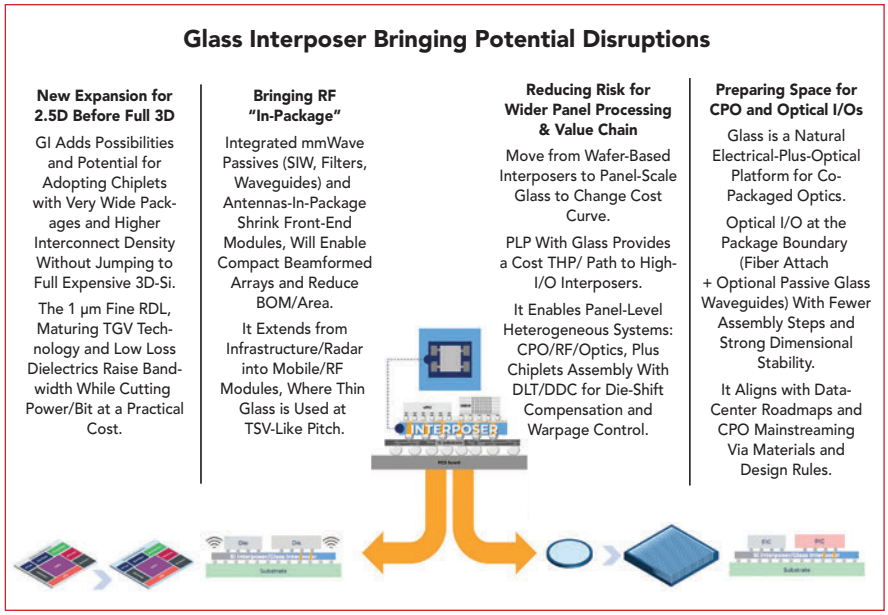

▲ Fig. 3 **Glass interposers bringing potential disruptions.** ***Source:*** **Glass Materials in Semiconductor Manufacturing 2025 report, Yole Group.**

GLASS-CORE SUBSTRATES

A glass-core substrate places glass in the role traditionally played by an organic core, the structural backbone of the IC substrate. Built-up dielectric layers and copper

qorvo®

Connecting the World Through Space

With system-level expertise and a broad product portfolio, Qorvo enables seamless connectivity across ground, airborne and space-based SATCOM platforms.

LEARN MORE at
qorvo.com/go/satcom

routing are then formed on one or both sides, often symmetrically, to manage warpage.

Data center servers and AI accelerators are reaching the limitations of organic IC substrates in terms of larger body sizes, higher layer counts and finer routing. These demands amplify the problems of warpage and dimensional drift. Glass, with a wide CTE spectrum and high stiffness, is positioned as a way to improve dimensional stability, reduce warpage and enable higher routing density. Intel's September 2023 announcement on developing glass-core substrates is a notable inflection point in the substrate-level glass industry. That announcement matters not only because of the technology, but because it signals ecosystem-changing dynamics: raw glass suppliers, chemical suppliers, laser equipment suppliers, new glass-based business models, inspection and assembly qualification. Since the announcement, the number of companies involved has exploded from research and development projects to the formation of consortia and the building up of pilot lines.

For RF, a glass-core substrate is not always about the last micron of line/space. It is often about geometry stability for arrays, in which phase consistency and calibration across temperature, lower dielectric loss foundations for mmWave feed networks and filters, better isolation structures enabled by vertical vias and stable build-up alignment and also the integration of RF and digital in a single substrate when radios incorporate significant local compute (beamforming, MIMO, AI-assisted calibration).

Interposers can improve performance quickly, but substrates are where volume economics live. Glass-core substrate (GCS) adoption is therefore less about "can it be built?" and more about "can it be built at the yield, cost and reliability required for high volume platforms?"

THE REAL SCALING PRIMITIVE: TGV KNOW-HOW

If glass interposers or GCS are the architecture, TGV is the primitive. In Si interposers, TSV technology is mature. In glass, the process window is different (drilling and etching, metallization adhesion, void-free fill and substrate edge warp and reliability error crack management). The industry target is clear: shrink via diameters, improve placement accuracy and scale throughput.

RF packaging uses glass in several additional ways that can become mainstream even if glass interposers or GCS take longer to scale.

Antenna-in-Package Arrays and Feed Networks

As arrays grow (more elements, tighter spacing), the feed network becomes a dominant source of loss and phase error. Glass offers a stable, low loss routing plane with the potential for fine pitch and tight tolerances, useful for beamforming modules (phased arrays for 5G/6G access, backhaul and radar) and also compact front ends where antenna, filters and transitions are co-located.

FLANN

1956
2026

Next-generation, high-capacity satellite links are pushing communications into frequencies above 40 GHz, where few components are space-qualified. With 50 years of millimetre-wave expertise, Flann delivers waveguide technology designed for these demanding environments.


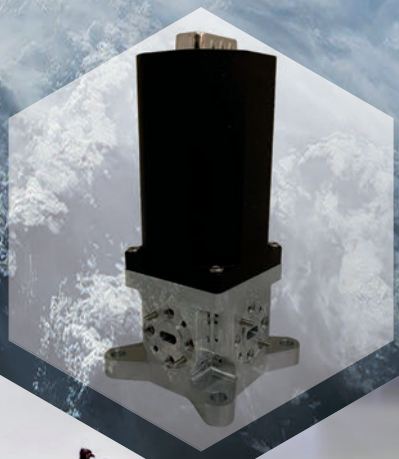


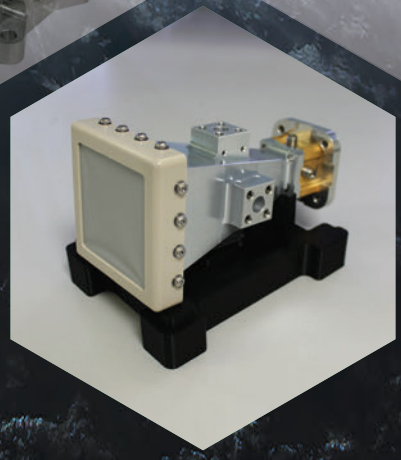
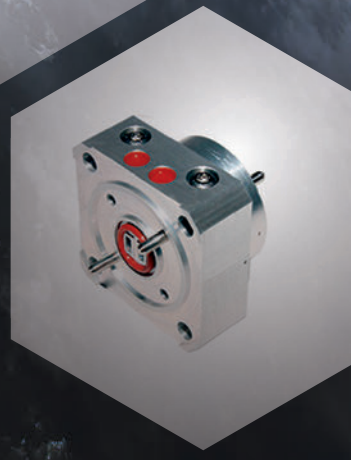

Our advanced design tools enable multipaction, corona, thermal, and vibration analysis to qualify designs before manufacture. Production is carried out in a purpose-built facility delivering flight-ready waveguide assemblies and components.

sales@flann.com
@flann-microwave

GUARANTEED PERFORMANCE FROM 1 GHz TO 1.1 THz

Integrated mmWave Passives

At D-Band and beyond, integrated waveguide structures become attractive. Glass supports dense vias and can be combined with cavities, including air features in some approaches, enabling compact low loss passive functions. The SIW, filters and waveguides are part of the "RF in-package" value proposition, shrinking discrete front ends into packaging-level integration.

Embedded Die and Cavity-Based RF Modules

Embedding RF die inside glass cavities shortens vertical RF paths and reduces transition discontinuities, often the hidden limiter at mmWave/sub-THz. This mirrors compute packaging's move toward embedding and stacking (high bandwidth memory, logic-on-logic), but with different design goals: impedance continuity, isolation and minimizing radiation and leakage.

Board-Level and System-Level Explorations

A small but important set of efforts explores glass-like materials or glass cores at larger scales (low loss backplanes, stable high speed routing or hybrid electrical/optical interfaces). Even when these are at an early stage, they reinforce the same ecosystem: drilling, metallization, inspection and panel handling.

GLASS: WHAT NEXT?

Glass is no longer just a low loss dielectric. It is increasingly being engineered as a multi-role packaging platform: as a carrier enabling thin-wafer and panel processes, as a glass interposer enabling dense vertical interconnect and fine RDL for 2.5D/3D chiplets and mmWave passives and as glass-core substrates aiming to deliver the dimensional stability and routing density needed for the next generation of large, high-end packages. The multi-entry view helps explain why momentum is accelerating: each role can mature in parallel, reinforcing ecosystem investment and pulling glass from specialty use into scalable production pathways.

For RF, the timing is particularly compelling. As front ends move from sub-6 GHz into mmWave and onward to sub-THz, advanced packaging becomes an RF component, and the substrate must deliver low dielectric loss, smooth conductors/interfaces and tight dimensional stability for fine routing and scalable interconnect density. Glass's property envelope, dielectric constant range, tunable CTE and ultra-smooth surfaces map directly onto these requirements, and its panel compatibility aligns with the industry's push to new manufacturing formats.

The remaining question is not whether glass works, but how fast the ecosystem can convert process maturity, especially around TGV formation/fill, panel handling, warpage control and RF/thermal co-design, into repeatable, cost-competitive, high volume manufacturing. That ramp will likely occur unevenly: RF infrastructure and specialty mmWave modules may adopt first where performance value is immediate, while AI/HPC and substrate-level adoption will accelerate as supply chains and panel yields reach the scale demanded by mainstream compute platforms. ■

PROVING SATELLITE AND RF PERFORMANCE.

ETS-Lindgren supports government, military, and commercial space organizations with advanced test, measurement, and shielding solutions that ensure satellite and radio-communication systems perform exactly as intended. From earth-orbiting satellite platforms and ground stations to secure RF links and space-to-ground communications, we help validate the electronic systems that keep global networks connected and protected.

Our capabilities span every stage of modern satellite and radio operations. We support the readiness of communications payloads, antennas, transceivers, telemetry and tracking systems, and secure SATCOM networks, and we engineered the world's largest RF microwave chamber for full-platform and large-aperture antenna testing. Through vertically integrated design, manufacturing, and services, ETS-Lindgren delivers the precision and reliability required for mission-critical RF performance on the ground and in orbit.

ETS-Lindgren supports satellite and communications programs around the world, delivering the precision, reliability, and performance required for mission-critical RF systems. We are *Committed to a Smarter, More Secure Future*.

For more information on our defense solutions, visit our website at www.ets-lindgren.com or contact your ETS-Lindgren representative.

Connect with us at:

COMMITTED TO A SMARTER, MORE CONNECTED FUTURE

ETS·LINDGREN®
An **ESCO Technologies** Company

Offices Worldwide | **ets-lindgren.com**

INVITED PAPER

Transceivers Versus Discreets in Satellite Applications

Bob Potter
Global Invacom Group, Canterbury, U.K.

The satellite ground segment market is undergoing significant evolution, driven primarily by the growth of low Earth orbit constellations and high-throughput satellites. As the number of satellites in orbit and the demand for better connectivity continue to increase, there is huge potential, but also a range of challenges and complexities that come with this evolution. The ground segment urgently needs to reinvent itself to keep up with the pace of change.

One area with room for innovation in the ground segment sector is the argument between transceivers and low noise block down-converters (LNB) and block up-converters (BUCs), otherwise known as discreets. For some, satellite transceivers are completely replacing discreets. Other users are more wary of ditching the discreets, fearing loss of flexibility, performance or functionality. This article discusses the key differences and similarities and highlights when users would need one versus the other.

TALKING TO THE SATELLITE: DISCREETS AND TRANSCEIVERS

Satellites operate at extremely high frequencies. For example, Ka-Band operates from 26 to 40 GHz, Ku-Band from 12 to 18 GHz and C-Band from 4 to 8 GHz. This is a stark comparison to most network connectivity equipment, which operates from around 70 MHz to 2.4 GHz. The industry needs a way to up-convert those signals to higher frequencies before transmission to the satellite. Additionally, ground systems must be able to convert incoming signals to the low frequency ranges after reception from the satellite for transmission to the antenna receiver unit. This is vital, as it allows the data to be processed for display on end-user devices.

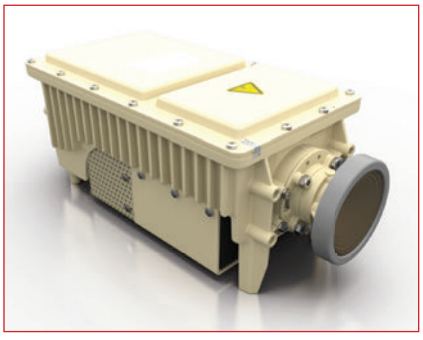

Fig. 1 XRJ transceiver from Global Skyware, part of the Global Invacom Group.

DISCREETS: SIGNAL CONVERSION

A discreet is the catch-all term for LNB and BUC, integral parts of any satcom system. BUCs convert low frequency signals into high frequency signals that can then be amplified and transmitted to satellites, whereas LNBs are designed to receive sensitive high frequency satellite signals from orbiting satellites and convert them to lower frequencies.

Satellite antennas require both elements to ensure that signals can be converted at both the transmit and receive ends. In this setup, the antenna will have a feed element connected to communicate with the BUC and LNB. In most cases, the feed element will consist of a feed horn, an orthomode transducer (OMT) and a polarizer. These will then be mounted on separate mechanical structures, which must be linked together using cabling and waveguides. As signals pass through these elements, signal loss is possible and must be minimized to avoid connectivity issues. This means both the LNB and the BUC must be close to the feed.

Transceivers: Transmit and Receive

Transceivers combine the transmit and receive functions of both LNBs and BUCs along with the feed horn, polarizer and OMT, into a compact single device. A transceiver, such as the multi-orbit XRJ transceiver shown in ***Figure 1***, can be mounted directly on the back of an antenna, with the feed on the other side directly connected to the transceiver. This reduces the amount of waveguide runs and requires only one mechanical structure, rather than three. This also makes for a more straightforward assembly. However, depending on the applications, they may

DC–18 GHz 2W SMA Fixed Attenuator

M–M and M–F Configurations | 1–10, 12, 15, 20, 30, 40 dB

Starting from
$ 33 /piece

VSWR
1.25:1 max

Inventory ready in
U.S. & Canada

Average Attenuation Accuracy
±0.1 dB typ

Speed guarantee
Ships within 24 hours

Product assurance
12 months warranty

Check live stock, full specifications, & terms at URFinc.com

URF

Fig. 2 **Using a transceiver reduces the physical space required and simplifies cabling and spares.**

not be a perfect replacement for a system of discreets.

DO TRANSCEIVERS MEAN LESS POWER?

Several arguments have been raised against switching to transceivers, including the risk of reduced power capability. BUCs, in particular, deliver very high power, making them ideal for applications such as broadcasting and telecommunications. While this is true, there is a perception that transceivers can only be low power, making them unsuitable for many applications. This perception is driven by port-to-port isolation within the transceiver. If isolation is poor, the transmitter noise floor desensitizes the receiver and limits data throughput, thereby reducing available power. However, new innovations, better engineering tools and precision fabrication have resulted in transceivers offering greater port-to-port isolation, making them more powerful than ever. This makes them comparable to discreets and powerful enough for most applications. The problem of potential interference between components within the same box requires transceiver manufacturers to both engineer and conduct extensive testing. This is not always to the same level as discreets because the component parts may be different each time. Careful engineering and extensive testing increase customers' confidence that a transceiver is designed and tested to ensure all components work together seamlessly.

When referring to transceiver power levels, it is often unclear whether specifications are defining saturated or linear power. Linear power (P_{Lin}) refers to the ability of an amplifier to increase the power of a signal without distortion. After that point, the signal will be distorted and limit the types of waveforms that can be transmitted to the satellite. Saturated power (P_{Sat}) is the maximum power an amplifier can deliver; however, at this level, the signal may be distorted, and data throughput can drop significantly. Often, transceivers are measured using P_{Lin} because it is a more realistic representation of the actual output achievable without signal distortion. However, many vendors, especially with discreets, will quote the maximum P_{Sat}, which is around twice the P_{Lin}. This can make it unclear and more challenging to compare actual performance.

Fig. 3 **Example of a transceiver.**

The Benefits of Integration

One of the most significant differences between the approaches is that transceivers are integrated into existing systems and replace multiple parts, including cabling, while discreets have external cabling. This has several effects on the signal.

Firstly, signals going through additional RF elements connected to the antenna experience more signal

TABLE 1

COMPARISON OF TRANSCEIVERS VERSUS DISCREETS

Feature	*XRJ Transceiver*		*BUC + LNB + FEED*	
Design	Integrated and compact	☑	Multiple units, from potentially multiple vendors Greater weight and higher power BUCs require waveguide and remote mouting from feed	☒
Performance	Improved G/T – lower loss in feed Zero mismatched connections between waveguide flange High power output 25 W = > 40 W P_{sat} Optimised losses in Tx and Rx RF chain	☑	System losses (noise figure) must be considered for each component Separate mounting for LNB and BUC Additional waveguide loss	☒
Installation	Simple connections, no risk of dirt/water ingress into RF chain	☑	Multiple waveguide connections must be adequately waterproofed	☒
Configuration	Single interface, Web Gui, CLI or OpenBMIP	☑	Multiple systems (LNB + BUC)	☒
Maintenance	Single unit for spares management	☑	Multiple units to be managed and held by maintenance teams	☒
Time to restore following fault	Single unit to replace, simple ruggedized IF and power connection	☑	Swap out of either LNB or BUC will require separation of waveguide from feed plus IF and power	☒

REMCOM®

Analyze Mobility and Performance of Body-Worn Devices

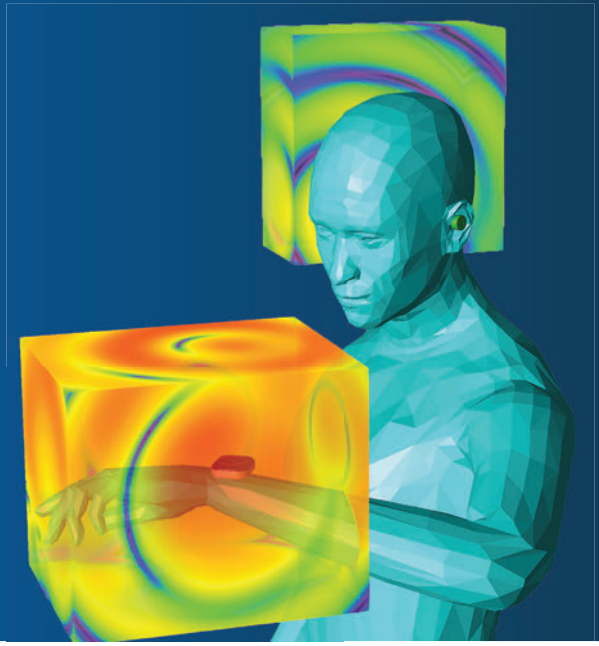

Electromagnetic Simulation Software from Remcom

Remcom's Huygens surface capability incorporates near-field antenna effects into simulations of antenna performance so that mobility, multipath, and interactions with body-worn devices may be analyzed in realistic environments.

- GNSS positioning
- NASA Artemis Program
- Body Area Networks (BANs) and sidelink communications
- 5G/6G connectivity for UAVs, automotive, and robotics

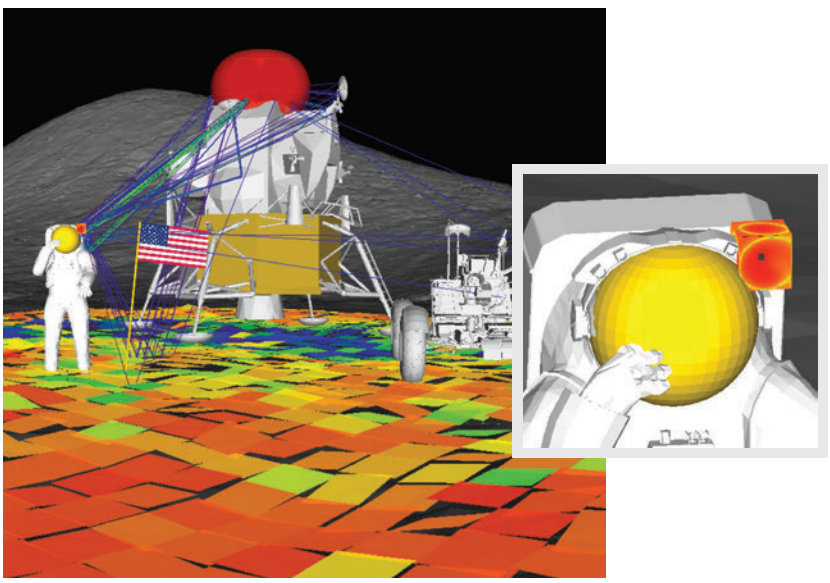

RF Digital Twin of Apollo 15 Mission: Wireless InSite simulation of coverage and multipath from an antenna mounted on the lunar lander to a near-field Huygens antenna on the astronaut's helmet.

Learn more at | **www.remcom.com/animate-on-body** ›››

For 30 years Remcom's software has enabled the world's most advanced engineering teams to deliver their devices to market.

+1.888.7.REMCOM (US/CAN) | +1.814.861.1299 | **www.remcom.com**

losses, as touched on above. In the case of a transceiver, the polarizer, OMT and feed horn are integrated, minimizing losses, whereas these are separate components when using discreets. As the signal passes from one stage to the next, losses will be introduced at each interface. Typically, this introduces a loss of approximately 0.3 dB. This integration reduces this value. Reducing losses and the number of elements the signal passes through will improve both the antenna gain-to-noise temperature ratio (G/T) and effective isotropic radiated power. This ultimately results in better performance.

In addition to simplifying the cabling and spares, using a transceiver dramatically reduces the physical space required, as shown in ***Figure 2***. This is particularly important for comms-on-the-move or other applications where space is a premium. Of course, fewer parts and fewer cables also make setup much easier and more efficient. Again, for comms-on-the-pause applications, especially in a defence setting, being able to set up quickly is an absolute must. In defence, it is not feasible to connect multiple parts, especially if they need to be connected in a specific order, as they will often be set up quickly and in challenging conditions.

Involving fewer components also brings the mean time between failure down. Additionally, in the integrated system, polarity switching is internal and automatic, making it easy to switch to a different frequency band or satellite with lower risk of error.

Another benefit of an integrated system is fewer exposed components. It is well known that RF solutions can be impacted by environmental elements, such as rain, snow, dust or ice. In some cases, this can be immediately detrimental; in others, it can simply shorten the equipment's lifespan. Therefore, it is valuable to prevent external elements from entering or affecting the electronics.

Flexibility Versus Accountability

Despite the benefits of integrated systems, there are downsides to consider. For example, if something fails, the entire transceiver must be replaced rather than a smaller component. This is the biggest deterrent to the integrated approach; however, it is rare in well-designed, thoroughly tested transceivers.

Furthermore, with discreets, because the parts are separate, users can choose to build the system to their requirements, selecting different vendors for each part and choosing those vendors based on the performance and quality of each individual component. This can provide greater flexibility in purchasing choices; however, it also introduces complexity and may pose interoperability challenges.

The most common scenarios where engineers choose discreets over transceivers are when they require high power. These use cases are limited, but there are key cases, such as transmitting to multiple

RF-LAMBDA

THE LEADER OF RF BROADBAND SOLUTIONS

EUROPE DEUTSCHLAND

RF SWITCHES

MM / MICROWAVE DC-90GHz

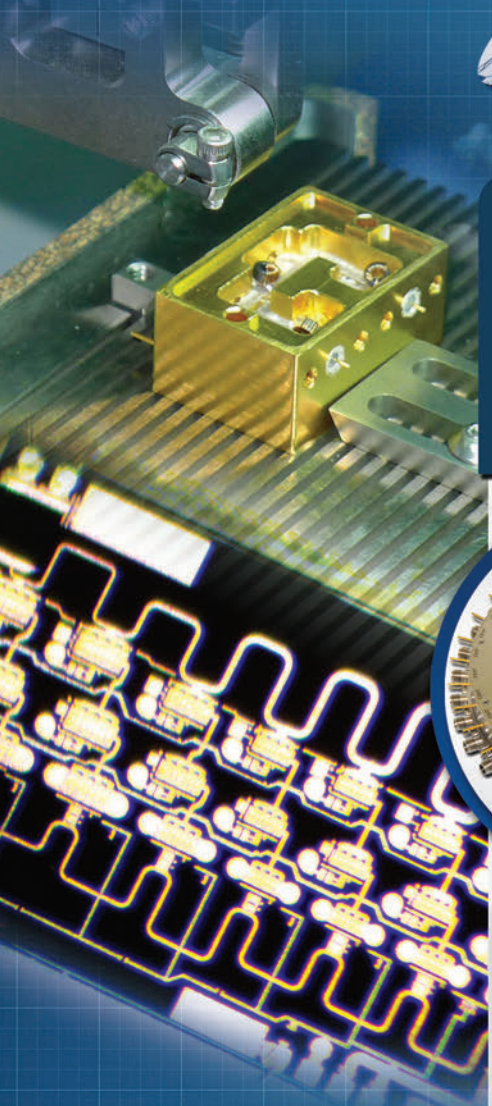

160 CHANNELS
mm/Microwave

0.05-20GHz
Filter Bank Switch Matrix
For Phase Array Radar Application Satellite communication.

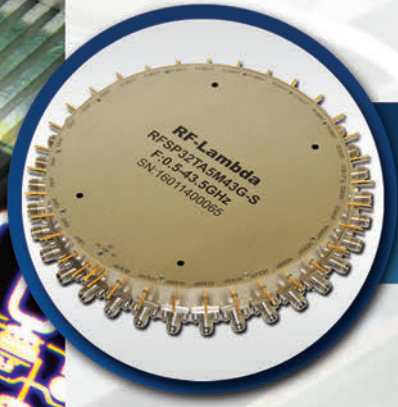

PN: RFSP32TA5M43G
SP32T SWITCH 0.5-43.5GHz

PN: RFSP16TA5M43G
SP16T SWITCH 0.5-43.5GHz

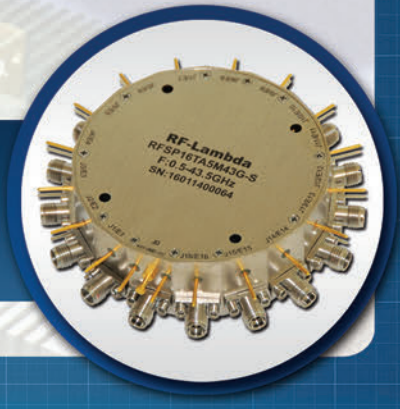

www.rflambda.com
sales@rflambda.com

1-888-976-8880
1-972-767-5998

San Diego, CA, US
Plano, TX, US
Ottawa, ONT, Canada
Frankfurt, Germany

carriers, where the power is being spread across multiple bandwidths, requiring more total power to distribute over each carrier. In most cases, satellite terminals operate with a single modem and a single carrier, but not always. For example, command posts for networks providing connectivity between teams and back to headquarters become more of a hub than a satellite terminal. This is most common in rapid-deployment scenarios, such as during a disaster. For instance, during a forest fire, teams must be quickly deployed around the affected areas. At the same time, they need to be connected to each other and any centralised operations to share intelligence. Another such scenario might involve a large forward-operating base in the defence sector. There are a couple of ways to handle this, including implementing multiple antenna systems in place, or using a bigger, powerful BUC and integrating multiple carriers.

Using a transceiver integrates multiple complex functions of the RF chain into one product, thereby lowering procurement, testing and assembly costs. The integrated system will have been developed by a single vendor. On the one hand, that removes the flexibility to pick and mix different elements from different vendors. However, on the other hand, that makes a single vendor accountable, simplifying the process of addressing any errors that might arise.

Transceivers themselves are flexible, allowing for simple and automatic polarity switching as mentioned. This makes it easy to change frequency band, satellite or orbit.

Fighting Gravity

Because discreets have more parts connected to the antenna, they are generally offset from the antenna's centre. This significantly affects the system's weight balance. Transceivers are typically mounted on the opposite side to the feed, which keeps them close to the centre and makes the system axis symmetric, as shown in ***Figure 3***. The closer to the centre you can position the RF elements, the less impact of the pull of gravity. In systems where elements are less central and are pulled downward, there is often strain on the motors, which can lead to frequent replacement. Improving the balance of the entire system is therefore likely to make the individual elements more robust and last longer.

Selecting the Right Product for the Application

Ultimately, the choice between transceivers or discreets will come down to a few factors, as shown in ***Table 1***. As mentioned, the power level is a key factor. It may also depend on the existing setup and whether the user needs to replace a single element. However, for new systems, transceivers can deliver enough power to be comparable with discreets in most applications. Transceivers can provide a neat and integrated solution that is easier to set up, is more resistant to the elements and has reduced signal losses due to fewer cables and parts to negotiate. ■

Featuring Keynotes • Technical Sessions • Workshops

EDI CON Online delivers essential technical training and information directly to engineers' desktops and mobile devices. Enjoy free, real-time training with simple registration and easy access.

EDI CON ONLINE

EDUCATIONAL DAYS

NOW AVAILABLE ON DEMAND

5G/6G, IoT, Radar/Automotive/SATCOM

SI/PI/PCB/Interconnect/EMI

EDICONONLINE.COM

Organized by horizon house

Official Publications

Microwave Journal

Signal Integrity Journal

INVITED PAPER

AI-Powered Digital Post-Distortion: Enabling Energy-Efficient 6G Uplink Communications

Andreas Oeldemann
Rohde & Schwarz, Munich, Germany

Dani Korpi
Nokia Bell Labs, Espoo, Finland

In cellular uplink scenarios, particularly at cell edges where signal strength is weakest, user equipment (UE) faces a fundamental tradeoff: operate the power amplifier (PA) efficiently near saturation, introducing severe nonlinear distortions, or back off to linear regions at the cost of reduced power efficiency and shorter battery life. This challenge intensifies as modulation orders increase. While 5G New Radio (NR) currently supports up to 256-QAM in the uplink, 6G research is exploring 1024-QAM and beyond to achieve the multi-gigabit data rates envisioned for next-generation applications.

Traditional digital predistortion (DPD) addresses PA nonlinearities at the transmitter, requiring sophisticated signal processing, feedback loops and PA characterization circuits that add complexity, cost and power consumption to user devices. For resource-constrained smartphones, IoT sensors and wearables, coping with this overhead becomes particularly challenging. Digital post-distortion (DPoD) fundamentally reverses this paradigm. Rather than the transmitter compensating for its own distortions, the receiver, which is typically a base station with more computational resources, performs the compensation. This architectural shift enables the UE to operate with simpler, power-efficient transmitters while maintaining link performance. This also enables the UE to resort to higher transmit powers when necessary.

The emergence of AI-powered DPoD techniques represents a step change beyond classical signal processing approaches. While traditional DPoD methods rely on predetermined mathematical models such as polynomial functions, AI-powered implementations leverage neural networks and machine learning (ML) to optimize compensation strategies directly from observed signals. The adaptability of AI-enhanced receivers becomes advantageous as 6G systems encounter increasingly complex scenarios, including the frequency range 3 (FR3) band, massive MIMO with many antenna elements and dynamic channel conditions that defy classical modeling approaches.

DPOD FUNDAMENTALS

The Nonlinearity Challenge in Modern Uplinks

PAs exhibit nonlinear behavior characterized by amplitude-dependent gain compression (AM-AM conversion) and phase distortion (AM-PM conversion). When driven near saturation to maximize efficiency, these nonlinearities become severe, introducing in-band distortion that degrades error vector magnitude (EVM) and out-of-band spec-

The right technology at the right time.

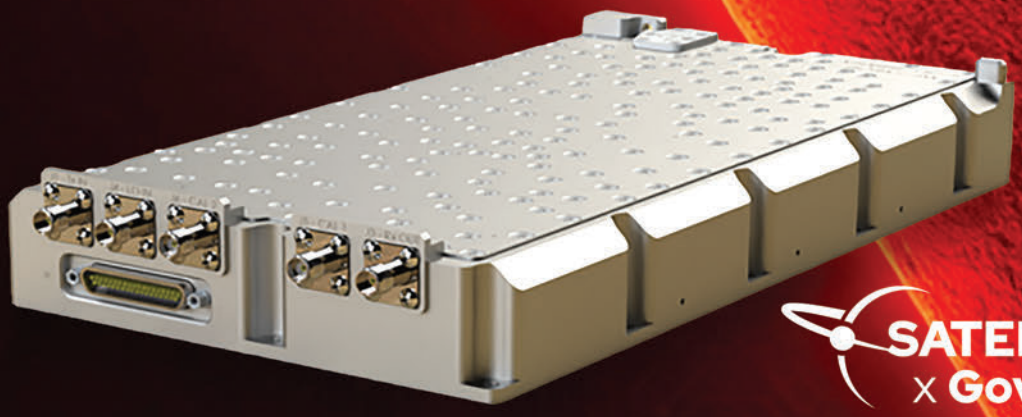

SATELLITE x GovMilSpace

VISIT US AT BOOTH #1631

At **KRATOS General Microwave**, we pioneer advanced microwave solutions tailored for the evolving needs of both traditional and the competitive "New Space" markets.

Whether supporting Low Earth Orbit (LEO), Medium Earth Orbit (MEO) or Geostationary Orbit (GEO) missions, our space-qualified products—such as Up/Down Converters, Frequency Synthesizers, Transmit/Receive Modules and many more — redefine reliability, efficiency and precision.

With a focus on delivering the best cost-performance combination, our solutions are designed to excel in both traditional space applications and the rapid timelines of "New Space" ventures. We ensure fast development cycles and uncompromising performance to meet your mission-critical needs.

Partner with **KRATOS General Microwave** to power your systems, long term partnership and drive the next era of space innovation.

FOR MORE INFORMATION, PLEASE CONTACT US: kratosmed.com/gmspace

KRATOS | General Microwave
Microwave Electronics Division

KRATOS®
READINESS DELIVERED

tral regrowth that violates emission masks.

For orthogonal frequency division multiplexing (OFDM) signals, high peak-to-average power ratio (PAPR) exacerbates this problem, as occasional high-amplitude peaks drive the PA into compression. DFT-spread OFDM (DFT-s-OFDM) was adopted in 5G uplink for its lower PAPR characteristics, which partially mitigates this. However, as modulation order increases to 256-QAM and beyond, even DFT-s-OFDM signals develop sufficient PAPR to cause distortion when amplifiers operate at high efficiency.

Why Receiver-Side Compensation?

DPoD relocates nonlinear compensation from the transmitter to the receiver, delivering several key advantages:

- **Energy Efficiency at the UE:** Removing DPD circuitry from the transmitter eliminates power-hungry feedback loops, observation receivers and real-time adaptation algorithms. These result in lower power consumption and reduced complexity, which extend battery life and ease thermal management requirements.
- **Centralized Computational Resources:** Base stations can leverage high performance CPUs, GPUs or dedicated AI accelerators to run sophisticated compensation algorithms without the size and power constraints faced by battery-powered UE.
- **Adaptive Learning:** AI-powered receivers can continuously learn from diverse user transmissions, covering varying PA characteristics, channel conditions and other impairments, to develop adaptive compensation strategies that can outperform traditional fixed-parameter approaches.
- **Relaxed Transmitter Specifications:** If receivers can reliably compensate for transmitter distortion, transmitter EVM requirements can be relaxed, enabling simpler, more energy-efficient PA designs that can operate closer to saturation for improved power efficiency and lower cost. On the downside, this can lead to out-of-band emissions due to spectral regrowth, therefore potentially reducing spectral efficiency.
- **Introducing Additional Flexibility:** Effective impairment compensation at the receiver side will facilitate more flexible UE operation and transmission signal quality. The UE can transmit uplink signals under different operating points, depending on its capabilities and the requirements of the network. In some cases, the UE can transmit very clean signals, and no receiver-side compensation is necessary. In some other cases, higher overall performance is achieved if the UE is allowed to transmit a distorted signal, which is corrected by the receiver.

TECHNICAL IMPLEMENTATION OF AI-POWERED DPOD

AI-powered DPoD solutions employ deep neural networks trained on representative data to learn how to compensate for both transmitter impairments and channel impairments. Various architectures have been explored, including Nokia Bell Labs' HybridDeepRx, a convolutional neural network (CNN)-based receiver tailored to address nonlinear impairments.[1]

This receiver builds on alternating between frequency and time-domain processing, extracting the benefits of both. That is, the model performs channel compensation and symbol-to-bit demapping with the frequency-domain layers, while the time-domain layers facilitate effective mitigation of amplifier-induced distortion.

Figure 1 illustrates the model architecture, with emphasis on the physical layer processing chain. The OFDM-modulated waveform is transmitted using a nonlinear PA. This results in compression of the transmitted signal, introducing distortion. Upon reaching the receiver, the signal will also have experienced multipath fading from the wireless channel.

In the receiver, the signal is first

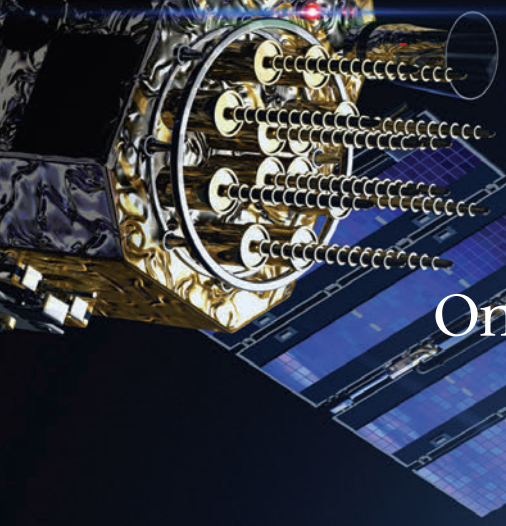

Performance.
Precision.
On the Ground, in the Air.
And Beyond.

See what we've been up to!

Space-Qualified

New Products

T32 Series TCXO

Since 1961, Greenray Industries has been a preferred provider of precision, high performance reference sources to many of the world's leading aerospace, defense and industrial manufacturers.

With a range of critical design innovations that enhance product performance and reliability, our quartz crystal oscillators help RF engineers realize their unique frequency control solutions.

On the ground, in the air – and beyond.

GREENRAY

LEO, MEO & Deep Space + Radar + SATCOM + Telemetry + Airborne & Mobile Communications + Smart Munitions + GPS

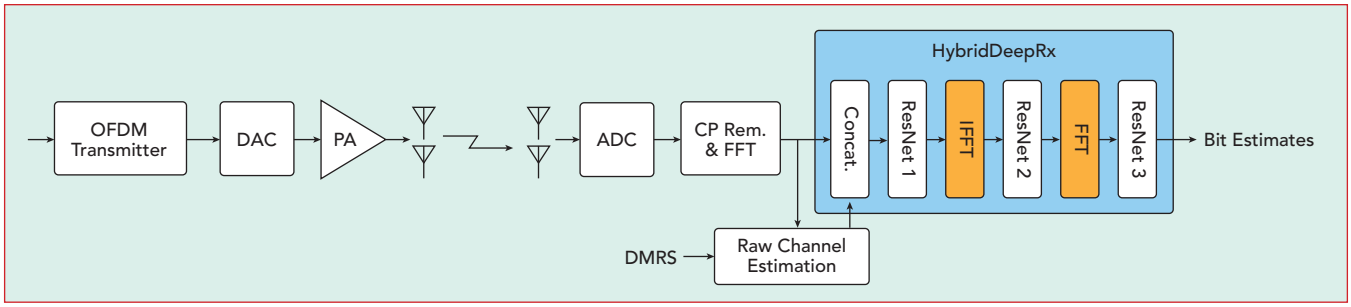

Fig. 1 **The HybridDeepRx AI receiver.** ***Source:*** **Nokia.**

OFDM demodulated through CP removal and fast Fourier transform (FFT), and a raw channel estimate based on the known pilot symbols is calculated. Then, the frequency-domain received signal and the raw channel estimate are concatenated and fed to the HybridDeepRx AI receiver. The model has its first ResNet section in the frequency domain, which it uses to compensate for the linear channel effects. After this, an inverse FFT (IFFT) is used to transform the ensuing latent signals to the time domain, where the model uses another set of ResNet blocks to compensate for the nonlinear distortion. Finally, another FFT is used to transform the latent signal back to the frequency domain, where a third set of ResNets is used to extract the log-likelihood ratio (LLR) estimates.

The training process of such an AI-driven receiver requires large datasets of paired transmitted bits and received signals collected across diverse channel conditions and PA operating points. The AI receiver model is trained as a whole, meaning that the only criterion is the accuracy of the output LLRs. Therefore, it is not possible to say conclusively what is done at which point of the receiver, although some rough deductions are of course possible (as done above).

Fig. 2 **HIL testbed to test Nokia Bell Labs' HybridDeepRx.**

While synthetic data can be used for training such a model, hardware-in-the-loop (HIL) testbeds are essential for validating AI model performance. Nokia uses Rohde & Schwarz's HIL testbed to validate the HybridDeepRx AI receiver.

EVALUATING AI-POWERED 5G RECEIVERS WITH HIL TESTING

To evaluate Nokia Bell Labs' HybridDeepRx under real-world conditions to test whether the AI-based receiver compensates for channel impairments and nonlinear PA distortion in 5G uplink signals, an HIL testbed was used. ***Figure 2*** shows the testbed, which leverages Rohde & Schwarz test and measurement solutions for signal generation, channel emulation, signal analysis and AI model inference.

An uplink scenario in which a mobile transmitter induces nonlinear distortion is evaluated by operating its PA near saturation. The HybridDeepRx AI receiver replaces the

MilliBox®
ANTENNA TEST SYSTEMS

Compact · Modular · Affordable

MMWAVE AND SUB-THZ OTA TEST SYSTEMS

OTA your Way !

Compact anechoic chambers
6GHz to 330GHz
Modular design
Many sizes & configurations
30cm to 3m far-field

3D DUT positioners
<0.1° absolute resolution
Open Python SW controller
Up to 3 rotation axes
Many sizes & types available

Ideal benchtop placement
Below deck instrument bays
Shorter wiring

Integrate with existing instruments
Many plot types included
Unlimited automation

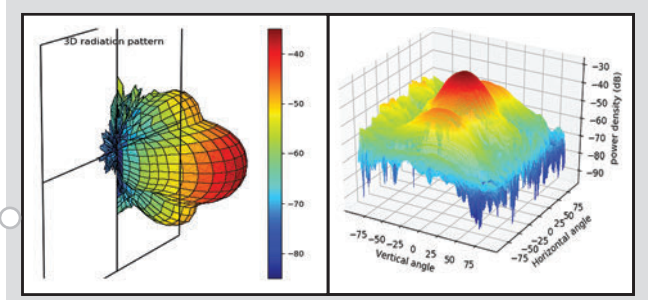

More Info

MilliBox
millibox@milliwavess.com
+1.408.892.9595
millibox.org

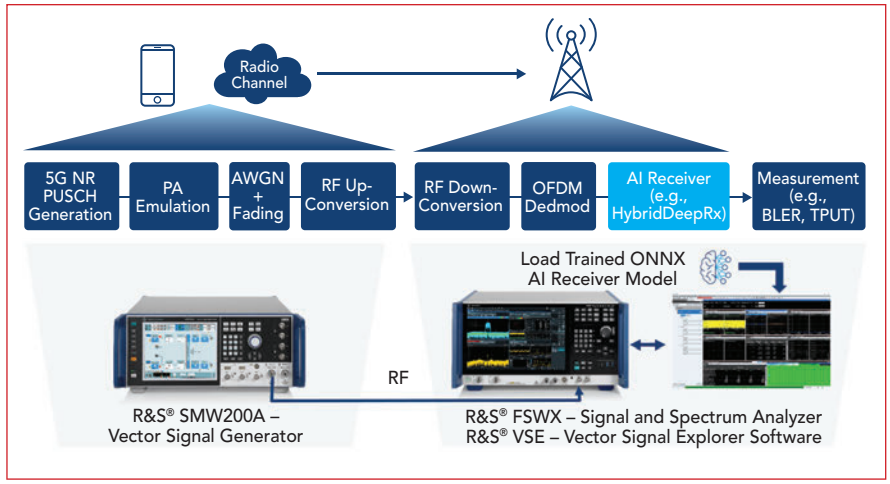

Fig. 3 **HIL AI Receiver testbed based on R&S SMW200A VSG, FSWX and VSE signal and spectrum analysis solutions.**

conventional OFDM receiver chain at the base station. ***Figure 3*** provides an overview of the testbed.

Testbed Components and Configuration

Signal Generation: An R&S SMW200A vector signal generator (VSG) produces the standard-compliant 5G uplink signal. Channel emulation capabilities introduce realistic fading and noise. Crucially, a PA model is applied to the generated waveform before the wireless channel to emulate the nonlinear distortion introduced by the PA at different operating points.

- **5G Waveform Generation:** The VSG forms the transmit side of the testbed. It generates a 5G NR uplink signal, configurable to emulate typical mobile device transmissions.
- **PA Emulation:** A key feature of the testbed is the ability to model the nonlinear behavior of a PA during signal generation. Instead of a physical PA, a mathematical model representing it is applied to the waveform that is transmitted by the R&S SMW200A. This allows controlled introduction of PA impairments without requiring an actual PA unit. The PA back-off setting, controlling the distance from saturation, is a crucial parameter for varying the level of distortion. This PA modeling approach allows researchers to rapidly iterate through different PA characteristics without requiring physical hardware changes, accelerating the development cycle.
- **Channel Emulation:** The R&S SMW200A incorporates channel emulation capabilities. This emulates the effects of the wireless propagation channel on the transmitted signal, adding realistic impairments. Configurable channel profiles can represent different deployment scenarios (urban, rural, etc.). The channel emulator can also be fed with wireless channel data generated in site-specific RF digital twins, for example, leveraging raytracing technology.
- **Signal Output:** The impaired 5G signal is output from the VSG and fed directly to the receive side of the testbed.

Signal Analysis and AI Inference: An FSWX signal and spectrum analyzer, paired with Vector Signal Explorer (VSE) software, both from Rohde & Schwarz, captures the impaired 5G uplink signal. The R&S VSE has been extended to load and execute custom AI receiver models, enabling inference of user-defined AI models directly within the measurement application.

- **Signal Capture:** The FSWX signal and spectrum analyzer captures the received, impaired 5G signal. Its wide bandwidth and high dynamic range ensure accurate signal acquisition.
- **VSE Software:** R&S VSE is the central control and measurement application. It performs several critical functions:
  - Demodulation and Baseband Processing: R&S VSE performs the initial demodulation of the

SPECTRUM UNLIMITED: FREQUENCY REUSE BY BEAMFORMING

SEEING IS BELIEVING

4-BEAM 4 WEEKS ACTUAL RESULTS

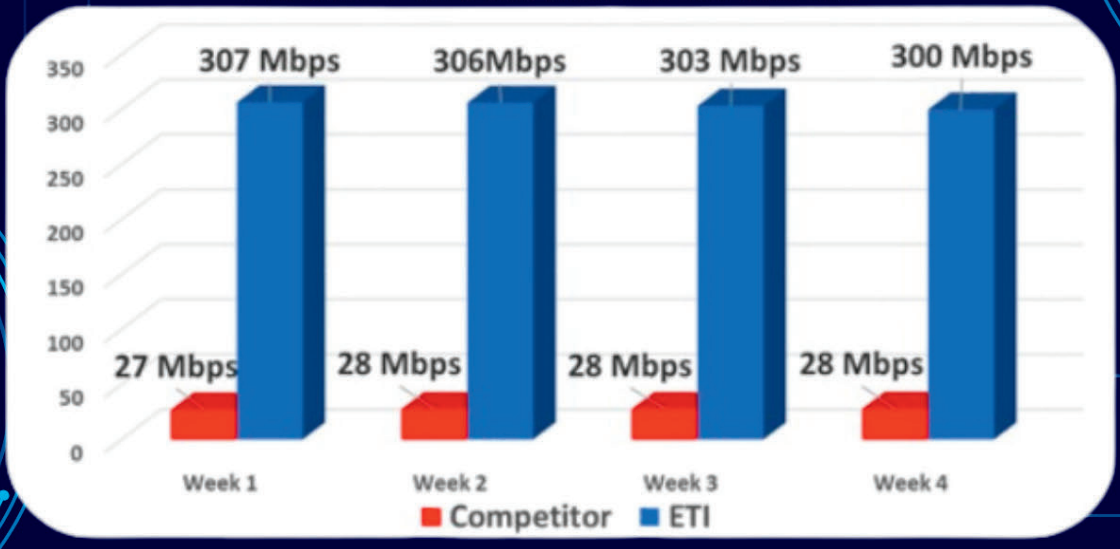

10 TIMES INCREASE OF SPEED!

SAME CHANNEL PER BEAM!

- LOW COST MULTI-BEAM ANTENNA SYSTEM
- NO ELECTRICITY COST
- NO SOFTWARE REQUIRED
- UP TO 2048 BEAMS PER SECTOR
- REPETITION OF TOTAL AVAILABLE SPECTRUM
- INCREASE CUSTOMER BASE UP TO 2048 TIMES

CATCH US IF YOU CAN...

et industries

WWW.ETIWORLD.COM | +1 (973) 394-1719 | SALES1@ETIWORLD.COM

5G signal, bringing it down to baseband.

- AI Model Loading and Execution: This is where the HybridDeepRx AI model is integrated. R&S VSE is specifically extended to support loading user-defined AI models provided in the open neural network exchange (ONNX) format.
- Neural Network Inference Engine: R&S VSE utilizes a GPU-accelerated inference engine to execute the HybridDeepRx model on the captured signal data. This includes calculations within the CNN and residual network architectures in both time and frequency domains.
- Configuration Flexibility: Users can configure specific sections of the receiver chain to utilize either the AI model (HybridDeepRx) or the conventional 3GPP algorithms for channel estimation, equalization and demapping.
- KPI Measurement: R&S VSE calculates key performance indicators (KPIs) such as block error rate, throughput and bit error rate. These metrics quantify the receiver's performance.

AI Model Integration and HybridDeepRx Processing: The HybridDeepRx model is loaded into VSE via an ONNX interface. The VSE utilizes GPU acceleration for neural network inference. It performs joint channel estimation, equalization and demapping. The configuration can switch between the neural-network-based demapper and a conventional 3GPP-compliant implementation.

- **Time/Frequency Domain Translation:** The model leverages FFTs and IFFTs to switch between frequency and time-domain processing, facilitating more accurate distortion mitigation.
- **Joint Estimation, Equalization and Demapping:** Unlike traditional receivers, HybridDeepRx performs these functions jointly within the neural network, improving overall detection accuracy.

Multi-Port Phase-Coherent Measurements

DPoD validation in MIMO systems requires observing signals across multiple antennas with precise phase relationships. The FSWX's multi-port architecture, the first signal and spectrum analyzer with this capability, provides up to two 4 GHz bandwidth paths with phase-coherent measurements. This enables several critical capabilities for DPoD research:

- **Simultaneous PA Characterization:** The FSWX measures amplifier input and output concurrently, capturing both frequency-domain spectral regrowth and time-domain constellation distortion in a single acquisition (see ***Figure 4***).
- **Phased Array Validation:** Users can verify beamforming performance across multiple antenna elements with maintained phase coherence.
- **True MIMO Analysis:** The FSWX observes spatial signal characteristics essential for understanding how nonlinear distortion propagates through MIMO channels.

The FSWX also offers cross-correlation capability, which represents a breakthrough in measurement sensitivity. By internally splitting a signal into independent paths and correlating the results, the analyzer effectively cancels its own noise floor, improving dynamic range by up to 15 dB in spectral measurements and up to 6 dB for in-band measurements. As ***Figure 5*** illustrates, this proves particularly valuable when measuring signals near or below the analyzer's native noise floor, such as characterizing receiver sensitivity or evaluating DPoD performance at cell edge conditions where signal-to-noise is marginal. For EVM measurements of high-order modulation (256-QAM, 1024-QAM), this extended dynamic range is essential for distinguishing true signal impairments from measurement system noise.

Wide Bandwidth Analysis for Beyond 5G Research

Looking toward 6G, the FSWX is also positioned for FR3 (7 to 24 GHz) research thanks to its internal analysis bandwidth up to 8 GHz. While current 5G NR specifies bandwidths up to 400 MHz in FR2, 6G research explores multi-gigahertz continuous signals to understand wideband

HIGH FREQUENCY Components

PPI
Passive Plus
RF & Microwave Components

HIGH QUALITY
RF/MICROWAVE PASSIVE COMPONENTS FOR HIGH FREQUENCY APPLICATIONS

Fundamental in radar systems and antennas, PPI components are indispensable for optimizing signal integrity, efficiency, and performance across high frequencies.

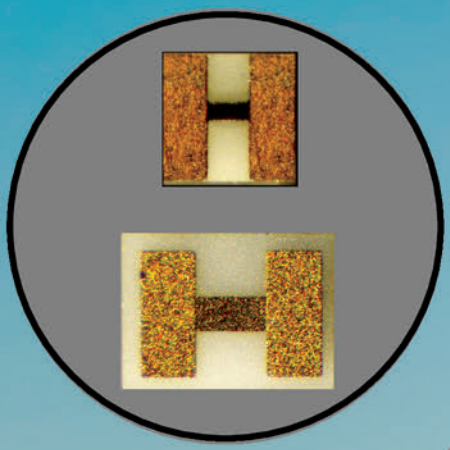

- **Broadband Capacitors**
  5 case sizes, 10nF & 100nF
  up to 67 GHz
- **Broadband Resistors**
  1209 & 2010 sizes
  up to 67 GHz
- **Broadband Conical Inductors**
  Flying Leads & SMT
  up to 110 GHz

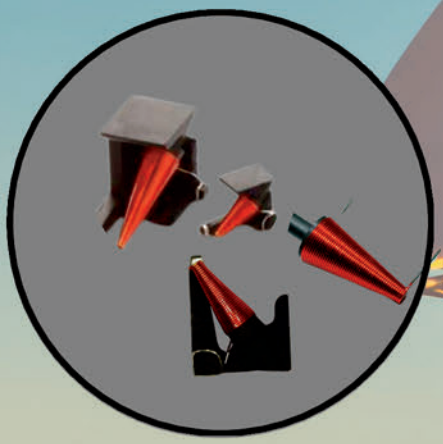

Reach out for availability

www.passiveplus.com
+ (631) 425-0938
sales@passiveplus.com

channel effects and develop appropriate channel models. With its advanced filter banks (replacing traditional YIG preselectors) and broadband analog-to-digital converters, the FSWX enables clean, wideband captures without artifacts, which are expected to prove helpful for evaluating AI-enhanced receivers operating across these extreme bandwidths.

Fig. 4 **Screenshot from FSWX showing dual-channel measurement of amplifier input and output.**

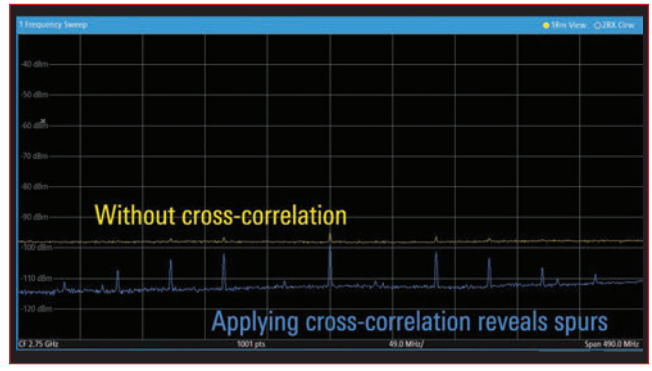

Fig. 5 **Cross-correlation capability revealing signals below the noise floor.**

AI Inference in Measurement Flow

Integrating neural network inference into measurement systems requires computational infrastructure that traditional test equipment typically lacks. The VSE software can run on a standard PC and supports loading ONNX models and running GPU-accelerated inference, effectively bridging the gap between ML frameworks (e.g., PyTorch, TensorFlow) and RF measurement systems. This capability allows researchers to iterate rapidly, train models on captured or simulated data, deploy to hardware for validation, collect new measurements and refine training — closing the development loop without requiring custom hardware or extensive system integration.

CONCLUSION

AI-powered DPoD fundamentally redefines the receiver's role in wireless systems, shifting it from passive signal recovery to active compensation for transmitter impairments. By leveraging base station computational resources and ML capabilities, DPoD can enable UE to use simpler, more energy-efficient transmitters while compensating for impairments at the receiver.

As the industry moves towards 6G, AI-driven DPoD is more than an incremental improvement. It typifies a broader shift to intelligent, adaptive network infrastructure that learns and optimizes rather than relying solely on predetermined algorithms. Equally important is the test and measurement ecosystem that enables this transition; advanced multi-port analyzers with AI inference capabilities will be vital to both research and practical deployment.

Advancing this vision requires sustained collaboration among algorithm developers, semiconductor vendors, network-equipment manufacturers, standards bodies and test and measurement providers. Success will be measured not merely by laboratory demonstrations but by real-world deployments in which billions of heterogeneous devices enabled by intelligent transmitters and AI-powered receivers deliver unprecedented gains in spectral and energy efficiency. ■

Reference

1. J. Pihlajasalo et al., "Deep Learning OFDM Receivers for Improved Power Efficiency and Coverage," *IEEE Transactions on Wireless Communications*, Vol. 22, No. 8, Aug. 2023, pp. 5518–5535.

OPHIR RF

High Power RF Systems

CLASS A LINEAR • 5-YEAR WARRANTY

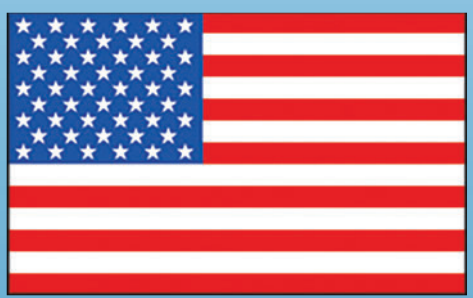

DESIGNED AND MANUFACTURED IN THE USA
SINCE 1992!!

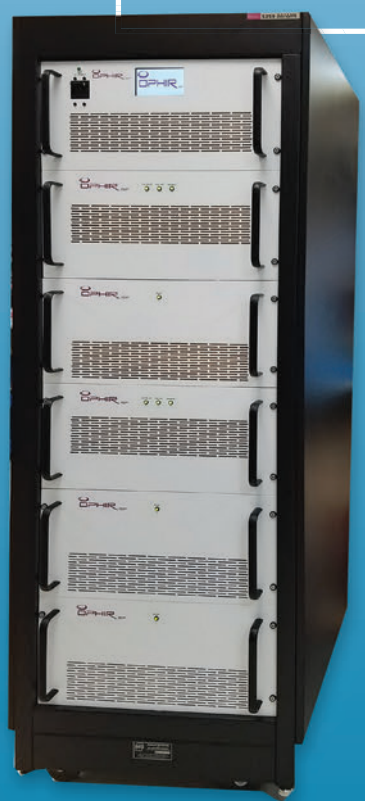

0.01-225MHz 5kW

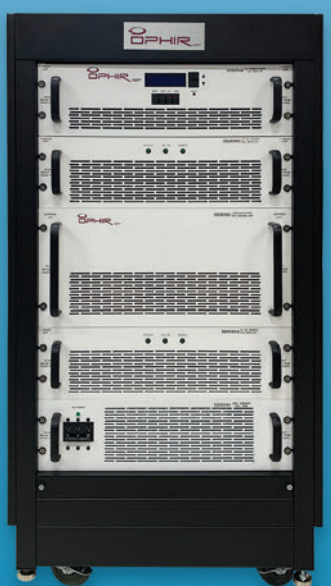

80-1000MHz 2kW

1.0-6.0GHz, 500W

6.0-18GHz, 250W

www.OphirRF.com
(310) 306-5556

Wideband High Gain Antenna Design Based on Multilayer Artificial Magnetic Conductor

Huanhuan Qi, Genyuan Du, Xiangqun Zhang and Yajing Yuan
Xuchang University, Xi'an, China

A wideband multilayer artificial magnetic conductor (AMC) structure comprises five periodic patch layers printed on different dielectric substrates with varying dielectric constants. The AMC structure is used as a ground plane for a printed wideband antenna to improve its gain. Over a 4.5 to 7.5 GHz 10 dB impedance bandwidth, its average gain exceeds 8 dBi with a maximum gain of 12 dBi.

In recent years, wideband antenna design has been a research focus with the rapid development of modern wireless communications.[1] Many designs have been proposed, such as a quasi-Yagi antenna that can have a 75 percent impedance bandwidth[2] and an L-probe feed patch antenna that can achieve an impedance bandwidth of 36 percent.[3] The gains of these antennas, however, are not very high, which limits their application.

To address this, much attention has been focused on metamaterials for metasurfaces,[4,5] lenses,[6] frequency selective surfaces (FSSs)[7] and AMCs.[8-12] For the AMC structure, a plane wave is reflected in-phase (between -90 and +90 degrees) rather than out-of-phase, as occurs on the surface of a perfect electrical conductor (PEC). Since the reflected phase of an AMC does not cause destructive interference between direct and reflected waves, many researchers have adopted it to improve antenna gain and directivity.

Scarborough et al.[8] employed an E-plane coupled closely-packed microstrip patch array loaded with a group of mushroom-like electromagnetic band gap (EBG) structures to effectively decrease lateral and backward radiation patterns by 13.19 dB and 7.76 dB, respectively. Mushroom-like structures can be considered as AMCs to replace the ground plane of an antenna to improve antenna gain and directivity.[13-15] However, for the mushroom-like structure, which provides shorted left-handed stub inductors through metallic via holes, large currents concentrated around the vias generate considerable loss, which degrades gain and radiation efficiency.[16] Fabrication of the structure is complex as well, increasing the antenna cost.

To decrease electromagnetic loss and simplify fabrication, the use of periodic patch-like mushroom structures has been attempted, named by some as patch-type AMC structures,[16-19] which have the same characteristics of in-phase reflection as mushroom-like structures and are insensitive to the electromagnetic wave incident angle.[20] However, because the AMC surface operates as a resonant mechanism, an antenna loaded with a monolayer AMC surface often exhibits a narrow bandwidth, which limits its practical application.

In this work, alternative and improved strategies are explored to address wideband gain enhancement. First, a new design methodology for constructing a multilayer AMC structure is introduced to broaden the

ERZIA

NEW SPACE

COTS Amplifiers Ready for Launch

Join us at

SATSHOWWEEK

BOOTH 3122

WWW.ERZIA.COM

in-phase reflection bandwidth. By using different dielectric constants and optimized patch sizes, the in-phase reflection bandwidth is significantly increased. Next, a wideband planar antenna with an impedance bandwidth from 3.8 to 7.5 GHz is designed. Finally, the multilayer AMC structure is employed as the antenna's ground plane to enhance gain.

Prototype antenna measurements confirm the multilayer AMC's performance. Due to the wideband in-phase reflection characteristics of the AMC, the antenna's average gain is significantly improved to greater than 9 dBi from 4.5 to 7.5 GHz, peaking at 12 dBi.

MULTILAYER AMC STRUCTURE

The in-phase reflection bandwidth of the AMC surface is a design focus issue, important for its application. To expand the bandwidth, the phase property is investigated. Although numerical experimental data through parametric analysis has been provided,[9] the theoretical basis is not adequate. Theoretical analysis of the reflection phase is given in detail here.

Assuming the incident wave penetrates on AMC surface, the phase delay Φ_d through the AMC structure is determined by calculating the ratio of the reflected (b_n) and incident (a_n) fields and is calculated with ***Equations 1*** through ***5***:

$$\phi_d = \angle \frac{b_n}{\alpha_n} = \angle \frac{\tau_1 \tau_2}{e^{jkt}\left(1 + \rho_1 \rho_2 e^{-2jkt}\right)} \quad (1)$$

$$\rho_1 = \frac{\eta - \eta_0}{\eta_0 + \eta} \quad (2)$$

$$\rho_2 = \frac{\eta_0 - \eta}{\eta_0 + \eta} \quad (3)$$

$$\tau_1 = \frac{2\eta}{\eta_0 + \eta} \quad (4)$$

$$\tau_2 = \frac{2\eta_0}{\eta_0 + \eta} \quad (5)$$

Where, τ_1, τ_2 and ρ_1, ρ_2 are the intrinsic transmission and reflection coefficients, respectively; η_0 and η are the intrinsic wave impedances of the air and dielectric regions, respectively; τ is the thickness of the substrate; ε_r is its dielectric constant and k and λ_r are the wave number and wavelength in the dielectric, respectively. By simplification, the phase delay in the AMC structure can be calculated with ***Equations 6*** and ***7***:

$$\phi_d = \tan^{-1}\left(\frac{1 + \varepsilon_r}{2\sqrt{\varepsilon_r}} \tan(kt)\right) \quad (6)$$

$$k = \frac{2\pi}{\lambda_r} \quad (7)$$

The patch-type AMC structure at resonance is equivalent to an LC parallel resonant circuit. The structure resonates within the frequency range where high impedance and in-phase reflection are met. The surface impedance of the patch structure is formulated in Equation 8:

$$Z_S = \frac{j\omega L}{1 - \omega^2 LC} \quad (8)$$

Where C and L are the equivalent capacitance and inductance given by Equations 9 and 10, respectively, determined by the patch width a, gap g, the thickness t and the permittivity of the substrate.[21]

The phase characteristic is mainly determined by the dielectric constant ε_r and the thickness τ. The size of the patch also has some effect. To broaden the bandwidth of the in-phase reflection, the thickness of the substrate can be changed. However, if the substrate is too thick to be found in nature, it cannot be applied. Dielectric loss should be considered at microwave and higher frequencies as well.

Another way of changing the dielectric constant is considered. In this work, a multilayer AMC structure is proposed. On one hand, a different dielectric constant for each layer is used to change the effective dielectric constant and broaden the bandwidth of in-phase reflection. On the other hand, the overall thickness is also changed with the multilayer structure. Furthermore, as air is filled between the layers, dielectric

MiCable

0.6~6GHZ
SURFACE MOUNT 90° HYBRID

Application Power Amplifier, Power Combining Network, Antenna Feed Network, Modulator & Phase Shifter

High Power Handling
50W

Low VSWR/I.L.
High Isolation

Excellent Amplitude & Phase Unbalance

Small Case Style
High Performance & Cost-Effective

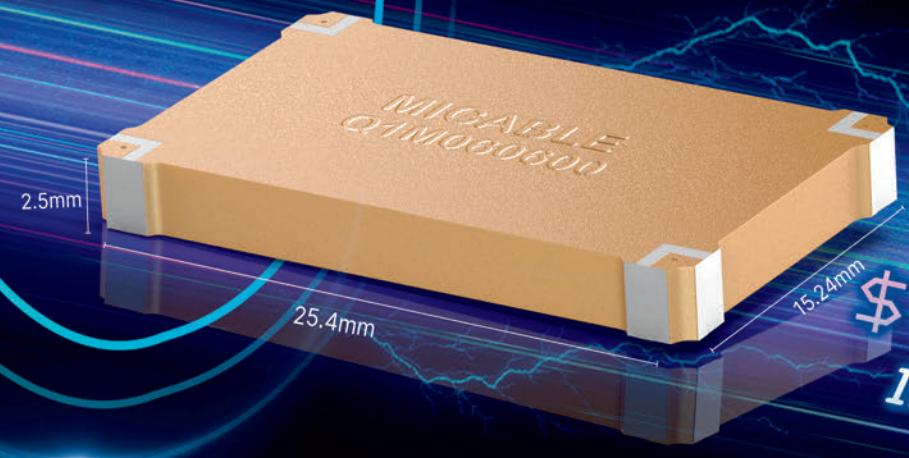

$58.45 10-49 pcs
IN STOCK

Freq. Range (GHz)	P / N	Nominal Phase Unbal. (Deg.)	Ports VSWR Max. (:1)	Insertion Loss* Max. (dB)	Amplitude Unbal. Max. (dB)	Phase Unbal. Max. (Deg.)	Isolation Min. (dB)	Power Max. (W)
0.6-6	Q1M060600	90	1.4	1.2	±0.8	±5	16	50

*Above Theoretical 3dB and Amplitude Unbalance

Test Curve (Q1M060600)

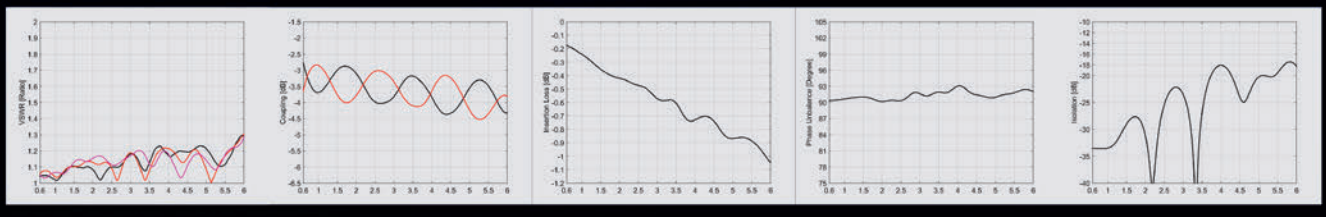

More Information-
Scan the QR Code

MIcable Inc.
www.micable.cn sales@micable.cn +86-591-87382856

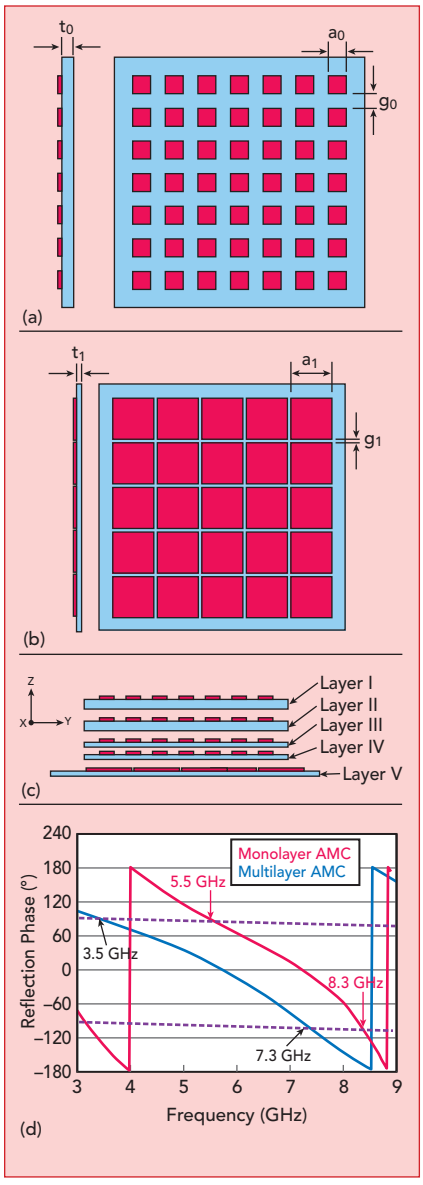

Fig. 1 Multilayer AMC structure: top view of layer I to layer IV (a), top view of layer V (b), side view of the multilayer AMC structure (c) and reflection phase characteristics of monolayer and multilayer structures (d).

loss is greatly reduced.

The multilayer AMC structure consists of five layers (see ***Figure 1***). The patches on the top two layers (Layers I and II) are constructed on FR-4 (ε_r = 4.4) with thickness τ_0 = 1 mm, and the other patches (on Layers III, IV and V) are printed on Rogers (ε_r = 3.5) with thickness τ_1 = 0.8 mm. The array of 7 × 7 square metallic unit cell patches for Layers I, II, III and IV all have the same dimensions.

An array of 5 × 5 metal unit cell patches for Layer V is designed with the patch width changed from a_0 to a_1, and the gap changed from g_0 to g_1. To expand the in-phase bandwidth, the parameters a_0, a_1, g_0 and g_1 are optimized to obtain an equivalent C and L that makes the phase and impedance vary slowly with frequency. Through numerical simulation, the parameters are optimized to a_0 = 4.8 mm, a_1 = 15 mm, g_0 = 4 mm and g_1 = 2 mm. The space between each layer of the multilayer structure is 2 mm.

For comparison, the reflection phase of a monolayer AMC structure is analyzed as well. For consistency, the thickness of the monolayer substrate τ =13.6 mm, which is the same as the height of the multilayer AMC. The patch width and the gap between adjacent patches in the monolayer substrate are the same as those of the top four layers of the multilayer AMC structure.

Figure 1d shows the reflection phase of the monolayer and multilayer AMC structures. Compared with the monolayer AMC structure, the lower frequency of the in-phase reflection band is extended from 5.5 to 3.5 GHz. Miniaturization of the AMC structure is thus achieved by reducing the lower cut-off frequency. Moreover, the phase variation with frequency is slower, which corresponds to a broader AMC bandwidth. The in-phase reflection band of the multilayer structure is from 3.5 to 7.3 GHz, while that of the monolayer structure is from 5.5 to 8.3 GHz. This is greater than a 30 percent increase in bandwidth, which is attributed to the multilayer structure providing more freedom for design optimization.

WIDEBAND HIGH GAIN ANTENNA DESIGN

Application of the AMC structure to the design of a wideband high gain antenna is presented here. First, the design of a wideband planar "reference antenna" is discussed. The multilayer AMC structure is then added as the ground plane. Full-wave simulations and measurements of the antenna are carried out to verify its performance.

From Ground to Orbit
RF Without Limits

Satellite communications continue to evolve — higher frequencies, tighter margins, harsher environments.

Power your mission with our space-qualified line card featuring industry-leading RF manufacturers, backed by design experts with deep technical expertise and global support—because reliability isn't optional in space. **Representing leading RF solutions across the RF signal chain:**

- **GaN & GaAs Power Amplifiers (Ku–Ka–Q-band)**
- **LNAs, Drivers & MMICs**
- **Frequency Conversion & Timing**
- **RF Front-End Modules**
- **High-Reliability Passives & Interconnect**

RichardsonRFPD
An Arrow Company

Engage with our Engineering Experts at

SATELLITE x GovMilSpace

BOOTH 3131

RichardsonRFPD
An Arrow Company

GUIDING INNOVATION FOR OVER 50 YEARS
RF, Wireless, IoT and Power Technologies

800.737.6937 | 630.262.6800
www.richardsonrfpd.com

Reference Antenna

The reference antenna layout is shown in ***Figure 2***. The height of the ground is denoted as lg. The parameter lg represents the length of the microstrip feedline as well, which plays a key role in impedance matching to the 50 Ω SMA input connector (see ***Figure 3***).

The curved portion of the feedline provides current to the radiators. Further simulation shows the input impedance also depends on the radius r (see ***Figure 4***). By optimizing the values of lg and r, making Re (Z_{in}) close to 50 Ω and Im (Z_{in}) near 0 Ω, $|S_{11}|$ < 10 dB can be achieved over a wide frequency range from 3.8 to 7.5 GHz (see ***Figure 5***). Measurements of a prototype antenna built on an FR4 substrate (ε_r = 4.4) agree well with the simulation. Optimized antenna parameters are listed in ***Table 1***.

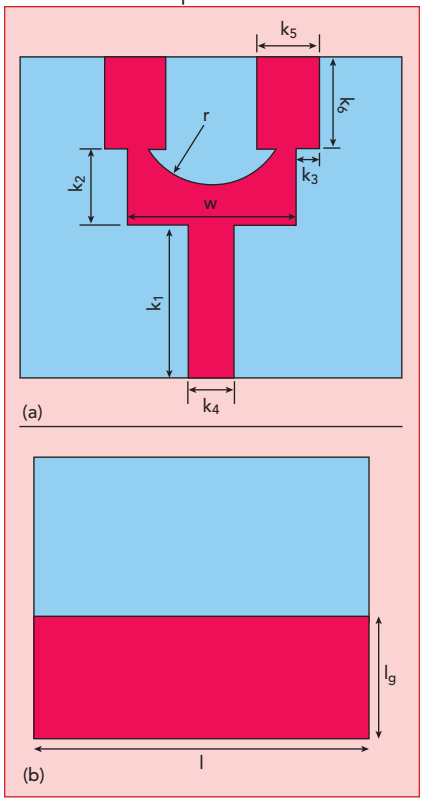

Fig. 2 Reference antenna schematic: top view (a) and bottom view (b).

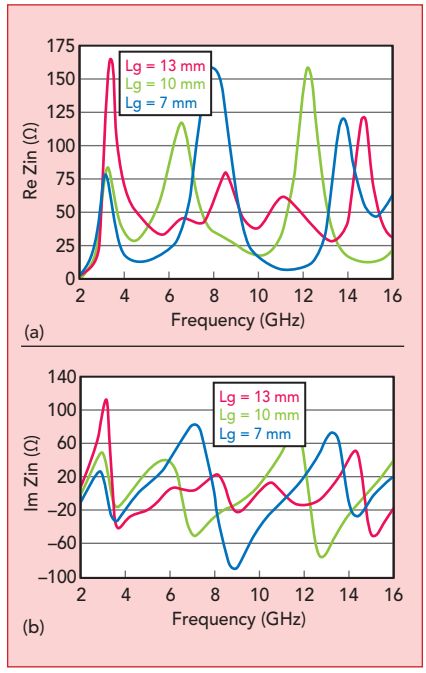

Fig. 3 Input impedance as a function of lg: real (a) and imaginary (b).

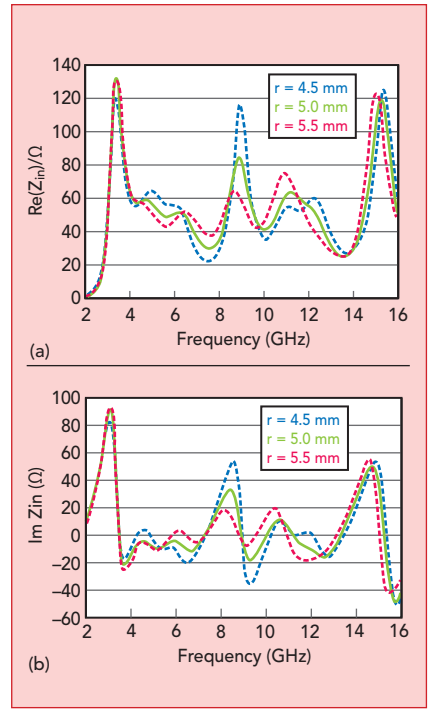

Fig. 4 Input impedance as a function of r: real (a) and imaginary (b).

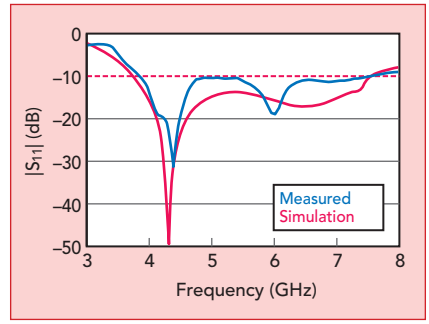

Fig. 5 Measured and simulated reference antenna $|S_{11}|$.

VNAs to 3.5 GHz Starting Below $3,000

from Copper Mountain Technologies

VALUE

- Value-priced VNAs designed for common S11 and S21 measurements, making them ideal for **testing antennas, filters, amplifiers, transmission lines and cables**
- Suitable for **lab, production, and field-testing** environments
- Software runs on **Windows or Lunux** operating system on a PC, laptop, tablet, or x86 single-board computer
- Compatible with **ARM processors**—can be operated via Raspberry Pi

Full Featured 2-Port 1-Path VNAs

Leaders in Customer Value

- Metrology-grade performance backed by CMT's **ISO/IEC 17025 (2017) accredited labs.**
- Advanced software features included.
- **Timely Support** from automation and applications engineers who function as part of your team to help configure and optimize measurements.
- Made in the **EU and USA**.

EXTEND YOUR REACH®

WWW.COPPERMOUNTAINTECH.COM

COPPER MOUNTAIN TECHNOLOGIES

TABLE 1
REFERENCE ANTENNA DIMENSIONS (MM)

k_1	k_2	k_3	k_4	k_5
10	5	1.5	3	4
k_6	l	r	lg	w
6	25	5.5	9	11

AMC-Backed Antenna

Although the reference antenna has a wide impedance bandwidth, the reduced area of the ground causes bidirectional radiation, resulting in low directivity in the forward radiation. The multilayer AMC structure acts as a reflector to improve radiation performance (see ***Figure 6a***). The distance between the reference antenna and the top layer of the multilayer AMC structure is denoted as h_2. Antenna impedance bandwidth is primarily affected by h_2 (see ***Figure 6b***). A value of h_2 = 9 mm is chosen so that the in-phase reflection band corresponds with the operating band to the greatest extent. This is the frequency range from 4.5 to 7.5 GHz.

To assess the influence of the multilayer AMC structure on antenna radiation performance more intuitively, gain is simulated with three different reflectors, including a PEC, monolayer AMC and multilayer AMC for comparison (see ***Figure 7a***). For the reference antenna, the gain in the forward direction is only about 3 dBi. With the PEC, gain is significantly improved.

With the monolayer AMC structure, the simulated gain is improved by approximately 1 to 2 dB compared to the PEC reflector. This is attributed to the in-phase reflection characteristics of the AMC structure. In addition, an array-like effect caused by the cells of the AMC structure, which can be considered as sub-radiators, also helps to improve antenna system gain.

With the multilayer AMC structure, gain is further increased. The incremental improvement is up to 3 dB with a maximum gain of 12 dBi. This is mainly attributed to a flatter in-phase reflection characteristic. Additional-

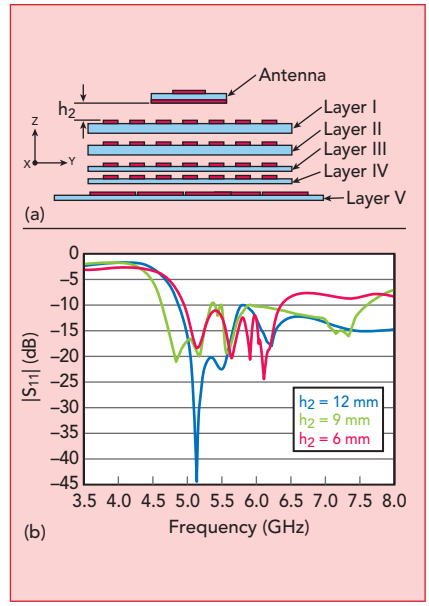

Fig. 6 Lateral view of the antenna and multilayer AMC structure (a) and simulated $|S_{11}|$ as a function of h_2 (b).

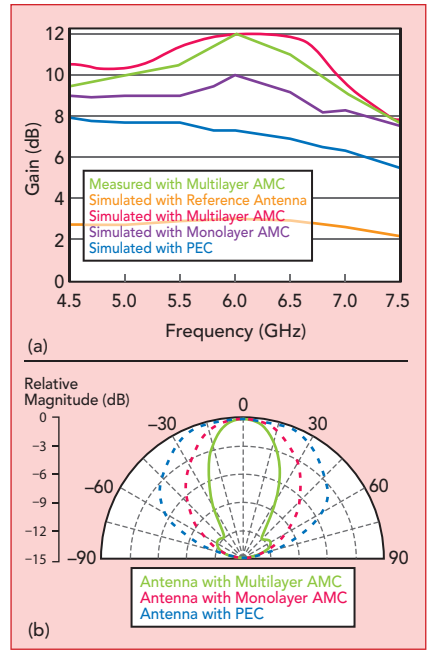

Fig. 7 Simulated and measured antenna gain (a) and simulated E-plane radiation patterns at 6 GHz (b) with different reflectors.

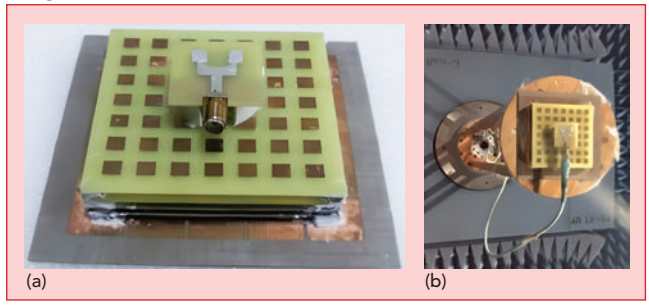

Fig. 8 Photograph of the multilayer AMC antenna (a), the antenna mounted in an anechoic chamber for test (b).

M-Wave DESIGN

High-Power Waveguide-to-Coax Transitions

2–20 GHz Solutions

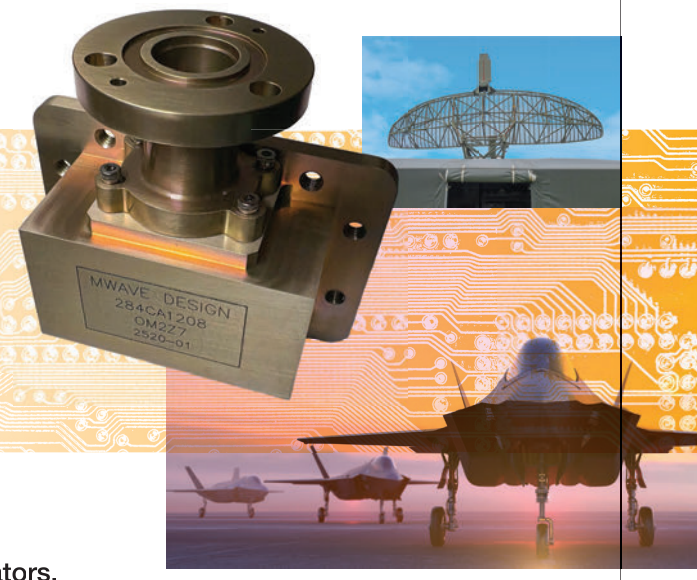

Delivering superior efficiency and power handling

Adapters, plumbing runs, couplers, combiners, isolators, circulators and fully integrated assemblies available

35+ Years Delivering Custom Solutions

Learn More
mwavedesign.com

TRM

Custom Passive RF & Microwave Solutions

Optimal Performance. Proven Solutions.

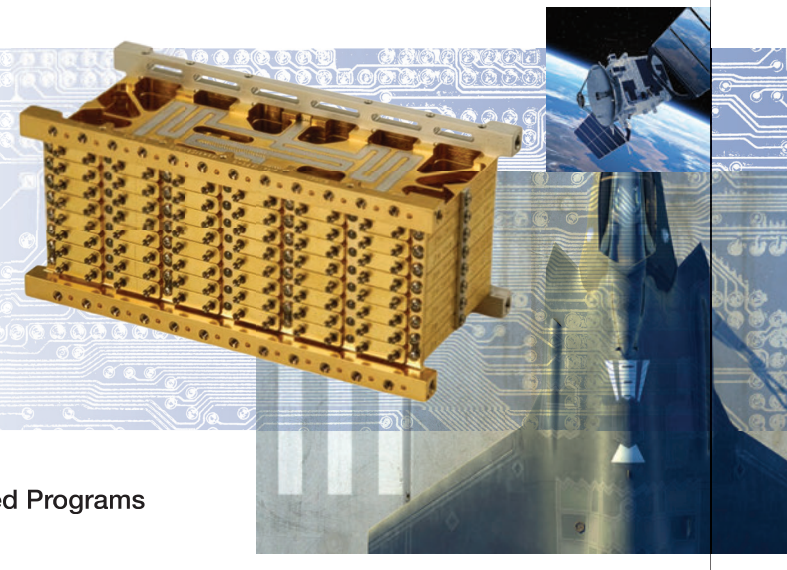

18+ Years Proven Support for Space-Qualified Programs

200+ Unique Products Delivered

Coming Soon: COTS Solutions for LEO Launch Support

Learn More
trmmicrowave.com

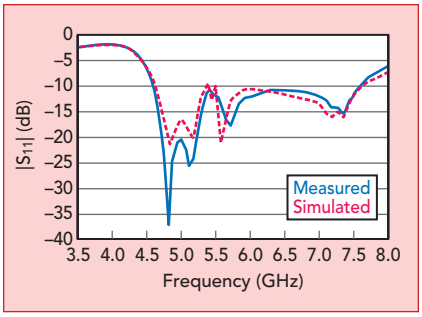

Fig. 9 Simulated and measured $|S_{11}|$.

ly, for the monolayer AMC structure, the thickness of the substrate is 13.6 mm, while for the multilayer AMC structure, the thicknesses of the five plates are 1 mm, 1 mm, 0.8 mm, 0.8 mm and 0.8 mm, respectively. This results in lower substrate loss and higher gain. Gain of the multilayer AMC antenna is measured as well (see Figure 7a), demonstrating close agreement with the simulation.

Simulated E-plane radiation patterns of the antenna with different reflectors at 6 GHz (see ***Figure 7b***) show that higher directivity with a narrower beamwidth is achieved with the multilayer AMC structure.

MEASUREMENTS

Performance of the prototype multilayer AMC-backed antenna (see ***Figure 8***), including $|S_{11}|$, gain and radiation patterns, is measured in a far-field anechoic chamber. Gain is shown in Figure 7a, $|S_{11}|$ is shown in ***Figure 9*** and measured radiation patterns are shown in ***Figure 10***. Measurements agree closely with the simulations.

$$C = \frac{\alpha(\varepsilon_0 + \varepsilon_r)}{\pi} \cos^{-1}\left(\frac{\alpha + g}{g}\right) \quad (9)$$

$$L = \mu t \quad (10)$$

CONCLUSION

A wideband and high gain antenna employs a five-layer AMC structure. The AMC acting as a ground plane is constructed by printing periodic patches on substrates with different dielectric constants to effectively broaden the frequency range of in-phase reflection. Attributing to this in-phase reflection characteristic, antenna gain from 4.5 to 7.5 GHz is significantly improved, achieving a maximum gain of 12 dBi. This wideband high gain antenna has potential communication systems applications. ■

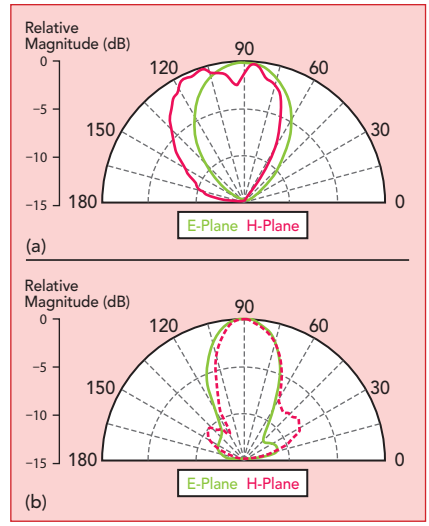

Fig. 10 Measured radiation patterns at 5 (a) and 6 (b) GHz.

ACKNOWLEDGMENT

This work was supported by the Science and Technology Research Project of Henan Science and Technology Department (Grant

HIGH POWER COUPLERS

5 - 500 Watts

Model #	Frequency (MHz)	Coupling (dB) [Nom]	Coupling Flatness (dB)	Mainline Loss (dB) [Typ./Max.]	Directivity (dB) [Typ./Min.]	Input Power (Watts) [Avg.]
SDCHP-125	10 - 250	18.5	0.5	0.1 / 0.4	24 / 19	30
SDCHP-140	10 - 400	18.75	1	0.5 / 0.85	27 / 22	25
SBCHP-1100	10 - 1000	10	0.5	1.2 / 1.4	17 / 15	5
KBK-HP-1100	10 - 1000	10	0.5	1.2 / 1.4	17 / 15	5
KDK-HP-255	20 - 550	20	0.4	0.25 / 0.35	23 / 18	27.5
SDCHP-255	20 - 550	20	0.4	0.25 / 0.35	23 / 20	27.5
SDCHP-335	30 - 350	20.1	0.85	0.24 / 0.32	24 / 20	75
SDCHP-484	40 - 840	19.2	0.9	0.3 / 0.4	24 / 20	30
SCCHP-560	50 - 560	14.6	0.7	0.48 / 0.65	23 / 20	75
SCCHP-990	90 - 900	15.2	0.6	0.52 / 0.64	20 / 17	38.3
SBCHP-2080	200 - 800	12.3	0.7	0.64 / 0.80	24 / 18	48.3
SBCHP-2082	200 - 820	11.0	0.5	0.74 / 0.9	22 / 19	22.5
KDS-30-30-3	27 - 512	27.5	0.75	0.3 / 0.4	23 / 15	50
KDS-30-30	30 - 512	27.5	0.75	0.3 / 0.4	23 / 15	50
KBK-10-225	225 - 400	11	0.5	0.6 / 0.7	25 / 18	50
KBS-10-225	225 - 400	10.5	0.5	0.6 / 0.7	25 / 18	50
KDK-20-225	225 - 400	20	0.5	0.2 / 0.4	25 / 18	50
KDS-20-225	225 - 400	20	0.5	0.2 / 0.4	25 / 18	50
KEK-706H	500 - 2500	31.5	2.5	0.28 / 0.4	18 / 12	100
SCS-8012D	800 - 1200	20	0.6	0.22 / 0.25	22 / 18	100
KEK-704DH-2	850 - 1250	30	0.25	0.20 / 0.30	28 / 25	500
KEK-704H	850 - 960	30 5	0.25	0.08 / 0.20	38 / 30	500
SCS100800-10	1000 - 8000	10.5	2	1.2 / 1.8	8 / 5	25
SCS100800-16	1000 - 7800	16.8	2.8	0.7 / 1	14 / 5	25
SCS100800-20	1000 - 7800	20.5	2	0.4 / 0.75	12 / 5	25
SCS-1522B	1500 - 2200	10	--	0.65 / 0.75	23 / 18	100
SCS-1522D	1500 - 2200	20	--	0.32 / 0.38	23 / 20	100
SCS1701650-16	1500 - 15500	17	2.5	1 / 1.4	16 / 5	25
SCS1701650-20	1700 - 15000	21	2.5	0.9 / 1.3	10 / 7	25
SDC360440-10	3600 - 4400	8.6	0.25	0.7 / 1.4	18 / 10	10
SDC360440-20	3600 - 4400	19	0.25	0.7 / 1.2	16 / 10	10

New Models!

Talk To Us About Your Custom Requirements

SYNERGY® MICROWAVE CORPORATION

Phone: (973) 881-8800 | Fax: (973) 881-8361
E-mail: sales@synergymwave.com | Web: www.synergymwave.com
Mail: 201 McLean Boulevard, Paterson, NJ 07504

No: 242102210067), the Key R&D Project of Henan Province-Research and Application of Key Technology (Grant No: 241111212500) and Henan Province Key R&D and Promotion Special (Technology Tackling Key) Project (No.232102210181, No.252102521071).

References

1. B. Hua, L. Han, Q. Zhu, C. -X. Wang, K. Mao, J. Bao, H. Chang and Z. Tang, "Ultra-Wideband Nonstationary Channel Modeling for UAV-to-Ground Communications," *IEEE Transactions on Wireless Communications*, Vol. 24, No. 5, May 2025, pp. 4190–4204.
2. A. Abbosh, "Ultra-wideband Quasi-Yagi Antenna Using Dual-Resonant Driver and Integrated Balun of Stepped Impedance Coupled Structure," *IEEE Transactions on Antennas and Propagation*, Vol. 61, No. 7, July 2013, pp. 3885–3888.
3. C. L. Mak, K. M. Luk, K. F. Lee and Y. L. Chow, "Experimental Study of a Microstrip Patch Antenna with an L-Shaped Probe," *IEEE Transactions on Antennas and Propagation*, Vol. 48, No. 5, May 2000, pp. 777–782.
4. H. -X. Xu, S. Tang, S. Ma, W. Luo, T. Cai, S. Sun, Q. He and L. Zhou, "Tunable Microwave Metasurfaces for High-Performance Operations: Dispersion Compensation and Dynamical Switch," *Scientific Reports*, Vol. 6, No. 38255, November 2016.
5. I. H. Abdelaziem, A. A. Ibrahim and M. A. Abdalla, "High Gain and Efficiency Dual-Band Antenna Using Meta-Surface," *AEU-International Journal of Electronics and Communications*, Vol. 148, May 2022.
6. M. Singh and M. S. Parihar, "High-Gain MIMO Antenna with Broad Beam Scan Range Using Anisotropic Planar Meta-Lens Array for Millimeter-Wave-Band 5G Applications," *IEEE Antennas and Wireless Propagation Letters*, Vol. 24, No. 2, February 2025, pp. 324–328.
7. S. Kundu and A. Chatterjee, "A Compact Super Wideband Antenna with Stable and Improved Radiation Using Super Wideband Frequency Selective Surface," *AEU-International Journal of Electronics and Communications*, Vol. 150, June 2022.
8. C. P. Scarborough, D. H. Werner and D. E. Wolfe, "Functionalized Metamaterials Enable Frequency and Polarization Agility in a Miniaturized Lightweight Antenna Package," *Advanced Electronic Materials*, Vol. 2, No. 2, February 2016.
9. Y. Jia, Y. Liu, H. Wang, K. Li and S. Gong, "Low-RCS, High-Gain and Wideband Mushroom Antenna," *IEEE Antennas and Wireless Propagation Letters*, Vol. 14, October 2014, pp. 277–280.
10. D. Sievenpiper, L. Zhang, R. F. J. Broas, N. G. Alexopoulos and E. Yablonovich, "High-Impedance Electromagnetic Surface with a Forbidden Frequency Band," *IEEE Transactions on Microwave Theory and Techniques*, Vol. 47, No. 11, November 1999, pp. 2059–2047.
11. X. Chen, Z. J. Su, L. Li and C. H. Liang, "Radiation Pattern Improvement in Closely-Packed Array Antenna by Using Mushroom-Like EBG Structure," *IET International Radar Conference*, April 2013.
12. L. Li, Q. Chen, Q. Yuan, C. Liang and K. Sawaya, "Surface-Wave Suppression Band Gap and Plane-Wave Reflection Phase Band of Mushroom-Like Photonic Band Gap Structures," *Journal of Applied Physics*, Vol. 103, No. 2, January 2008.
13. P. Chen, X. D. Yang, C. Y. Chen and Z. H. Ma, "Broadband Multilayered Array Antenna with EBG Reflector," *International Journal of Antennas and Propagation*, September 2013.
14. S. X. Ta and T. K. Nguyen, "AR Bandwidth and Gain Enhancements of Patch Antenna Using Single Dielectric Superstrate," *Electronics Letters*, Vol. 53, No. 15, July 2017, pp. 1015–1017.
15. A. A. Ibrahim and W. A. E. Ali, "High Gain, Wideband and Low Mutual Coupling AMC-Based Millimeter Wave MIMO Antenna for 5G NR Networks," *AEU-International Journal of Electronics and Communications*, Vol. 142, December 2021.
16. K. Agarwal, N. Nasimuddin and A. Alphones, "Wideband Circularly Polarized AMC Reflector Backed Aperture Antenna," *IEEE Transactions on Antennas and Propagation*, Vol. 61, No. 3, March 2013, pp.1456–1461.
17. S. Trinh-Van, O. H. Kwon, E. Jung, J. Park, B. Yu, K. Kim, J. Seo and K. C. Hwang, "A Low-Profile High-Gain and Wideband Log-Periodic Meandered Dipole Array Antenna with a Cascaded Multi-Section Artificial Magnetic Conductor Structure," *Sensors*, Vol. 19, No. 20, October 2019.
18. S. J. Orfanidis, "Reflection and Transmission in Electromagnetic Waves and Antennas," *Rutgers University*, 2008.
19. D. Feng, H. Zhai, L. Xi, S. Yang, K. Zhang and D. Yang, "A Broadband Low-Profile Circular-Polarized Antenna on an AMC Reflector," *IEEE Antennas and Wireless Propagation Letters*, Vol. 16, September 2017, p. 2840–2843.
20. L. Tang and Z. Zhang, "Ultrawide Bandwidth Rectangular Patch Antenna Over Artificial Magnetic Conductor," *IEEE International Conference on Microwave and Millimeter Wave Technology (ICMMT)*, May 2012.
21. D. Sievenpiper, "High-Impedance Electromagnetic Surfaces", Ph.D. Dissertation, Department of Electrical Engineering, UCLA, Calif., USA, 1999.

MiCable

SSMP 40GHz Female Right Angle

C25F Series MILLIMETER WAVE CABLE ASSEMBLY

Ideal for connection and jumper requiring extremely limited installation space and high reliability

NEW

3mm Min. Bend Radius

Excellent Phase Stability vs. Temp.

Excellent Mechanical/Temp. Stability

High Freq. **Low** Loss **Low** VSWR

Small Size for **High** Density Arrangement

VSWR

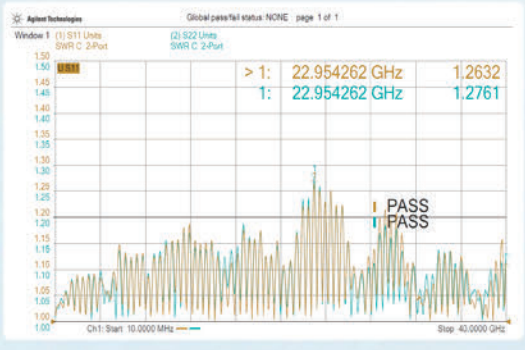

Cable Diameter	1.42mm
Frequency	DC~40GHz
Cable Attenuation	7.69dB/m@40GHz
VSWR	<1.40@40GHz
Shielding Effectiveness	<-90dB
Phase Stability vs. Flex.	<±4°@40GHz
Phase Stability vs. Temp.	<200ppm@-15°C~+35°C <400ppm@-40°C~+70°C
Amplitude Stability vs. Flex.	<±0.1dB/m@40GHz

More Information-
Scan the QR Code

MIcable Inc.

www.micable.cn sales@micable.cn +86-591-87382856

Enabling NASA's Venus Radar with Ultra-Low Phase Noise OCXOs

Wenzel Associates, Inc.
Austin, Texas

When the European Space Agency's (ESA) EnVision spacecraft, as shown in ***Figure 1***, launches for Venus, one of its key instruments, NASA's Venus Synthetic Aperture Radar (VenSAR), will rely on a 10 MHz oven-controlled crystal oscillator (OCXO) from Wenzel Associates as a critical frequency reference. VenSAR is scheduled to launch in November of 2031, and its mission is to generate coherent radar data for high-resolution imaging, topography and surface property analysis. The accuracy of those data products begins with frequency precision.

Fig. 1 **Artist's rendering of the EnVision spacecraft.**

Synthetic aperture radar systems depend on phase-coherent signal generation over long time intervals. Any frequency instability or phase noise from the oscillator translates directly into image phase errors, degrades resolution and reduces radiometric accuracy. For a deep-space mission like EnVision, the oscillator must provide exceptional stability, ultra-low noise and consistent performance under environmental stress.

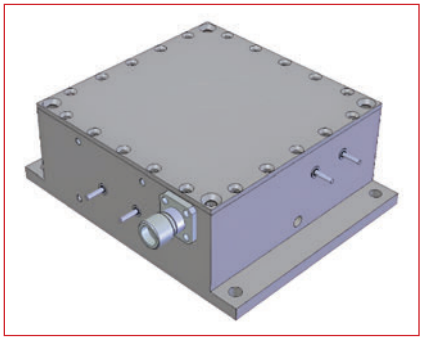

Fig. 2 **Artist's rendering of the 10 MHz OCXO.**

DESIGN FOR FREQUENCY INTEGRITY

The VenSAR OCXO, as demonstrated in ***Figure 2***, uses a quartz crystal resonator from Croven Crystals, optimized for minimal acceleration sensitivity and low aging. Featuring a stress-compensated cut (SC-cut) quartz crystal and a specialized mounting structure inside a hermetically sealed

RF-LAMBDA

THE POWER BEYOND EXPECTATIONS

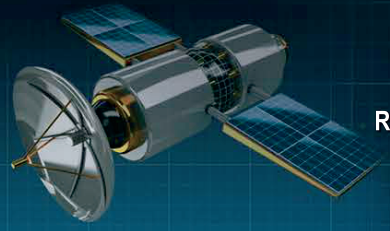

ITAR & ISO9001
Registered Manufacturer
Made in USA

RF T/R MODULES UP TO 70GHz

DREAM? WE REALIZED IT

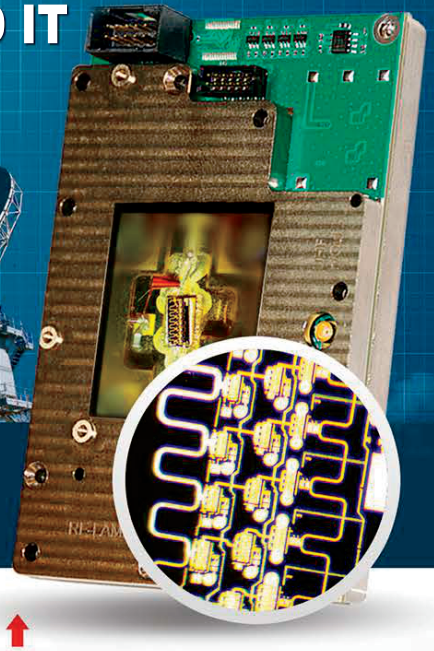

LOW LOSS **NO MORE CONNECTORS**
GaN,GaAs SiGe **DIE BASED BONDING**
SIZE AND **WEIGHT REDUCTION 90%**

HERMETICALLY SEALED
AIRBORNE APPLICATION

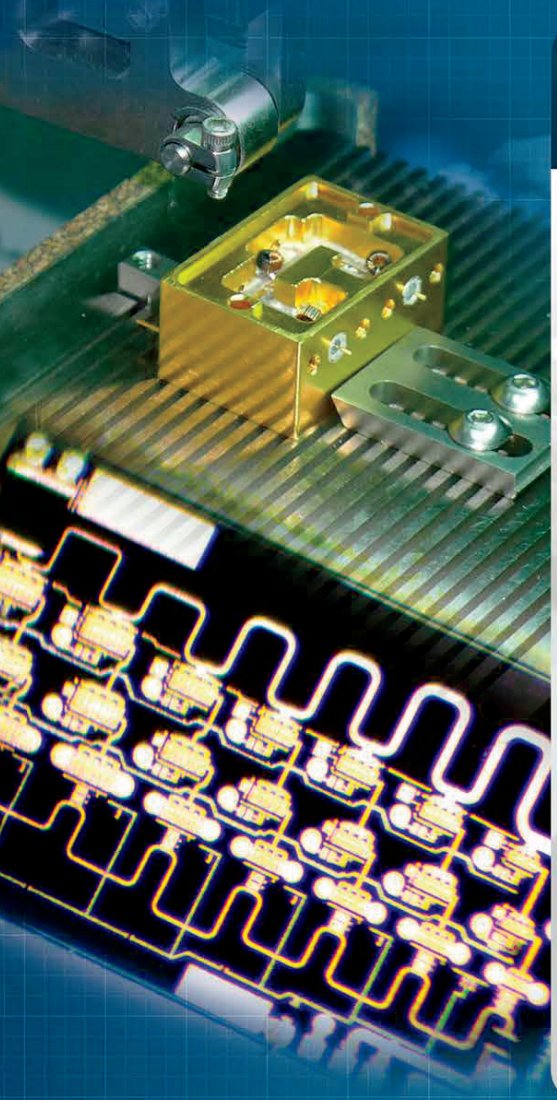

SATCOM TR MODULE
RX 50GHZ TX 22GHZ

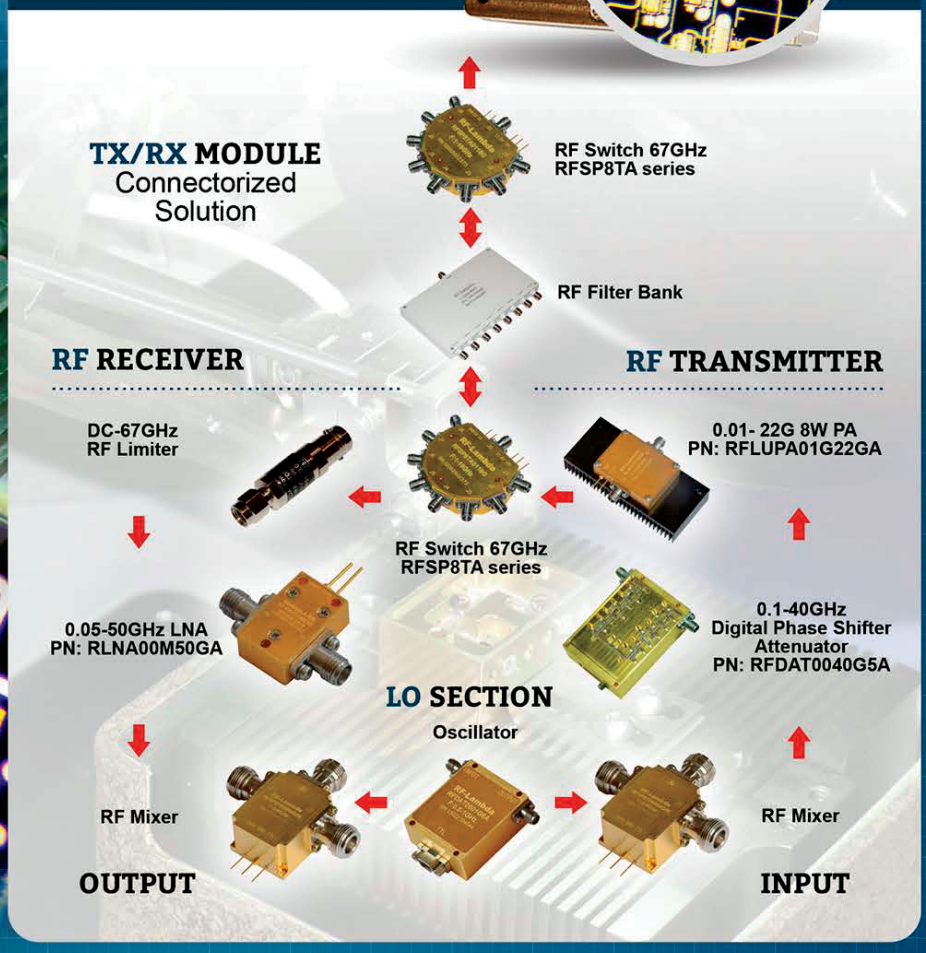

www.rflambda.com
sales@rflambda.com

1-888-976-8880
1-972-767-5998

San Diego, CA, US
Carrollton, TX, US
Ottawa, ONT, Canada
Frankfurt, Germany

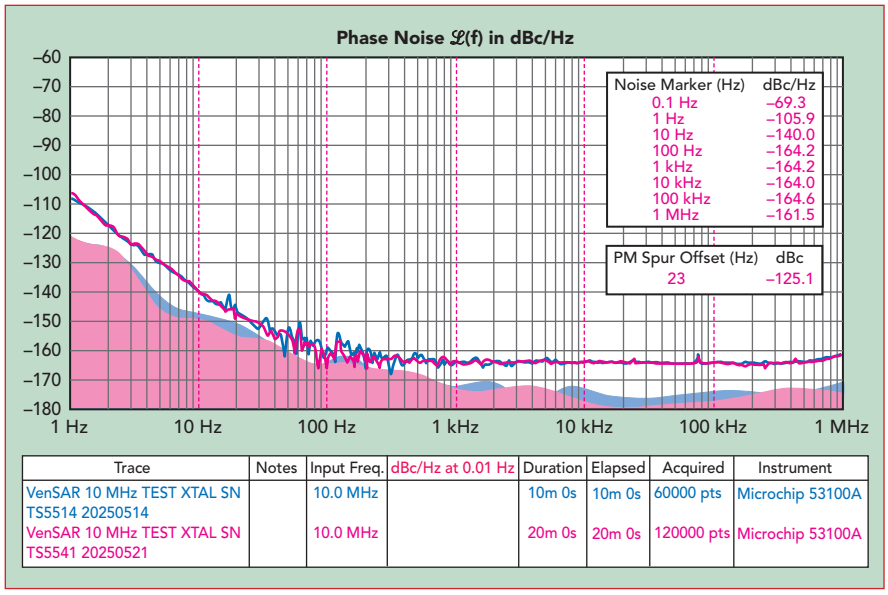

Trace	Notes	Input Freq.	dBc/Hz at 0.01 Hz	Duration	Elapsed	Acquired	Instrument
VenSAR 10 MHz TEST XTAL SN TS5514 20250514		10.0 MHz		10m 0s	10m 0s	60000 pts	Microchip 53100A
VenSAR 10 MHz TEST XTAL SN TS5541 20250521		10.0 MHz		20m 0s	20m 0s	120000 pts	Microchip 53100A

▲ Fig. 3 **Phase noise plot of the 10 MHz OCXO showing –164 dBc/Hz at 10 kHz offset.**

housing, the quartz crystal resonator is designed to minimize the effects of external vibration on frequency stability. The addition of a proportionally controlled oven circuit ensures the quartz crystal resonator and circuitry are maintained at a stable temperature, minimizing the effects of environmental temperature changes on frequency stability. Both the quartz crystal resonator's low g-sensitivity design and thermal regulation are essential for achieving optimal fractional frequency stability over the mission's demanding performance specifications.

Output signal phase noise is a key performance parameter for radar coherence. ***Figure 3*** shows that the oscillator achieves phase noise levels of -105 dBc/Hz at 1 Hz offset and -164 dBc/Hz at 10 kHz, enabling high dynamic range and fine Doppler resolution. Achieving these noise levels requires careful management of flicker noise in sustaining amplifier circuits and control of microphonic effects within the oven cavity. The design incorporates low noise discrete transistor amplifiers, has a high-Q resonator circuit and is designed to be robust during mechanical shock.

Electrical design also focuses on filtering and isolating power supply noise and output signal buffering. Each stage is optimized to reduce additive phase noise and ensure load insensitivity. Proportional heater controllers provide thermal stability. All active components are chosen based on NASA EEE-INST-002 and JPL Parts Engineering Technical Standards. They are selected based on resistance to total ionizing dose and single-event effects, ensuring predictable behavior through the mission's radiation exposure profile.

SPACE QUALIFICATION AND ENVIRONMENTAL TESTING

Qualification testing for the VenSAR OCXO follows a rigorous process derived from NASA standards for spaceflight hardware. Thermal vacuum testing verifies oven regulation across the full operating temperature range under vacuum conditions. Thermal cycling and temperature shock testing ensure startup reliability and long-term drift characteristics. Vibration and shock tests simulate launch stresses with random vibration profiles. ***Figure 4*** shows the device set up for environmental testing.

Extended aging tests characterize frequency drift and validate long-term predictability, while burn-in and step-stress testing screen for early-life failures. Final performance verification includes phase noise measurement

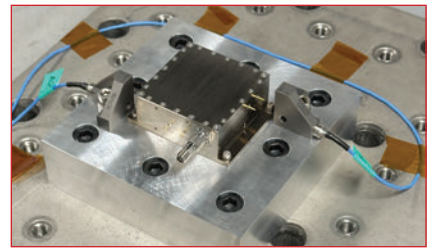

▲ Fig. 4 **Preparing the device for pyroshock testing.**

using cross-correlation analyzers, Allan deviation analysis and frequency-temperature coefficient testing. Each oscillator's test data is captured and documented to provide full pedigree traceability for the mission.

CONCLUSION

The OCXO design builds on Wenzel Associates' decades-long space flight heritage across multiple NASA programs, including Mars Curiosity and Perseverance, Europa Clipper and NISAR. Experience from these missions directly informed the design of the VenSAR oscillator. The result is a highly stable, low-drift frequency source with demonstrated reliability in long-duration missions. The VenSAR OCXO represents the intersection of precision crystal engineering, thermal control and environmental resilience. Each design decision, from crystal cut and mounting to oven temperature control and component selection, was made to ensure high frequency stability performance under the mechanical, thermal and radiation stresses of interplanetary flight.

By combining ultra-low phase noise performance with space qualification, Wenzel's oscillator will enable NASA and ESA engineers to push radar imaging performance further than before. Once EnVision begins its journey to Venus, the oscillator's precision 10 MHz signal will serve as the timing foundation for a mission designed to reveal a new view of our neighboring planet.

VENDORVIEW

Wenzel Associates, Inc.
Austin, Texas
www.quanticwenzel.com

SIX DAYS ■ THREE CONFERENCES ■ ONE EXHIBITION

EUROPE'S PREMIER MICROWAVE, RF, WIRELESS AND RADAR EVENT

EUROPEAN MICROWAVE WEEK
EXCEL, LONDON
4th-9th OCTOBER 2026
www.eumw.eu

EUROPEAN MICROWAVE WEEK 2026

SUBMIT YOUR PAPER ONLINE

EXCEL LONDON, UNITED KINGDOM

4TH – 9TH OCTOBER 2026

To electronically submit a technical paper for one or more of the three conferences, all you have to do is:

1. Visit our website www.eumw.eu
2. Click on `CONFERENCES' to view the individual conference details
3. From the Home page, click on "More info" under the "Authors" heading for author instructions on abstract submission

EuMA EUROPEAN MICROWAVE ASSOCIATION

Media partner: Microwave Journal

Co-organiser: horizon house

Technical co-sponsors: MTT-S IEEE MICROWAVE THEORY & TECHNOLOGY SOCIETY; IEEE AP-S Antennas and Propagation Society; AESS; Electron Devices Society

EuMIC THE EUROPEAN MICROWAVE INTEGRATED CIRCUITS CONFERENCE

EuMC THE EUROPEAN MICROWAVE CONFERENCE

EuRAD THE EUROPEAN RADAR CONFERENCE

Supported by: IEEE; EurAAP; APMC 2026; QMAS; esa THE EUROPEAN SPACE AGENCY

SUBMIT PRELIMINARY PAPERS ONLINE AT WWW.EUMW.EU BY 27TH MARCH 2026

High Linearity V-Band Amplifiers Increase Satcom Data Rates

mmTron, Inc.
Redwood City, Calif.

Significant advances in technology during the past 30 years have enabled humanity to achieve the goal of connecting anyone, anytime, anywhere on the planet. It began with the commercialization of mobile phones and the evolution from analog voice to digital data. In parallel, the development of much lower-cost and consequently more frequent rocket launches enabled constellations of satellites to cover the globe. In low Earth orbit (LEO) and very low Earth orbit (VLEO), the lower radiation levels and shorter mission lifetimes reduce the need for traditional, space-qualified components, enabling the use of commercial semiconductors and significantly lowering satellite payload costs.

Successful commercialization of these LEO systems is evident from the services offered by Starlink, orbiting approximately 9000 satellites, and Eutelsat OneWeb, with 660 satellites. Amazon is developing Amazon Leo, a constellation numbering more than 3000, and Starlink plans another 7500 satellites in VLEO. These systems provide broadband data services using user terminals developed for each constellation. A new generation of constellations promises a direct connection between the satellite and mobile phones. AST SpaceMobile's phased array satellite is designed to receive signals directly from phones and relay them through a ground gateway back through the mobile operator to the cloud.

To provide the high data rates users expect, satellite systems require wide bandwidth gateway channels. To support the ever-increasing demand for data, which is accelerating with AI, satellite systems are moving gateway links from Ku- and Ka-Band to higher mmWave bands, such as V- and E-Band.

Responding to this shift, mmTron has introduced high linearity power and low noise amplifiers (LNAs) for the V-Band satellite downlink. Covering 37 to 44 GHz, the amplifiers maximize linearity for high data rates and high efficiency to minimize satellite power consumption. They are fabricated on a space-qualified GaN process, which combines the power and efficiency advantages of GaN with the reliability pedigree for satellites.

TMC315 POWER AMPLIFIER

Covering 37 to 44 GHz, mmTron's TMC315 power amplifier (PA) provides 39 dBm output power at 1 dB compression and 40 dBm saturated. To enable closed-loop control of the output power, the PA has an integrated, temperature-compensated power detector.

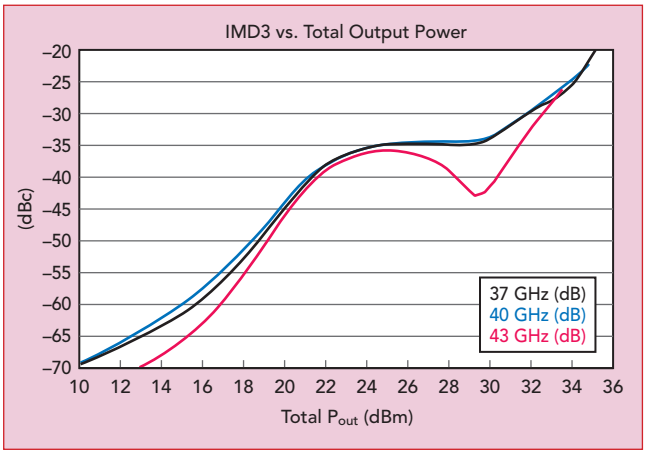

▲ Fig. 1 **TMC315 measured IMD3 versus total output power at 37, 40 and 43 GHz.**

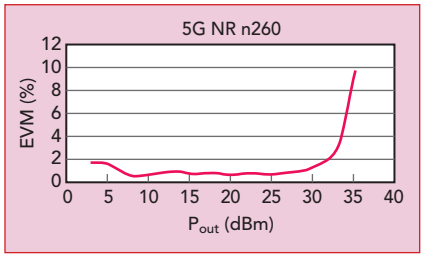

▲ Fig. 2 TMC315 EVM performance with a 5G NR signal in the n260 band.

Demonstrating the linearity of the TMC315, the third-order intermodulation (IMD3) is better than -33 dBc at 31 dBm output (see ***Figure 1***), and the third-order output intercept point (OIP3) is 44 dBm. Driven with a multi-carrier 5G NR modulated signal in the n260 band (37 to 40 GHz), the error vector magnitude (EVM) measures below 2 percent up to 32 dBm output (see ***Figure 2***).

In addition to high linearity, the PA achieves a power-added efficiency (PAE) of approximately 25 percent, as shown in ***Figure 3***. High PAE is important to minimize satellite power consumption and simplify the thermal design of the payload.

With three amplifier stages, the TMC315 provides greater than 20 dB small signal gain and better than 10 dB return loss across the operating frequency range (see ***Figure 4***).

The PA maintains output power, linearity and efficiency performance across a wide range of drain bias, from 18 to 28 V, offering flexibility to system designers.

TMC316 DRIVER/LNA

The TMC316 amplifier is the second amplifier mmTron is introducing. With frequency coverage from 32 to 44 GHz, it can be the driver amplifier for the TMC315 or used as a standalone LNA.

The TMC316 provides 27 dBm output power at 1 dB compression and 28 dBm saturated, with 32 dBm OIP3. The small signal gain is 17 dB (see ***Figure 5***), and the noise figure is 5.5 dB.

Like the TMC315, the TMC316 maintains good output power, linearity and efficiency across a wide range of drain bias, from 18 to 28 V.

BARE DIE, TAB AND PACKAGED OPTIONS

Both amplifiers are available as bare die, mounted on tabs or packaged in air-cavity, 5 × 5 QFNs. The TMC315 die measures 3.0 × 2.5 × 0.1 mm and the TMC316 is 3.0 ×1.5 × 0.1 mm.

With the tab configuration, the amplifiers are soldered to CuMoCu tabs, ensuring a void-free attachment to a high thermal conductivity base that removes heat from the device and reduces channel temperature, extending lifetime. The coefficients of thermal expansion of the CuMoCu tab and the amplifier's SiC backside are well matched, which ensures mechanical reliability with temperature changes.

These V-Band amplifiers are the latest products in mmTron's large portfolio of MMIC products, including mmWave PAs and LNAs, wideband distributed amplifiers covering DC to 180 GHz, front-end modules, mixers, multipliers, multifunction ICs and interfaces for high speed data converters.

mmTron's recognized expertise is highly linear and efficient mmWave PAs for satcom, fixed wireless access and other high data rate mmWave communications systems. mmTron's wide bandwidth products are also used in aerospace and defense and instrumentation.

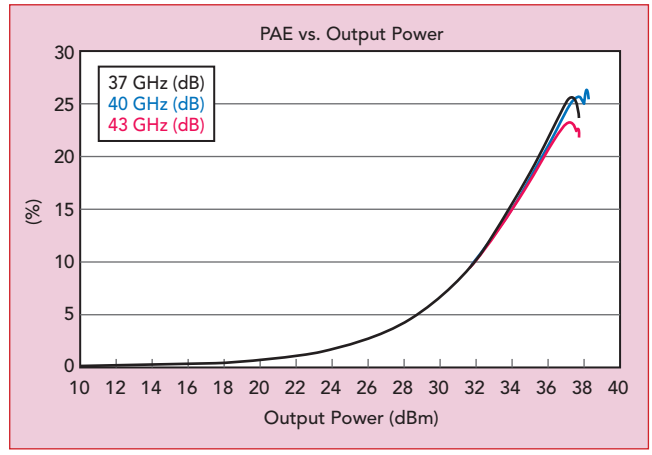

Fig. 3 TMC315 measured PAE vs. output power at 37, 40 and 43 GHz.

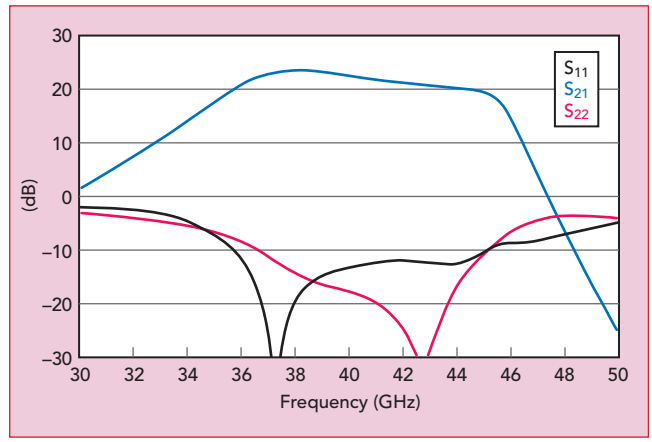

Fig. 4 TMC315 small signal gain and return loss versus frequency.

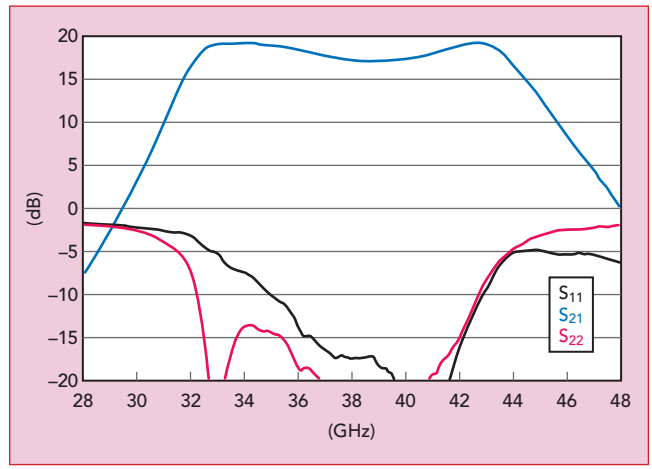

Fig. 5 TMC316 small signal gain and return loss versus frequency.

mmTron, Inc.
Redwood City, Calif.
www.mmtron.com

SATELLITE x GovMilSpace

MARCH 23-26 | WASHINGTON, DC

WHERE SPACE SYSTEMS GET PRESSURE-TESTED

TECH SEMINAR: 16 PEER-EVALUATED SESSIONS FOR ENGINEERS & SYSTEM ARCHITECTS

Exhibit Hall access • Implementation-ready takeaways

You'll get breakthrough solutions you can put to work immediately:

- Software-defined space systems
- Resilient network architectures
- RF awareness & tactical edge systems
- Optical communications & PNT
- Interoperable satcom standards

...and more.

FREE Exhibit Hall Pass + 20% Tech Seminar Discount

Scan to register or use code MJ4SAT26 at www.satshow.com

Broadband Power Divider Ready for Wi-Fi 6 Through Wi-Fi 8

MECA Electronics' new 802-S-5.000 broadband power divider operates across 2.00 to 8.00 GHz frequencies, spanning the needs of S- and C-Bands and Wi-Fi 6E through Wi-Fi 8. This two-way power divider uses a Wilkinson configuration with SMA connectors. The 802-S-5.000 delivers an amplitude balance of 0.3 dB and phase balance of 4 degrees, performance previously challenging to find outside of narrowband products.

Since MECA products are fully designed and manufactured in the U.S., the 802-S-5.000 answers the call for aerospace and defense industry applications. It has a maximum insertion loss of 0.5 dB and a typical isolation of 22 dB, and with an operating temperature of -55°C to +85°C, the product is eligible to be screened and ruggedized for harsh environments.

MECA designed the 802-S-5.000 with compact size, broadband capability and precision performance to meet emerging telecommunications needs in 5G and 6G platforms. The innovation allows operators to streamline integration and production costs, while a 36-month warranty from the manufacturer provides operational assurance.

MECA Electronics is an integral partner to every part of the RF and microwave industry, providing innovative solutions to even the most complex problems since the company was founded in 1961. Always made in America, MECA has developed a reputation as a trusted resource for RF/microwave applications in defense, satellite and telecommunications, helping engineers and supply chain managers meet operational objectives for more than 65 years.

MECA Electronics, Inc.
Denville, N.J. (973) 625-0661
www.e-MECA.com

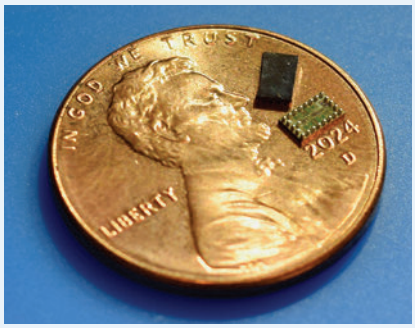

Ultra-Low Power, High Performance Beamformer ICs

Electronically steered antennas (ESAs), also known as phased arrays, are rapidly becoming the platform of choice for satellite communications (satcom) on Earth and in space. ESAs are low-profile, versatile and fast, allowing for LEO/MEO/GEO deployments across fixed and mobile satellite services. However, system power and IC costs continue to impede their wide-scale adoption; conventional analog beamforming solutions are power hungry and expensive.

Oso Semiconductor is introducing a reimagined microarchitecture for the beamformer IC. Through its ultra-low loss beamforming IP, Oso Semi adopts a sub-array level amplification approach where only one amplifier is needed for a four-element subarray, after the coherent signal is combined (for receive) or before it is split (for transmit).

The reduction in per-channel amplifiers and lossy phase shifters results in a 4x reduction in power per channel for the receive (under 12 mW), a 2x reduction in power per channel for the transmit (under 80 mW) and a shrinking of silicon area to nearly half, which directly reduces the IC cost of the ESA. Oso Semi's designs also result in improved receiver (Rx) linearity by up to 10 dB and improved transmit noise figure by up to 6 dB, while maintaining Rx noise figure within 20 percent of state-of-the-art designs and delivering an OP1dB of 12 dBm. ESAs designed using Oso Semi's chips result in a 40 to 50 percent reduction in total system power for transmit and receive, eliminating the need for heavy heat sinks with active cooling and unlocking low-power, portable applications.

With products targeting Ku- and Ka-Bands, Oso Semiconductor is ready to help system designers build the next generation of satcom flat panel terminals.

Oso Semiconductor
Mountain View, Calif.
www.ososemi.com

MAKING WAVES

Scaling Precision: Synchronization Strategies for High-Channel ADC/DAC Architectures

This video presents a practical and scalable solution for synchronizing a high number of ADCs and DACs, an increasingly critical requirement in modern radar, communications, EW and instrumentation systems.

Analog Devices
www.analog.com

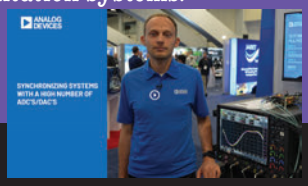

RF Measurements for NR in Non-Terrestrial Networks

Watch this brief video to learn about Anritsu's user-friendly test solution designed for RF measurements of NR NTN technology.

Anritsu
https://resources.goanritsu.com/

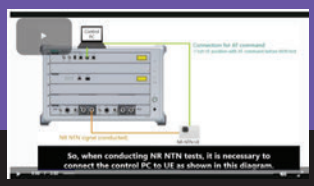

Lexicon of Balun and Transformer Configurations

Choosing the right transformer for a given application can be overwhelming. This article explains the functions and key parameters for each of the 22 different transformer and balun configurations in Mini-Circuits' product portfolio.

Mini-Circuits
https://blog.minicircuits.com

Innovative Power & RF Solutions for Robotic Technology

This paper highlights how advanced RF connectivity and power management technologies address critical design challenges, including precise motion control, robust communication and optimized energy efficiency — accelerating robotic innovation.

Qorvo
www.qorvo.com

RFMW Presents the Most Innovative Products of 2025

RFMW shares the company's Most Innovative RF, Microwave, and Power Management Products of 2025. This year has delivered remarkable breakthroughs that are shaping the future of our industry, and we're just getting started.

RFMW
https://rfmwblog.com/

Automotive Measurements with R&S ELEKTRA

In this video, Product Manager EMC Software Reiner Goetz gives a general introduction to Rohde & Schwarz's new EMC software R&S ELEKTRA and highlights some features that are relevant for automotive standards.

Rohde & Schwarz
www.rohde-schwarz.com

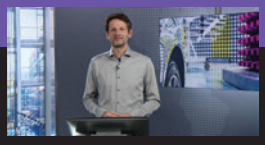

EUROPE'S PREMIER MICROWAVE, RF, WIRELESS AND RADAR EVENT

EUROPEAN MICROWAVE WEEK
EXCEL, LONDON
4th-9th OCTOBER 2026
www.eumw.eu

EUMW 2026 RADIATING CHANGE

EUROPEAN MICROWAVE WEEK 2026

THE EUROPEAN MICROWAVE EXHIBITION

EXCEL LONDON, UK

6TH – 8TH OCTOBER 2026

- 10,000 sqm of gross exhibition space
- Around 5,000 attendees
- 1,700 - 2,000 Conference delegates
- In excess of 300 international exhibitors (including Asia and US as well as Europe)

INTERESTED IN EXHIBITING?

Please contact one of our International Sales Team:

Richard Vaughan,
International Sales Manager
rvaughan@horizonhouse.co.uk

Gaston Traboulsi, France
gtraboulsi@horizonhouse.com

Mike Hallman, USA
mhallman@horizonhouse.com

Victoria and Norbert Hufmann,
Germany, Austria & Switzerland
victoria@hufmann.info
norbert@hufmann.info

Katsuhiro Ishii, Japan
amskatsu@dream.com

Jaeho Chinn, Korea
inter11@jesmedia.com

CALL +44(0) 20 7596 8742 OR VISIT WWW.EUMW.EU

NEW PRODUCTS

COMPONENTS

SPST Absorptive Switch

VENDORVIEW

PMI Model P1T-DC18-60-T-SFF-HSLVT is a single pole, single throw, absorptive switch that offers ultra-low video transient performance while providing ultra-fast switching speed of 6 ns; high isolation of 60 dB min. to 12 GHz, 70 dB min. to 18 GHz; and 4.5 dB max. insertion loss. This switch module contains an integral TTL driver and the DC supply voltage is only -5 VDC. Includes SMA female connectors in a housing that measures 1.0 × 1.0 × 0.5 in.

PMI Planar Monolithics
www.quanticpmi.com

Compact, Broadband Blocking Capacitors

VENDORVIEW

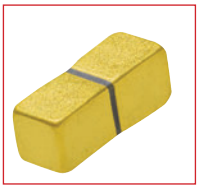

Knowles' Milli-Cap® broadband blocking capacitors are designed to minimize parasitics and deliver stable, low loss performance across wide frequency ranges. Their ultra-high series resonance and very low inductance make them ideal for demanding RF applications like test equipment, fiber-optic modules and broadband mmWave systems. With 0201, 0402 and 0602 footprints, they conserve board space while behaving like ideal capacitors, ensuring signal integrity and efficiency where every fraction of a dB matters.

RFMW
www.rfmw.com

CABLES & CONNECTORS

Miniature Coaxial Connector

Hirose launched a 1.0 mm coaxial connector that complies with the IEEE Std. 287 and supports frequencies up to 110 GHz. Featuring a compression-mount center contact, the 1.0 mm Series coaxial connector supports varying PCB thicknesses from under 1 mm to several mm — providing greater design flexibility. Eliminating the need for soldering, the 1.0 mm Series also features a screw (threaded) mount to reduce mounting complexity. The 1.0 mm Series is commonly used in test and measurement systems, as well as high frequency sensing and communication applications.

Hirose
www.hirose.com

High Power Surface-Mount 90° Hybrid

VENDORVIEW

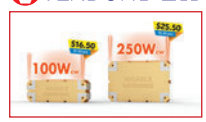

Mlcable released the new two models of 2 to 6 GHz high-power surface-mount 90-degree hybrid. With CW power handling capability of 100 W and 250 W. It has low insertion loss, excellent VSWR ≤1.3:1, extremely good amplitude and phase unbalance, high isolation, excellent stability and heat dissipation ability in a small package. It is suitable for power amplifier, power combining network, antenna feed network, modulator and phase shifter applications.

Mlcable Inc.
www.micable.cn

Microstrip Isolator

Protect your signal chain from reflected power without sacrificing space or signal integrity. The 2W9 Series 29 to 31.5 GHz microstrip isolator provides ultra-low insertion loss (<1 dB), 18 dB isolation and 2 W forward power handling, making it the ideal safeguard for sensitive RF components in extreme satcom environments. Compact, RoHS-compliant and surface-mount ready, this isolator is built for high performance reliability with zero compromise. Get the edge in your RF designs.

Renaissance Electronics AEM
www.aeminc.com/RF

AMPLIFIERS

Broadband 40-60 GHz Amplifier

VENDORVIEW

Model SBP-4036033436-1919-EP offers 34 dB small-signal gain over the 40 to 60 GHz frequency range and +36 dBm saturated output power. The amplifier features WR-19 waveguide input/output with anti-cocking UG-383/U-M flanges and operates from a

+20 VDC / 3.6 A supply.

Eravant
www.eravant.com

1300 W High Power Amplifier

VENDORVIEW

When test setups demand brute force with surgical precision, the AMP20130 delivers. This rack-mountable solid-state amplifier provides over 1300 W CW across 80 to 1000 MHz, with 61 dB gain and excellent P1dB performance. Designed for EMI/RFI, CW/Pulse and high-efficiency communication systems, it features a Class A/AB linear design, built-in protection circuits, extensive monitoring, a large local LCD display and remote interfaces. Built for the lab. Ready for the field.

Exodus Advanced Communications
www.exoduscomm.com

12 dB Gain CATV Amplifier

VENDORVIEW

The QPL1841 is a GaAs pHEMT single-ended MMIC RF amplifier IC featuring 12 dB of gain and low noise from 5 to 850 MHz. This high linearity IC is designed to support broadband CATV DOCSIS 4.0 applications, such as nodes, amplifiers and remote PHY devices, as well as fiber to the home, home gateways and cable modems. The combination of low noise, excellent distortion and low gain makes this suitable for drop amps and other distribution amps.

Qorvo
www.qorvo.com

15-18 GHz High Power Amplifier

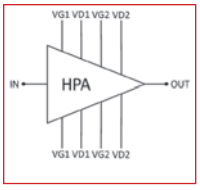

The CHA8315-99F is a monolithic GaN high power amplifier operating from 15 to 18 GHz and delivering an output power of 43.5 dBm with an associated PAE of 45 percent. It exhibits 23 dB small-signal gain. The overall power supply is 20 V/1.16A. The circuit is designed for defence applications but offers performance suited for a wide range of microwave applications. The part is manufactured on a robust GaN HEMT technology and is available as a die.

United Monolithic Semiconductors
www.ums-rf.com

SYSTEMS

QBUC Series from EM Research

The EM Research Quad-Band Block Up-converter (QBUC) integrates four switch-selectable RF bands in an ultra-compact 6.7 × 2.5 × 0.6 in. package, the smallest available based on published product specifications. Supporting L-Band through Ka-Band operation, the QBUC features internal filtering, low phase noise, integrated gain control and excellent spurious performance. QBUC enables flexible multiband system architectures while minimizing SWaP.

EM Research
www.emresearch.com

ANTENNAS

Conical Horn Antenna

VENDORVIEW

URF's 2 to 18 GHz dual polarized quad-ridged conical horn antenna is engineered for RF testing and measurement applications. This high performance wideband antenna delivers exceptional port isolation (≥ 28 dB) and a low VSWR (≤ 2.0:1). Achieve 16.5 dBi typical gain and 20 dB minimum cross polarization, making it the ideal microwave component for precision system integration. Now live in stock at $4,800 each.

URF
www.urfinc.com

TEST & MEASUREMENT

Handheld Analyzer

VENDORVIEW

Keysight Technologies, Inc. introduced the N99xxD-Series FieldFox handheld analyzer, the latest evolution of Keysight's FieldFox family. Purpose-built for precision and portability, the new D-Series enables 120 MHz gap-free IQ streaming, high speed data transfer and seamless field-to-lab integration. Today's RF environments are becoming increasingly complex and dynamic, as mission-critical, commercial and consumer systems converge across the spectrum. From 5G and radar to emerging 6G and satcom, engineers face mounting challenges in identifying interference, capturing transient events and characterizing wideband signals without data loss.

Keysight Technologies, Inc.
www.keysight.com

MICRO-ADS

Reviewed by Ajay K. Poddar

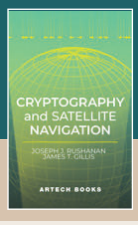

Bookend

Cryptography and Satellite Navigation

By Joseph J. Rushanan, James T. Gillis

The book "Cryptography and Satellite Navigation" is a concise guide that links cryptographic security with satellite navigation. It explores essential cryptographic methods to protect positioning, navigation and timing data in modern systems. This book provides an introduction to cryptography's critical role in secure communication and navigation, and explains the three primary cryptographic methods: ciphers, hashes and asymmetry. Additionally, the book explores the implications of quantum computing on the future of cryptography.

This book stands out with its detailed table of contents and is divided into nine chapters covering key topics. Part I introduces Satellite Navigation (SatNav), including Chapter 1: Introduction and Chapter 2: Overview of Satellite Navigation. Part II explores Cryptography, featuring Chapter 3: Symmetric Cryptography, Chapter 4: Hashing, Chapter 5: Public Key Cryptography and Chapter 6: Cryptographic Protocols. Part III addresses the security of SatNav with Chapters 7 through 11, covering topics from cryptography in the SatNav enterprise to future directions. The authors explain the three fundamental cryptographic techniques: symmetric ciphers for confidentiality, hashes for data integrity and asymmetric cryptography for privacy and authentication using digital signatures. These concepts are further elaborated through discussions on protocols protecting navigation signals in systems like Galileo and GPS.

This book offers a forward-looking analysis of quantum computing's implications for cryptographic security, particularly in SatNav systems. It discusses emerging challenges in a post-quantum era and presents practical applications, including real-world examples that make complex concepts accessible. The authors balance depth with clarity, catering to both cybersecurity and satellite engineering professionals and newcomers alike. Case studies, such as the Galileo navigation system, showcase how digital signatures protect navigation data, while symmetric ciphers enhance data protection. Overall, the book highlights the vital role of cryptography in the technology landscape, preparing readers for future challenges.

ISBN: 9781685690311
Pages: 370
To order this book, contact:
Artech House
us.artechouse.com

LEARNING CENTER

Microwave Journal

Keep these can't-miss online events on your radar in 2026!

Online Panels

March 4
Chiplets and 3D Heterogenous Integration

This panel of experts will discuss the challenges of advanced packaging technologies such as Chiplets and 3D Heterogenous Integration including integration, stacking, signal integrity and thermal concerns. The group will discuss simulation, testing and performance advantages of these approaches.

August 26
Digital Twins and AI

This panel of experts will discuss the benefits and challenges of developing digital twin models along with how AI is being used to assist in modeling and design of RF and microwave circuits.

Registration coming soon at mwjournal.com

1/2 DAY SUMMITS

March 18	Satellite and Space
April 22	Extreme RF (ex. Space, Quantum Computing, High Power, High Frequency, mMIMO, Harsh Environment, etc.)
May 20	AI in RF
October 21	Advancements in Military Radar & EW
November 11	5G/6G & IoT

For Sponsorship Information Contact your MWJ Sales Rep today!
mwjournal.com/salesoffices

Advertising**Index**

Sales Representatives

Eastern and Central Time Zones
Carl Sheffres
Group Director
(New England, New York, Eastern Canada)
Tel: (781) 619-1949
csheffres@mwjournal.com

Michael Hallman
Associate Publisher
(NJ, Mid-Atlantic, Southeast, Midwest, TX)
Tel: (301) 371-8830
Cell: (781) 363-0338
mhallman@mwjournal.com

Pacific and Mountain Time Zones
Scott Blackburn
Western Reg. Sales Mgr.
(CA, AZ, OR, WA, ID, NV, UT, NM, CO, WY, MT, ND, SD, NE & Western Canada)
Cell: (303) 819-3958
sblackburn@mwjournal.com

International Sales
Michael O'Kane
Tel: +44 (0) 1875 825 700
Cell: +44 (0) 7961 038 245
mokane@horizonhouse.com

Germany, Austria, and Switzerland (German-speaking)
Victoria and Norbert Hufmann
Tel: +49 911 9397 6442
victoria@hufmann.info
norbert@hufmann.info

Korea
Jaeho Chinn
JES MEDIA, INC.
Tel: +82 2 481-3411
inter11@jesmedia.com

China
Shanghai
Linda Li
ACT International
Tel: +86 136 7154 0807
lindal@actintl.com.hk

Shenzhen
Linda Li
ACT International
Tel: +86 136 7154 0807
lindal@actintl.com.hk

Beijing
Cecily Bian
ACT International
Tel: +86 135 5262 1310
cecilyb@actintl.com.hk

Hong Kong
Floyd Chun
ACT International
Tel: +86 137 2429 8335
floydc@actintl.com.hk

Taiwan, Singapore
Simon Lee
ACT International
Tel: +852 2838 6298
simonlee@actintl.com.hk

Japan
Katsuhiro Ishii
Ace Media Service Inc.
Tel: +81 3 5691 3335
amskatsu@dream.com

Submitting ad material?
Visit: www.adshuttle.com/mwj
(866) 774-5784
outside the U.S. call
+1-414-566-6940

Ed Kiessling
(781) 619-1963
ekiessling@mwjournal.com

Corporate Headquarters: 685 Canton Street, Norwood, MA 02062 • Tel: (781) 769-9750

µCeramIQ®

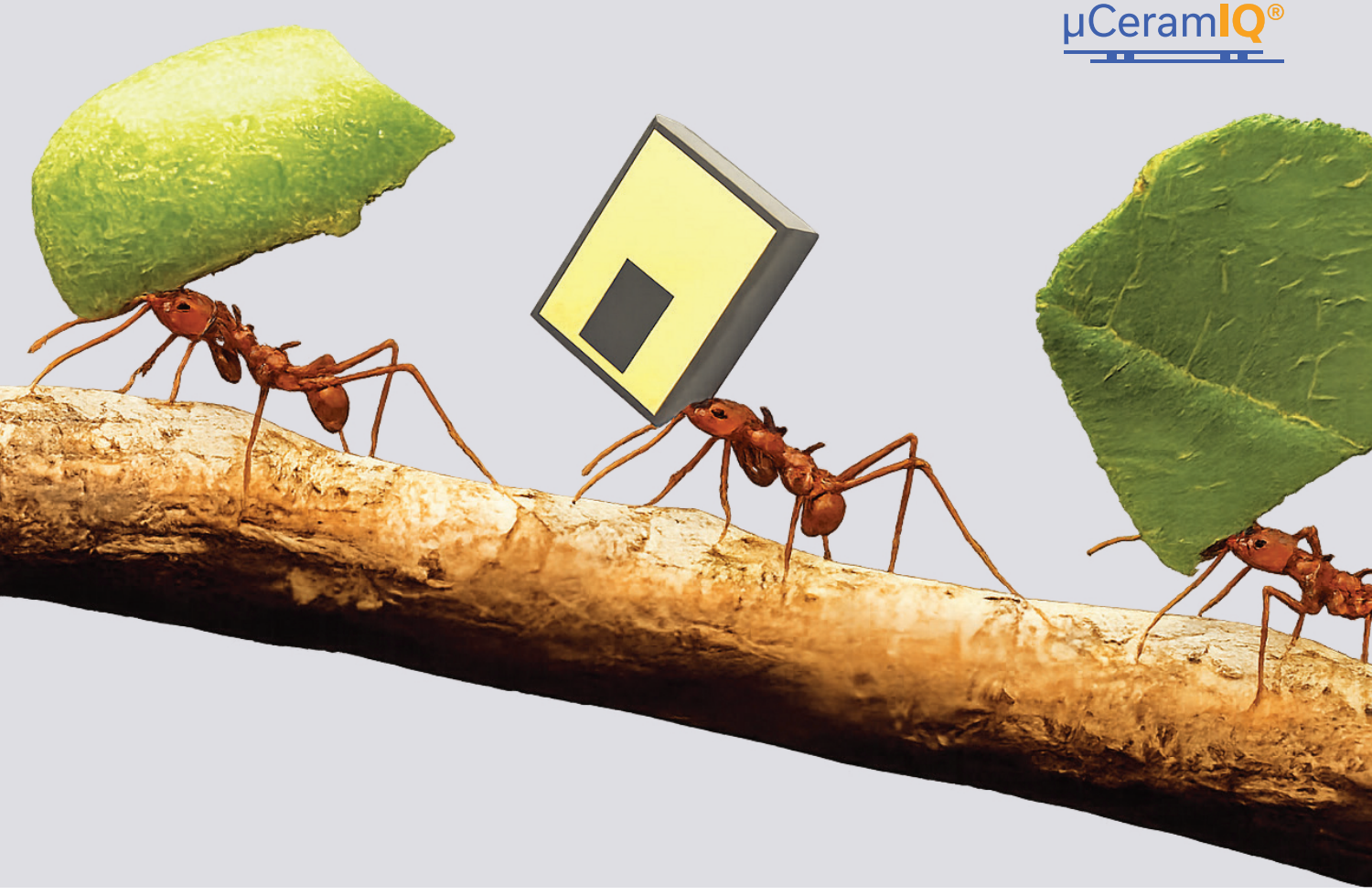

LFHK / BFHK / HFHK SERIES

Small but Mighty

Carrying the Load for High-Rejection and SWAP-C

LEARN MORE

- High pass, low pass & band pass models
- Passbands from DC to 36 GHz
- Stopbands up to 67 GHz
- Rejection up to ≥90+ dB
- Footprint as small as 1008

Protected by US Patents 11,638,370 and 11,744,057

Mini-Circuits®

Infineon CSS: New UWB Lab Drives Intelligence at the Edge

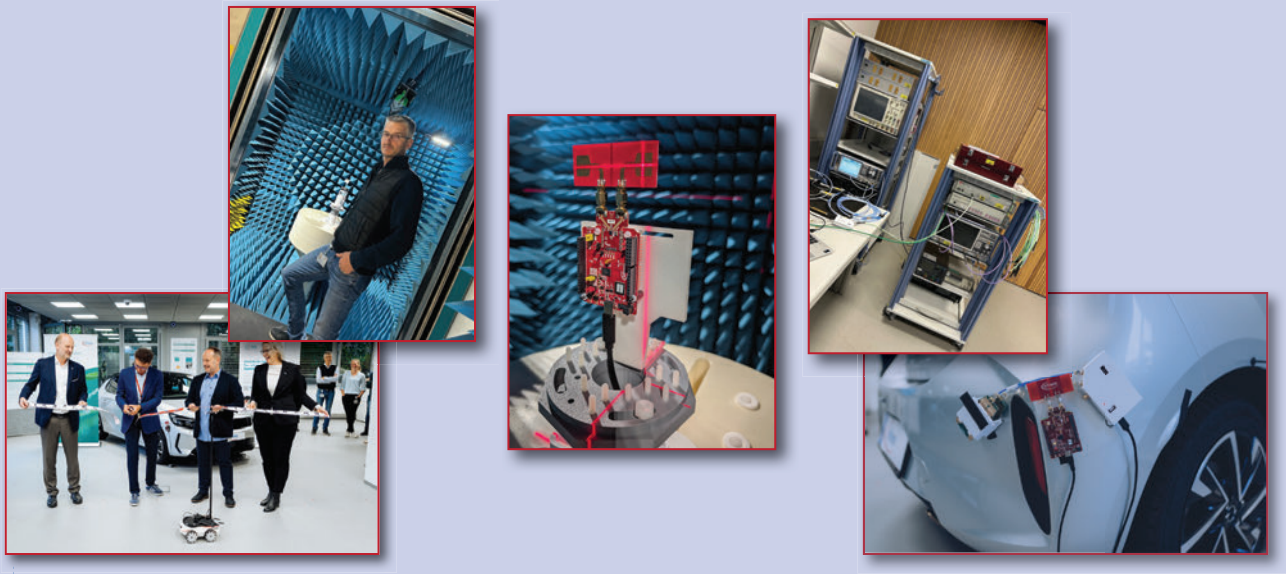

Infineon Technologies is a global semiconductor company focused on making life easier, safer and greener, as well as shaping worldwide digital transformation. Infineon has four divisions, including Automotive, Green Industrial Power, Power and Sensory Systems and Connected Secure Systems (CSS). The CSS division focuses on providing holistic solutions to deliver low-power computing, smart connectivity and built-in security.

One of the emerging enabling technologies for this mission is ultra-wideband (UWB). Infineon CSS recently made several strategic moves to support the development and testing of UWB. These steps were the acquisition of the Swiss company 3db Access, participation in and driving of the worldwide UWB standards, strategic development setup in the organization and the setup of a dedicated UWB application lab. 3db Access was a pioneer of UWB highly integrated transceivers with a focus on secured and low-power UWB ranging for car access systems, and Infineon acquired them in 2023 to learn from and build upon their expertise. The acquisition was driven by Infineon's recognition of the growing importance of UWB technology, which offers precise localization, sensing, secured communication and high speed data transfer, making it an attractive technology for applications that require high accuracy and reliability. The creation of the Infineon UWB Application Lab is the result of close collaboration between experts from Infineon and Silicon Austria Labs (SAL). By pooling expertise and working together, the teams fostered knowledge sharing and joint innovation, turning the vision of the lab into reality.

Infineon plans to leverage UWB technology to advance solutions in several key industries, including automotive and mobility, IoT and smart devices, tap-free payment and public transportation and industrial applications. UWB will power and ease secured keyless car access in combination with near-field communication and Bluetooth Low Energy (BLE) smartphones, wearables and key fobs, as well as address new applications such as child presence detection. UWB-enabled keyless access will also find its way into homes, powering smart door locks and doorbells. Additionally, UWB will support untracked (indoor) navigation for malls, car parks or events and provide spatial awareness for smart home automation. It will add convenience to several payment-related use cases, such as public transport and retail, without compromising security. Finally, UWB will enable precise localization for robotics, asset tracking, logistics and warehouse management.

The new Infineon UWB Application Lab, located in Graz, Austria, is equipped with state-of-the-art infrastructure and tools, including motion-capture systems, an antenna chamber, autonomous robots and wireless control technologies, designed to enable flexible testing and ensure precise and reproducible test environments. The UWB lab supports the Infineon vision of driving decarbonization and digitalization together with customers and the ecosystem. It helps to explore and optimize the UWB technology for its target applications, in combination with other technologies and in different form factors. It is an important milestone to move from product offering to system understanding to accelerate development and shorten time-to-market.

Infineon continues to serve the industry through state-of-the-art design, test and commercialization. Infineon, through its new UWB Application Lab, is dedicated to advancing UWB technology to further the automotive, IoT, public transportation and industrial applications industries.

www.infineon.com

SPECTRAN® V6

BEYOND REALTIME

Setting **the Mobile Benchmark**

The **ULTIMATE** Real-Time Spectrum Analyzer Tablet

8 | 18 | 55 | 140 GHz 2x 490 MHz RTBW

HIGH-END SPECTRUM ANALYZER:

- 9 kHz up to 140 GHz
- Optional Tx (Generator)
- 2x 490 MHz Bandwidth
- 3 THz/s Sweep Speed
- 16-Bit ADC
- -170dBm/Hz | 4dB NF
- IQ Recording & Playpack
- 8h Continuous Runtime
- Temp. Range -40° to +60°
- GPS & Time Server
- Opt. Handle & Stand
- Incl. RTSA-Software

RUGGED PREMIUM PC POWER:

- 15.6" 1500nit FullHD Touchscreen
- AMD 8-Core 8845HS CPU
- 64 GB LPDDR5 RAM
- Up to 64 TB Highspeed SSD
- 2x M.2 2280 & 3x M.2 2242
- Many I/Os incl. USB4, SD & HDMI
- SIM slot, opt. WiFi, Bluetooth, 5G
- SFP+ 10G Ethernet, SATA, RS232
- Rugged Aluminum Casing
- Hot-Swap Batteries
- Front & Rear Cameras, Smart Pen
- Windows or Linux

MADE IN GERMANY

www.aaroniausa.com
ubuy@aaroniausa.com
+1 (214) 935-9800

www.aaronia.com
mail@aaronia.de
+49 6556 900 310

AARONIA AG®
WWW.AARONIA.COM

WERLATONE 60TH ANNIVERSARY

A STEP AHEAD

SOLUTIONS FOR EVERY MILITARY PLATFORM

COMMUNICATIONS | EW | RADAR

DC TO X-BAND

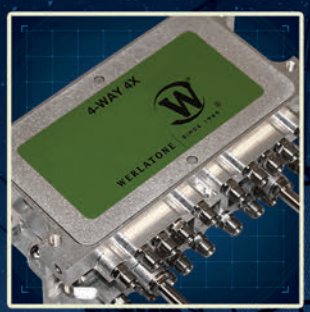

INTEGRATED SUB-ASSEMBLIES

BEAMFORMERS

WAVEGUIDE SOLUTIONS

E-PLANE COMBINERS

FIXED | AIRBORNE | GROUND MOBILE | SHIPBOARD

WE OFFER A VARIETY OF POWER LEVELS RANGING FROM 10 W CW TO 20 KW CW

WERLATONE'S HIGH POWER, MISMATCH TOLERANT® SOLUTIONS
ARE DESIGNED TO OPERATE IN EXTREME LOAD MISMATCH CONDITIONS.

BRING US YOUR CHALLENGE | WWW.WERLATONE.COM

WERLATONE 60TH ANNIVERSARY

LEARN MORE

Editor's Note: This is the second of a two-part article on advanced coaxial filter design. Part 1, published last month, discussed the design and analysis of the filter building blocks, and Part 2 discusses their use in advanced filter design, with examples.

Part 1 discussed the properties of filter building blocks containing strongly coupled posts that offer new possibilities for advanced coaxial (combline) filter designs. Equivalent circuits based on the individual resonances of the posts cannot be used to reliably describe the behavior of these structures because of the strong coupling between the posts. Instead, sets of electromagnetic (EM) resonances that satisfy the boundary conditions are used. The resulting equivalent circuits are either fully transversal or contain locally transversal sub-circuits, depending on the strength of the coupling between the cascaded blocks. The validity of similarity transformations that result in topologies with unusually strong coupling coefficients is questionable, even though they yield the correct frequency response. Such coupling matrices obscure the physics of the problem and fail to predict the correct behavior of filtering structures. However, topologies that match the post layout can be used to optimize a filter in connection with a full-wave solver or measurement.

In Part 2, examples of dual-post and triple-post units are used to illustrate the key findings. The basic knowledge of the real functionality of these special resonator configurations allows their consideration in advanced filter implementations using well-established classical design methods, without limitation by the design approach. This is demonstrated with an example of a second order inline filter providing one transmission zero by using a combination of single and transverse dual-post resonators. This fundamental understanding of the special properties provides the prerequisite for a variety of novel filter solutions.

Properties of Building Blocks Comprising Strongly Interacting Posts and Their Consideration in Advanced Coaxial Filter Designs: Part 2

Smain Amari
Royal Military College, Kingston, ON, Canada

Mustafa Bakr
University of Oxford, Oxford, U.K. and University of Leeds, Leeds, U.K.

Uwe Rosenber
Mician Global Engineering GbR, Bremen, Germany

Understanding of the real filter functionality allows basic design consideration for a systematic filter design, like pre-investigations of the resonators in view of unloaded Q and spurious mode distance, as well as pre-design of couplings with assessment of initial structural dimensions. Moreover, it is a prerequisite for the consideration of well-established filter design methods providing systematic tuning of filter resonances and couplings in case of an EM-CAD supported design (e.g., considering "port tuning") and of course for the tuning of the final hardware. It is a basis for the application of well-established filter design methods without any general limitations.

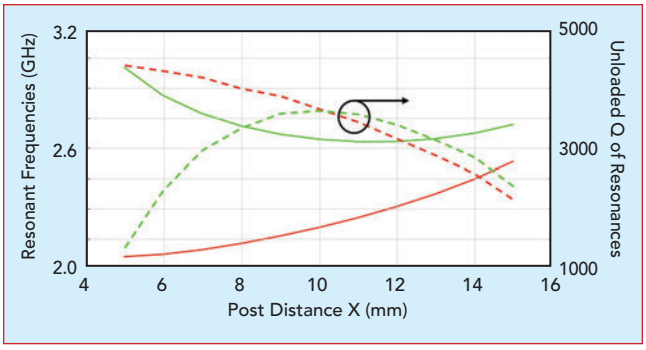

Fig. 1 Transverse dual-post properties according to Figure 2b in Part 1 of this article for different post distance: red curves – dominant (even) mode, green curves – odd mode.

The approach by Macchiarella et al.[1] produces a final design that meets specifications; however, it does not provide a good initial design where single resonators and pairs of interacting resonators are designed as in the classic approach. It relies on an EM-CAD "port tuning" method considering the subsection of the dual-post together with the adjacent single-post resonators. This structure is optimized (tuned) to satisfy the characteristic between the ports, which of course corresponds to the original design; however, with an overdetermined equivalent circuit model, i.e., with a higher number of elements (five couplings, four resonators) than that of the original design (three couplings, three resonators).

An optimization/"tuning" of the configuration with a higher number of variable physical parameters will finally satisfy the defined port characteristics. Moreover, the combination of the dual-post with the adjacent single-post resonators yields a general design limitation, e.g., dual-post resonators may also be directly coupled without any intermediate single-post resonator, also situated close to an interface coupling.

The transverse dual-post resonator is used in the following as an example to introduce basic filter design considerations when using resonators with close-post configurations.

BASIC DUAL-POST RESONATOR DESIGN

One essential aspect in filter design is the investigation of appropriate resonators in view of unloaded Q and spurious-free bands. Thus, the respective properties of a transverse dual-post resonator according to Figure 2b in Part 1 of this article have been explored for different post distances. The results in ***Figure 1*** show that the frequency distance between the dominant mode and the second mode decreases with increasing post distance.

In addition, the unloaded Q of the basic mode has a maximum for the close-post distance, while it decreases with larger post spacing. In the case of the second mode, the unloaded Q reaches a maximum at some post spacing (center), approximately 10 mm in this case. This is due to the stored EM energy between the posts for the second mode, causing higher surface currents for close distances. The decrease for larger spacings can be attributed to increasing currents close to the side wall, which also holds for the basic mode.

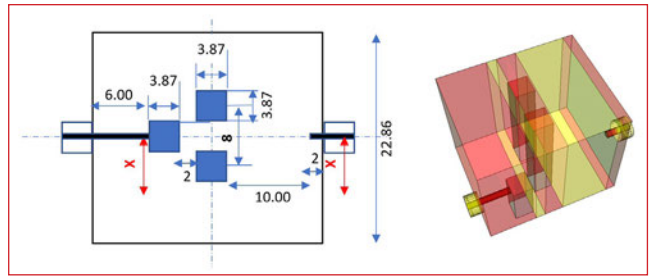

Fig. 2 Configuration for input coupling investigation: housing height = 22.86, dual-post height = 22.00, coupling post height = 10, coax input y offset from center = -2.5 and coax output y offset from center = 4.0 (mm).

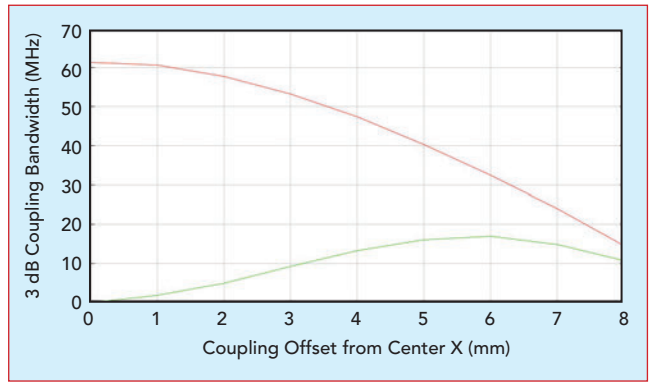

Fig. 3 3 dB coupling bandwidth of dual-post modes according to the configuration in Figure 2: red – basic mode (at 2.23 GHz), green – second mode (at 2.77 GHz).

For the application of the second mode in a filter design, the post height and spacing can be used to achieve a compromise between the unloaded Q and the distance of the basic (spurious) mode. The post footprint may also be considered for a final "fine-tuning" of these parameters.

CONSIDERATION OF RESONATOR COUPLINGS

Another important filter design aspect is the suitable implementation of the resonator couplings. This holds for the input/output couplings as well as for the inter-resonator ones.

Input/Output Coupling Design

For the input/output coupling investigation, a type of loop coupling is applied; i.e., a stub is located in front of the dual-post resonator, which is associated with the penetrating inner conductor of the coaxial interface at the end-wall (see ***Figure 2***). Other coupling configurations may also be treated in a similar manner.

A weak probe coupling is considered with a convenient distance at the opposite end-wall for the indication of the 3 dB coupling bandwidth, which is directly related to the dedicated input coupling and external Q, respectively. Evidently, an increase in the longitudinal distance between the coupling configuration and the resonator yields a decrease in the 3 dB coupling bandwidth and thus the related effect on the dedicated coupling. In the case of the dual-post resonator, the bandwidth variation has been explored when changing the coupling location in the transverse direction.

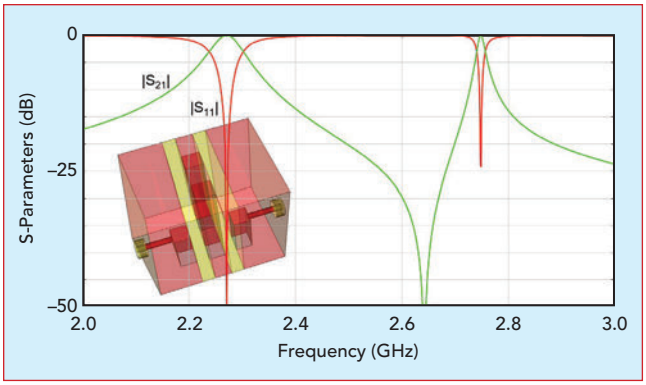

Fig. 4 **Dual-post singlet analyzed response with coupling stub offset in the same direction.**

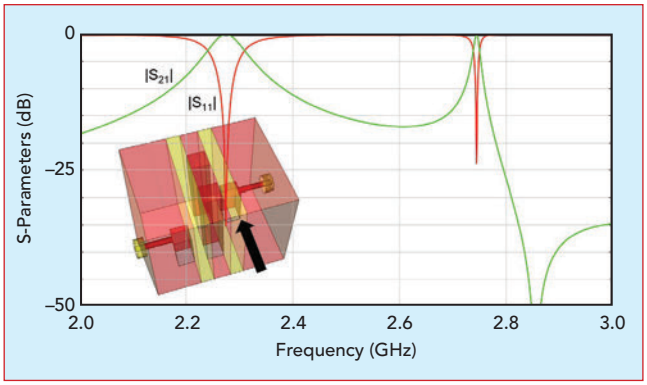

Fig. 5 **Dual-post singlet analyzed response with coupling stub offset in the opposite direction.**

The coupling coefficients to each of the two resonances of the dual-post unit are shown in ***Figure 3***. In detail, the coupling to the dominant mode has a maximum (3 dB bandwidth) at the waveguide center, an increasing transverse center offset of the coupling location yields a decrease of the 3 dB bandwidth due to diminishing magnetic field components.

In the case of the second (odd) mode, the 3 dB bandwidth is evidently zero (no coupling) at the center location. However, an offset location yields a coupling of this mode with a maximum at a center offset of approximately 5.7 mm for the used dimensions.

These results are easily understood by noting that the coupling to the two resonances is determined by the evanescent TE_{10} and TE_{20} waveguide modes, respectively, in the waveguide section between the input stub and the dual-post unit. Evidently, the TE_{10} mode with its lower cut-off frequency will always exhibit stronger coupling. The magnetic Hx fields of the evanescent TE_{20} mode vanish at the center location with maxima at the quarter waveguide widths, which directly corresponds to the reduced couplings of the second dual-post mode (see Figure 3).

Coupling Transformation Properties/Singlet

The coupling transformation properties of the second (odd) mode of the transverse dual-post unit, and its singlet-like behavior, can be easily verified with the configuration in Figure 2, but using the couplings at the input and output. The bypass coupling is mostly through the TE_{10} evanescent mode of the waveguide

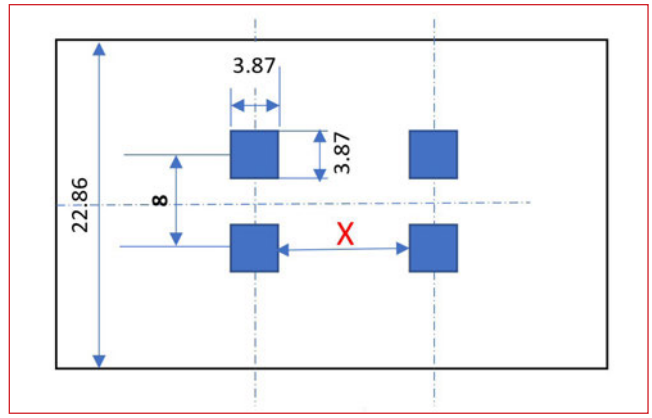

Fig. 6 **Configuration for investigation of inter-resonator couplings of dedicated dual-post resonances. Housing height = 22.86 and post height = 22 mm.**

that does not interact with the resonance (second mode of the dual-post resonator), but it causes a bypass coupling between the input and output, while the basic spurious mode has a negligible impact on the bypass coupling due to the large frequency distance.

When the input and output ports are placed on the same side of the symmetry plane of the configuration, as shown in ***Figure 4***, the generated transmission zero (TZ) is below the resonant frequency of the odd mode. The full-wave results shown in Figure 4 confirm this statement.

To move the TZ above the resonant frequency of the odd mode, the input and output ports must be placed on opposite sides of the symmetry plane of the posts, as shown in ***Figure 5***. Again, the full-wave results shown in Figure 5 confirm this conclusion.

Thus, the transverse dual-post constitutes a real singlet based on the odd mode resonance at the filter passband frequency and bypass coupling of the evanescent TE_{10} mode, like the waveguide implementation that relies on TE_{201} and TE_{10} cavity modes.[2] Experimental validation of this general behavior has been provided by the examples given by Macchiarella et al.[1] and Bastioli et al.[3]

These configurations can be designed using standard filter design methods, considering the respective couplings of the dual-post resonator with the adjacent filter input/output ports and/or resonators, where the cross-coupling can almost be determined by the complete distance bypassing the dual-post. There is only a minor impact by the spurious basic mode due to its large frequency distance. There is no advantage to a more elaborate higher-order equivalent circuit model, which includes the spurious resonance that cannot be controlled.

Inter-Resonator Coupling

For the investigation of inter-resonator couplings, the well-known resonance analysis is applied. First, a configuration with two identical dual-post units is explored by varying the separation distance between them (see ***Figure 6***).

The resonance analyses yield four resonant frequencies: two are dedicated to the dominant dual-post

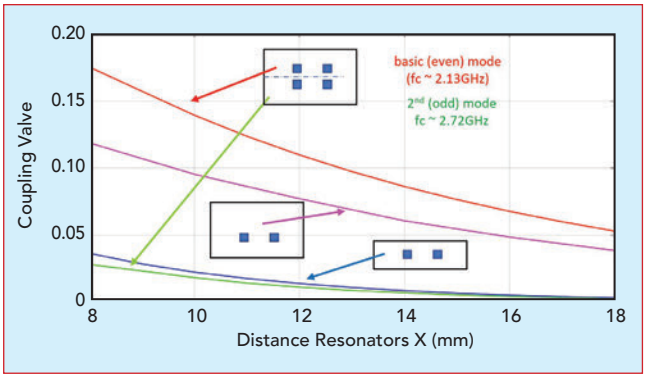

Fig. 7 **Coupling values of inter-resonator couplings: dual-post configuration, basic mode – red; second mode – green; single-post configuration with same envelop configuration and center offset, post height 20.85 mm adjusted (fc = 2.72 GHz) – magenta; centered single posts in half-width envelope – blue.**

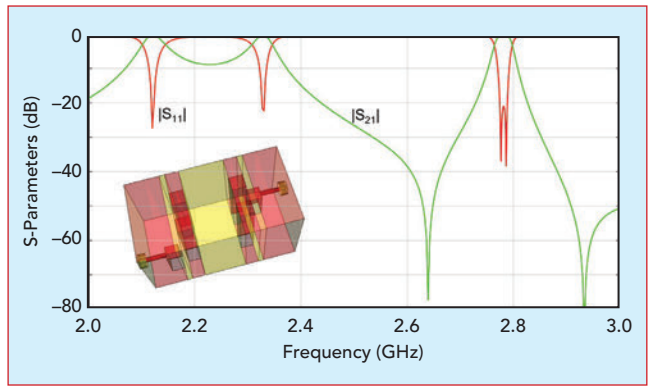

Fig. 8 **Dual-post doublet analyzed response with opposite offset spacing of coupling stubs.**

mode, while the other two are dedicated to the second mode. The deduced coupling values of the assigned modes are shown in ***Figure 7***. The coupling between the dominant modes is substantially stronger (more than 5x) than that between the second (odd) modes.

The analyses of half the configuration in Figure 6, considering an electric wall in the longitudinal symmetry plane (i.e., half waveguide width with center offset single-posts), yield identical results as the second mode. This demonstrates that the coupling of the second mode in this configuration relies solely on the TE_{20} waveguide mode and not on the fundamental TE_{10} mode. There will be a certain increase in the coupling values when considering the single-post resonators centered inside this half-width waveguide envelope (see Figure 7).

Another coupling analysis is carried out for the altered original configuration, considering only one post (with center offset) of each pair. In this case, the post height is modified (20.85 mm) to have the same resonant frequency as the second mode. Although this configuration exhibits weaker coupling values than those achieved for the dominant mode of the dual posts, in comparison with the second mode couplings, they are more than 3x stronger (see Figure 7).

The method for the coupling analyses is based on identical resonating configurations. Consequently, the application to different resonator types is critical (as in the combination of a dual-post with a single-post). However, the analyses of initial filter designs have shown that couplings between dual- and single-post resonators are of the same order of magnitude as that obtained for the second mode dual-post resonators. This is attributed to the fact that the second dual-post mode can only be coupled by odd mode field components, i.e., couplings with single-post resonators in this configuration are only possible if they exhibit a center offset relative to the dual-post.

An assessment of the footprint dimensions of the third order filter (see Macchiarella et al.,[1] Figure 6) confirms the above analyses. Indeed, the coupling of the single-post resonators with the dual-post (odd mode) resonator at a close distance is due entirely to the TE_{20} waveguide mode, while the bypass coupling between the two single posts can be (almost entirely) attributed to the TE_{10} mode and results in much stronger coupling despite the longer distance.

Inline Dual-Post Doublet

The basic understanding of the physics of close-post resonator configurations reveals many new design possibilities to be included in advanced filter designs. The knowledge that the second mode of transverse dual-post resonators is always coupled by the TE_{20} mode, while the TE_{10} mode provides strong bypass coupling, has been considered by the singlet design above.

The singlet configuration can also be extended by a second dual-post resonator for the realization of an inline second-order building block, providing a pair of TZs (see ***Figure 8***). Also in this configuration, the opposite offsets of input and output couplings are important for the coupling sign transformation (M_{SL}). The response clearly exhibits two spurious resonances below the passband.

The use of standard filter design methods allows the consideration of such basic configurations for advanced filter implementations. For example, the inline dual-post doublet can be combined arbitrarily with other (e.g., single-post) resonators to provide an inline quadruplet in higher-order filter designs.

Second Order Filter Design Example

The following example introduces a systematic filter design that relies on well-established methods while considering an implementation with dual- and single-post resonators. It also enables the identification of design limitations, e.g., resulting from the general TE_{10} bypass couplings when using the second dual-post mode, i.e., there is always a bypass coupling.

The second order filter characteristic is specified to have a center frequency of 2.775 GHz, a 20 MHz bandwidth (return loss: 20 dB) and a TZ at 2.7 GHz. This response is satisfied by the normalized coupling matrix of ***Equation 1***:

$$M = \begin{bmatrix} 0 & 1.2074 & -0.2443 & 0 \\ 1.2074 & 0.3559 & 1.6116 & 0 \\ -0.2443 & 1.6116 & -0.2973 & 1.2300 \\ 0 & 0 & 1.2300 & 0 \end{bmatrix} \quad (1)$$

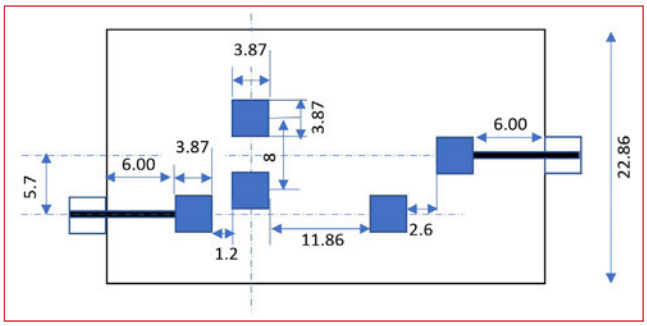

Fig. 9 **Initial filter configuration after assessment of resonator, input/output and inter-resonator coupling dimensions.**

The filter implementation considers the second mode of a dual- and a single-post resonator. Thus, the first design step is related to the determination of the two different resonator types as described above. The second step is related to the design of the input and output couplings of the assigned resonators. As shown above, the maximum coupling of the dual-post resonator is achieved at a transverse offset of 5.7 mm. Hence, the required coupling is adjusted by the longitudinal distance between the coupling stub and resonator.

The configuration of the single-post output coupling considers a centered location of the coupling stub, while the post is transversally offset by 5.7 mm. (The post offset accounts for the later inter-resonator coupling with the second mode dual-post resonator, while the central coupling location avoids a parasitic coupling with the second dual-post resonance mode.) The adjustment of the required output coupling is made in the same manner, i.e., by varying the longitudinal distance of the stub.

Once the configurations of the required interface couplings have been determined, they can be combined for the second order filter with the intermediate coupling length. Based on the considerations above, the initial length (11.86 mm) for the required coupling is estimated by two single-post resonators in the half-width waveguide envelope. The filter dimensions obtained by these initial systematic steps are given in ***Figure 9***.

The response (see ***Figure 10***) of this initial configuration shows a second order filter with the required bandwidth, 17 dB return loss and a frequency offset of about 4 MHz. Thus, this pre-dimensioning, which relies on well-esablished filter design methods, needs only minor adjustments of resonators and couplings to meet the original specifications, as shown by the analyzed results.

Note that, apart from the related offset locations of the input coupling and the single-post resonator, the cross-coupling is not considered for this initial design. Due to the above evaluation, there is always a bypass coupling of the second mode of the dual-post resonator in such structures by the dominant TE_{10} waveguide mode, since this mode does not interact with the dual-post resonator but with interface couplings and single-post resonators.

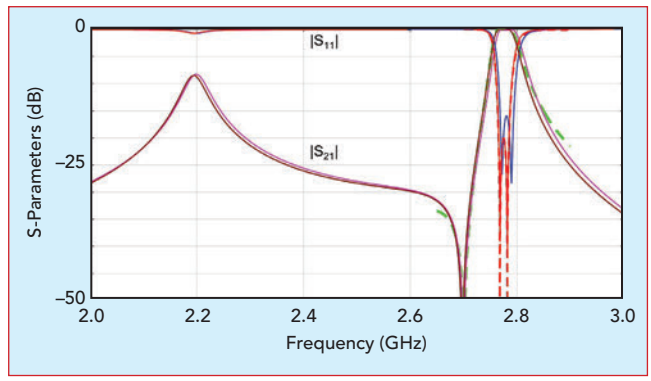

Fig. 10 **Second order filter design with dual- and single-post resonators initial configuration (see Figure 19) synthesized characteristic: $|S_{11}|$ (blue), $|S_{21}|$ (magenta). Results after minor tuning of coupling M_{12} and resonators: $|S_{11}|$ (red), $|S_{21}|$ (green).**

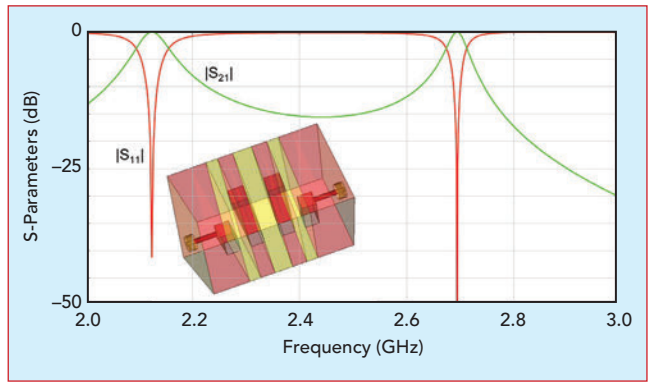

Fig. 11 **Analyzed response of an inline dual-post resonator.**

For the present configuration, the bypass coupling results mainly from the distance of the input coupling to the single-post, while the couplings of the dual-post resonator (toward the input and single-post), also depend on the associated sub-lengths. A TZ location closer to the passband requires a stronger bypass coupling, while the other couplings must remain with a similar strength.

Although all dedicated couplings depend on their respective longitudinal distances, they can be adjusted individually according to the need for a desired filter function (TZ location). For example, the bypass coupling M_{s2} is increased by reducing the distance between the dual- and single-post resonators. To keep the respective main coupling M_{12} (almost) constant, the transverse center offset of the single-post resonator location must be reduced (see above investigations). Consequently, the knowledge of the real functionality supports the systematic, straightforward filter designs using well-established methods.

ADDITIONAL VERIFICATION EXAMPLES

Inline Dual-Post Resonator

First, an inline dual-post unit is considered. The input and output are aligned with the posts of the unit, as shown in ***Figure 11***. As discussed in Part 1 of this article, this unit is not able to generate a TZ at a finite frequency. This is confirmed by the analyzed full-wave results shown in Figure 11. The behavior is identical to

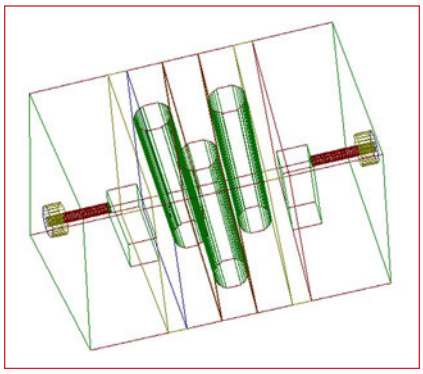

Fig. 12 **Fourth order filter design; dashed lines – synthesis of "box-section" characteristic; solid lines – analyzed responses of implementation.**

that of TE_{101} and TE_{102} waveguide cavity modes in inline filters.[4]

Triple-Post Unit (Doublet)

As discussed in Part 1 of this article, the triple-post unit can generate up to two TZs at finite frequencies. Only one TZ is generated when the coupling coefficients are constrained, according to Equation 10c in Part 1 of this article. Even if this constraint is not satisfied exactly, one TZ will be located far away from the passband, especially when the dominant even mode resonates at a sufficiently distant frequency below the passband. It was also demonstrated that the remaining TZ satisfies an approximate TZ-shifting property.

The triple-post configuration (see Figure 6 in Part 1 of this article) is used with necessary input and output coupling, symmetrically placed at both sides, to realize a second order (doublet) filter. Note that the footprint and housing cross sections are according to Figure 2.[5] The input and output of the filter coupling stubs are used with a conductive connection to the interfacing coaxial lines (see ***Figure 12***). The stub location and height are optimized to achieve a second order filter characteristic using the triple-post dimensions of Figure 6 in Part 1 of this article. The obtained characteristic is shown in ***Figure 13***. The configuration provides an equi-ripple passband from 2.747 to 2.759 GHz (return loss 22 dB) with a TZ above the passband at 2.767 GHz.

Solely adjusting the heights of the posts results in an almost mirrored image of the response with the TZ moved below the passband. The spurious mode far below remains practically unchanged (see Figure 13 and ***Figure 14***). In detail, the height of the inline dual posts of the triple configuration is reduced to 21.912 mm, and the height of the single-post is increased to 22.042 mm. ***Figure 15*** shows both responses over a frequency range around the passband. This clearly demonstrates doublet behavior with the TZ-shifting property. Although the possibility of shifting the TZ by adjusting the resonant frequencies was mentioned by Bastioli et al.,[5] the equivalent circuit used in the design does not exhibit this property.

These results show that triple-post structures are adequately described by models that rely only on those resonances that contribute to the passband. Their designs can be carried out by following well-established filter synthesis and design methods. There is no real need for elaborate overdetermined models and synthesis techniques that include spurious resonances far away from the passband, which cannot be controlled and contribute very little to the passband.

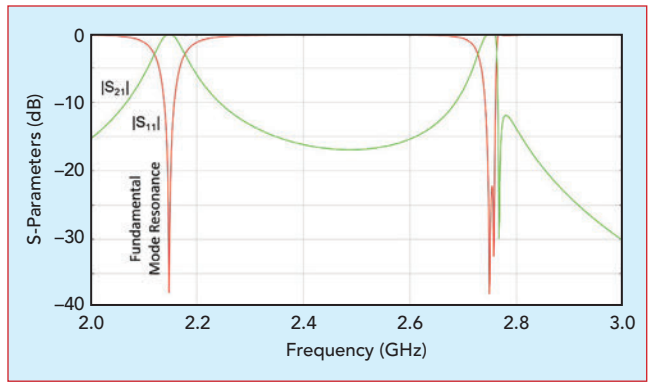

Fig. 13 **Response of configuration in Figure 4 (height of all posts = 21.95 mm).**

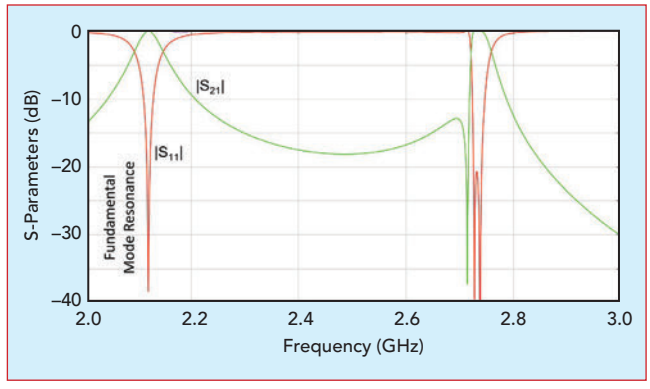

Fig. 14 **Response of configuration in Figure 4 (post heights: inline pair = 21.912 mm, single post = 22.042 mm).**

Design of a Fourth Order Box-Section Filter

A fourth order filter implementation considers a triple-post doublet section as the basic building block, coupled at both sides with single-post resonators to realize a fourth order filter with one TZ. The filter response has a center frequency at 2.662 GHz. The bandwidth is 76 MHz (equi-ripple return loss 25 dB) with a TZ below the passband at 2.61 GHz. According to the above findings, the configuration corresponds to a box-section coupling scheme, i.e., the respective normalized coupling values for the filter response are given by ***Equation 2***:

$$M = \begin{pmatrix} 0 & 1.1402 & 0 & 0 & 0 & 0 \\ 1.1402 & 0.0964 & 0.9398 & 0.4229 & 0 & 0 \\ 0 & 0.9398 & 0.3934 & 0 & -0.9398 & 0 \\ 0 & 0.4229 & 0 & -1.0211 & 0.4229 & 0 \\ 0 & 0 & -0.9398 & 0.4229 & 0.0964 & 1.1402 \\ 0 & 0 & 0 & 0 & 1.1402 & 0 \end{pmatrix} \quad (2)$$

The synthesis represents a narrow band characteristic close to the passband without any spurious effects.

The dashed lines in ***Figure 16*** show the response of the synthesized coupling matrix. The implementation is shown by the inset. The central triple-post doublet and the single resonators are situated in a straight housing (like that described by Bastioli et al.[5]) The single posts are conductively coupled with the coaxial interfaces at the opposite end walls. The different couplings between the single posts and the triple-post resonances are adjusted by the transverse offset locations of the single posts and the inline distance. The

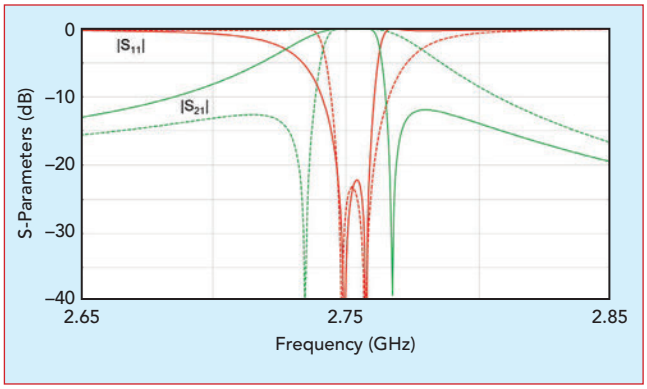

Fig. 15 **Narrowband responses of the initial doublet filter (Figures 13 and 14) with adjusted resonator post heights (zero-shifting property).**

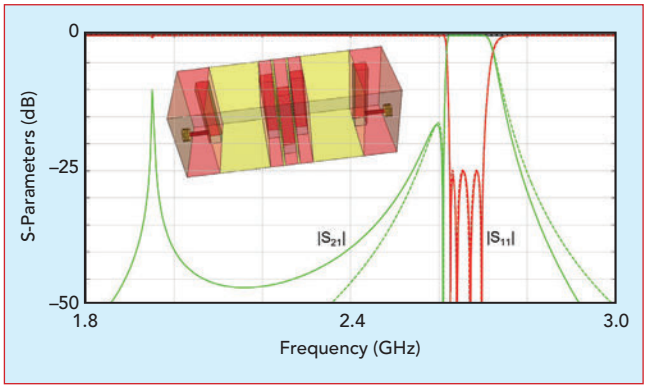

Fig. 16 **Fourth order filter design: dashed lines – synthesis of "box-section" characteristic; solid lines – analyzed responses of implementation (shown in inset).**

resonances of the doublet are conveniently controlled by separate adjustment of the dedicated two inline posts and the single post beside the two.

The analyzed characteristics of the configuration in Figure 16 coincide accurately with the ideal response of the coupling matrix. As expected, the spurious fundamental mode resonance of the triple-post unit appears far below the passband, resulting in an impairment of the ideal ("box-section") filter response with increasing distance from the passband. Toward lower frequencies, there is a reduced rejection, while toward higher frequencies, an increase in rejection is observed.

It should be noted that this design also exhibits the "zero-shifting" property as demonstrated by the response in ***Figure 17***, which follows from Figure 16 by solely adjusting the heights of the posts. As the analyzed results show, the fundamental mode resonance remains far below the passband. However, the achieved response does not provide an accurate mirror image of the initial design (see Figure 16); i.e., the passband is narrower with a higher return loss (> 30 dB), and the TZ is closer to the band. This is attributed to the spurious effects described above and requires some minor adjustments of the couplings to achieve an accurate mirror image of the initial response.

Triplet Filter Design with Inline Dual-Post

An inline dual-post resonator (see Figure 2a in Part 1 of this article) is selected for a triplet filter design to further validate its basic properties. The dual-post configuration is coupled to single-post resonators in a triangular arrangement with the latter resonators connected via conductive couplings with coaxial interfaces (see ***Figure 18***). For the cross-coupling, an inductive window is considered in the separation wall between the single-post resonators. The passband of the third order filter characteristic is from 2.598 to 2.680 GHz (equi-ripple return loss = 17 dB), and a TZ is located below the passband at 2.555 GHz. The dashed lines in ***Figure 19*** show the response of the synthesized coupling matrix.

Fig. 17 **Fourth order filter design (see inset of Figure 8). TZ shifts above the passband solely by small adjustments of post heights.**

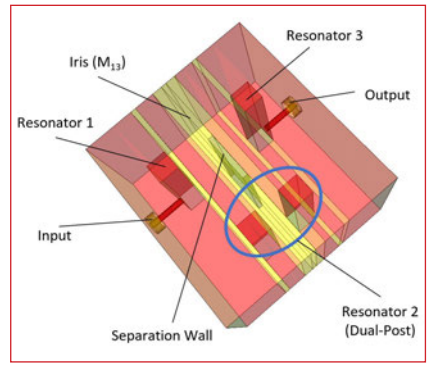

Fig. 18 **Configuration of triplet filter with dual-post resonator.**

Note, for the realization of the TZ below the passband, a transformation of the coupling sign is mandatory and therefore, the use of the second (odd) mode. The dual-post height in the final design is 22.06 mm. The analyzed response of this configuration is shown in Figure 19 (solid lines), together with the ideal response. Good agreement between the two is achieved. Analysis over a wide frequency range

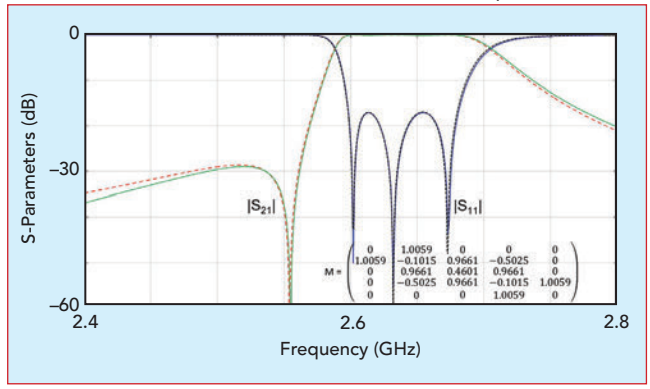

Fig. 19 **Response of triplet filter design (see Figure 18); synthesis (dashed), analyses (solid). Inset: coupling matrix.**

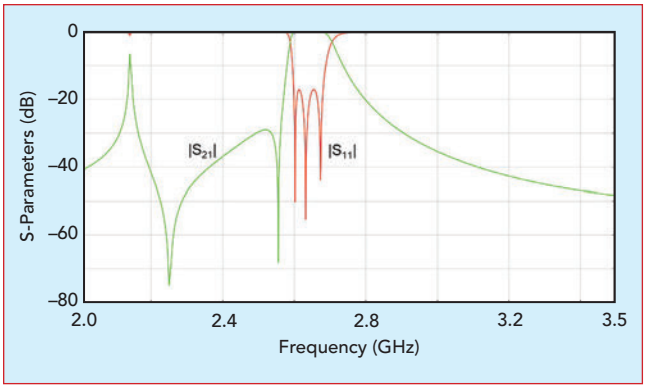

Fig. 20 **Analyzed wideband response of triplet filter design of Figure 18.**

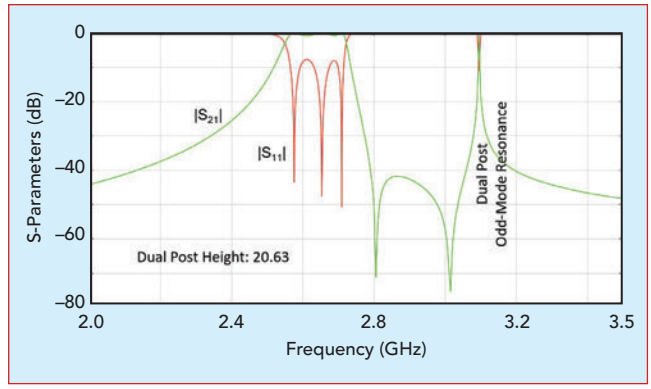

Fig. 21 **Analyzed wideband response of triplet filter design in Figure 18, but with a reduced height of the dual-post unit.**

shows the spurious fundamental resonance far below the passband as expected (see ***Figure 20***).

The properties of the special dual-post resonator configuration (see Figure 18) are simply demonstrated by exchanging the second (odd) mode and the fundamental mode allocations. That is, the resonances of both dual-post modes have been moved toward higher frequencies by solely reducing the height of the dual posts in the structure.

The analysis of this identical configuration with only a reduced dual-post height of 20.63 mm exhibits a transformation of the coupling sign. The computed response (see ***Figure 21***) shows a third order filter characteristic with moderate return loss (~8 dB), but with the TZ above the passband; additionally, the odd mode is now the spurious far above the passband (see Figure 21). No attempt was made to improve the return loss of a typical value of 20 dB because the intention is to show the sign transformation that comes with only adjusting the heights of the posts of the dual-post unit.

The simple interchange of even and odd modes for a dedicated filter implementation will not yield a mirror image of the responses. The modes exhibit different field strengths for the couplings with the other resonators (posts). Note that this feature is different from the zero-shifting property of doublet configurations that involve the frequency interchange of the assigned resonances ("self-couplings, *Mxx*").

Instead, this involves the interchange of the roles played by the two resonances of the dual-post unit. In the first design, the even fundamental mode is spurious and located below the passband. In the second design, the odd mode is spurious and located above the passband. This operation allows different transformations of the coupling coefficients and extends the design possibilities.

The additional TZ that is present in these two filters can be explained by the interference of the signal going through the coupling iris between the posts at the input and the output and the spurious resonance. In the first case (see Figure 20), the bypassed mode is even. Around the spurious resonance, the filter acts as a singlet with all coupling coefficients of the same sign, hence the TZ above the resonance. In the second case (see Figure 21), the spurious mode is odd. This means that one coupling coefficient is negative. Around the spurious resonance, the filter is equivalent to a singlet with one negative coupling coefficient, hence the TZ is below the resonance.

REFERRED EXPERIMENTAL VALIDATION

Measured results of filter designs with close-post configurations have been provided in several recent papers.[1,3,5-7] Photos of hardware realizations were also provided in the same references. The main goal of this work is not to design and manufacture new filters based on the same structures; instead, it is to explain the underlying physics of the relevant basic building blocks to enable straightforward systematic design and tuning by using well-established filter design methods. Moreover, it will be the key to many novel and innovative design ideas.

The elaborate and questionable syntheses in combination with EM-optimization techniques in recent papers[1,3,5-7] produce working filters. The point demonstrated by this work is that the same filters can be designed in a straightforward way by using classic design methods that are familiar to all filter designers if the proper equivalent circuits are used. The example of a fourth order filter is used to illustrate this point.

The fourth order filter design of Bastioli et al.[5] is like the fourth order box-section filter described here. Because of the orthogonality of the solutions to Maxwell's equations in a given volume, the eigenresonances of the triple-post unit are not coupled to each other. Given that the bandwidth of the filter is not large, the coupling coefficients of the resonances of the triple-post unit to the input and output resonators are not strong. This means that they can be treated as localized resonators.

The spurious (fundamental) mode provides coupling between the input and output resonators that is small and practically constant over the narrow passband. The result is the coupling scheme (box-section with small bypass coupling) shown in ***Figure 22***.

A comparison of the filter response from Bastioli,[7] in their Figure 15, with a synthesized characteristic considering one TZ only (box-section without bypass), exhibits some small deviations in rejection; i.e., rejection above the passband is a few dB higher, whereas below is a few dB lower. This is directly attributed to the weak spurious

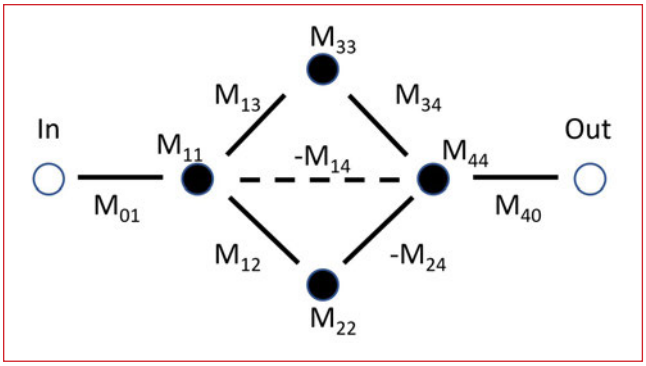

Fig. 22 Real coupling scheme of the introduced 4-pole filter (see Bastioli,[7] Figures 12 through 15) representing physical resonances of configuration ($M_{34} = M_{13}$; $M_{24} = M_{12}$; $M_{44} = M_{11}$).

fundamental mode bypass coupling in the box-section scheme (see Figure 22), which yields an extra TZ far above the passband; i.e., the corresponding normalized coupling values are given by ***Equation 3***:

$$M = \begin{pmatrix} 0 & 1.0390 & 0 & 0 & 0 & 0 \\ 1.0390 & 0.1029 & 0.8984 & 0.2365 & -0.1046 & 0 \\ 0 & 0.8984 & 0.1143 & 0 & -0.8984 & 0 \\ 0 & 0.2365 & 0 & -1.0136 & 0.2365 & 0 \\ 0 & -0.1046 & -0.8984 & 0.2365 & 0.1029 & 1.0390 \\ 0 & 0 & 0 & 0 & 1.0390 & 0 \end{pmatrix} \quad (3)$$

Note that all elements of this coupling matrix have typical values, contrary to the unrealistic values that result when using the triplet resonator scheme representations.[5,7]

The weak spurious mode coupling is an inherent parasitic effect in this doublet configuration with the triple-post structure; its accurate strength depends on the final physical implementation (mainly on the distance of the spurious fundamental mode resonance from the passband). It cannot be controlled completely as part of the design. It makes little engineering sense to include it in the model upon which the design is based. The best that can be done is to push it as far away from the passband as possible by reducing the distance between the strongly interacting posts. However, the knowledge of its effect from a first iteration may be incorporated to a certain extent in the initial synthesis of such a filter design. Final adjustments of the relevant dimensions of the filter in the design can compensate for the small distortions that may be caused by the spurious resonance.

The basic knowledge of this triple-post dual-mode resonator functionality allows similar basic design considerations (as provided in Part 1 of this article of the dual-post singlet resonator, e.g.) to optimize unloaded Q and spurious mode distance, as well as coupling properties with other resonator types.

The above investigations regarding properties of the triple-post resonator implementation are identical with the central footprint and housing dimensions from Bastioli et al.[5] in their Figure 12, which are part of their realized fourth order filter design (see a photo of the filter in their Figure 14, with measured results in their Figure 15). The passband of their realized filter, however, is substantially lower than the resonant frequencies in this investigation. This is attributed to the different heights and loadings of the posts (the heights of their posts are 22.86 mm with additional dielectric loading at the top, without further information). Nevertheless, this does not change the principal physical properties of such close triangular post configurations.

Also, the experimental results provided by Zeng et al.[7] validate the real physical behavior of the close-post configurations in coaxial filter designs introduced above, i.e., all these filter designs rely on standard synthesis methods where the number of resonators within the configuration is identical to that of the filter order. Consequently, their introduced synthesis is misleading. It introduces extra "redundant resonances," but without giving any physical representation of such redundant resonant circuits. A filter characteristic is finally achieved using commercial EM-CAD optimization techniques.

CONCLUSION

The investigations of building blocks with strongly coupled posts have shown that the individual posts are not pivotal to the design of filters containing these structures. Because of the strong coupling between posts that share the same volume, resonances localized around the post are not physical. Instead, the resonances of the complete block and their properties must be examined to identify those features that are relevant to the design of filters that contain one or more of such structures.

Similarity transformations yield coupling matrices that conserve the frequency response of the entire filter but not necessarily the dominant "internal" physics of these structures because of the strong coupling and the boundary conditions. Nevertheless, coupling matrices based on localized resonances can be and have been successfully used to optimize the filter in connection with the full-wave response of the entire filter or subsections that consider these structures with adjacent single-post resonators.

However, classic design methods based on pairs of resonators will most likely fail when applied to such coupling matrices. Using resonances that satisfy the boundary conditions and contribute to the passband is essential to understanding how these structures work and how to use them in interesting and innovative designs. These filters can be designed by following well-established methods if they are based on an equivalent circuit (coupling matrix) that contains only those physical resonances that contribute to the passband.

Knowledge of the real functionality is a prerequisite for the systematic application of standard design methods for a convenient geometrical pre-design of the desired filter configuration, considering also different kinds of resonators without general design limitations.

As an example, the usual basic considerations for the pre-design of a second order filter with one TZ are introduced for an implementation using dual- and sin-

gle-post resonators. The analysis results of the initial configuration, obtained by the application of this classical design approach, provide almost the desired filter characteristic response without any EM-optimization/tuning.

The filters described in this article have all been designed using well-established methods. The effect of spurious resonance is then addressed by a final adjustment of the filter dimensions in connection with the equivalent circuit and a field solver. ■

References

1. G. Macchiarella, S. Bastioli and R. V. Snyder, "Design of In-Line Filters with Transmission Zeros Using Strongly Coupled Resonators Pairs," *IEEE Transactions on Microwave Theory and Techniques*, Vol. 66, No. 8, August 2018, pp. 3836–3846.
2. S. Amari and U. Rosenberg, "Characteristics of Cross (Bypass) Coupling Through Higher/Lower Order Modes and Their Applications in Elliptic Filter Design," *IEEE Transactions on Microwave Theory and Techniques*, Vol. 53, No. 10, October 2005, pp. 3135–3141.
3. S. Bastioli and R. V. Snyder, "Evanescent Mode Filters Using Strongly Coupled Resonator Pairs," *IEEE MTT-S International Microwave Symposium*, June 2013.
4. U. Rosenberg, "New `Planar' Waveguide Cavity Elliptic Function Filters," *25th European Microwave Conference*, September 1995.
5. S. Bastioli, R. V. Snyder and G. Macchiarella, "Design of In-Line Filters with Strongly Coupled Resonator Triplet," *IEEE Trans. Microwave Theory and Techniques*, Vol. 66, No. 12, December 2018, pp. 5585–5592.
6. Y. Zeng, Y. Yang and M. Yu, "Flexible Design of Generalized Strongly Coupled Resonator Triplet Filters by Regulating Redundant Resonant Modes," *IEEE MTT-S International Microwave Symposium*, June 2021.
7. Y. Zeng, Y. Yang, M. Yu and S. Bastioli, "Synthesis of Generalized Strongly Coupled Resonator Triplet Filters by Regulating Redundant Resonant Modes," *IEEE Transactions on Microwave Theory and Techniques*, Vol. 70, No. 1, January 2022, pp. 864–875.